

# Methods for the Radiological Characterisation of the FiR 1 TRIGA Research Reactor Decommissioning Waste

by Tarryn Ackermann

*Thesis presented in fulfilment of the requirements for the degree  
of Master of Science in the Faculty of Science at  
Stellenbosch University*



Supervisor: Dr P Kotiluoto (VTT Technical Research Centre of Finland)  
Co-supervisor: Prof RT Newman (Stellenbosch University)

March 2017

## **Declaration**

By submitting this thesis electronically, I declare that the entirety of the work contained therein is my own, original work, that I am the sole author thereof (save to the extent explicitly otherwise stated), that reproduction and publication thereof by Stellenbosch University will not infringe any third party rights and that I have not previously in its entirety or in part submitted it for obtaining any qualification.

Copyright © 2017 Stellenbosch University

All rights reserved

## Abstract

Every nuclear reactor will eventually reach the end of its life time. With more than 60 new power reactors currently under construction, the need for understanding the safe decommissioning of a nuclear reactor is as important as ever. Among those reactors at the end of their life time is the VTT owned, FiR 1 TRIGA Mark II Research Reactor in Espoo, Finland.

The FiR 1 decommissioning project is reviewed as a whole, as well as the requirements set by regulatory authorities relating to decommissioning waste and the environment. Special focus is placed on full site characterisation in terms of activity measurements. During this part of the procedure, an activity inventory of all activated components and structures is determined. The activity inventory has been determined computationally through the use of MCNP and ORIGEN-S, and this is explained on a general level. However, the results thereof require validation through physical measurements. These physical measurements are performed using  $\gamma$  spectroscopy for three different types of samples (concrete, Flual and aluminium) using the In Situ Object Counting System (ISOCS<sup>TM</sup>). In addition, 13 barrels containing ion-exchange resin are characterised and compared with accepted release levels.

Measurements are performed and interpreted using Genie<sup>TM</sup> 2000 software, to determine activity concentrations for validation of computationally determined activities. Algorithms used in the Genie 2000 software are outlined to better understand how the activity concentrations are determined.

For the concrete sample, measured and predicted activities for  $^{60}\text{Co}$  and  $^{152}\text{Eu}$  agree with an uncertainty of 11% and 2%, respectively. While unsystematic differences are initially found for the cases of Flual and aluminium, it is understood that the most probable cause is the assumed material compositions in the calculations. After ICP-MS leading to more accurate knowledge of the Flual and aluminium sample compositions, there is much better agreement between computational and measured results. The differences are still large, but systematic. The calculated values are consistently one order of magnitude larger than the measured values, except for  $^{59}\text{Fe}$  in the aluminium sample, for which the values agree to the same order of magnitude. The 13  $\gamma$  spectra for ion-exchange resin barrels all look similar, with some barrels more active than others, as would be expected for an inhomogeneous sample. In every barrel,  $^{60}\text{Co}$  and  $^{137}\text{Cs}$  is found, with the  $^{137}\text{Cs}$  suspected to come from a leaking fuel rod.

Although much time and effort was spent on the analysis of a small number of samples relative to the number of samples in the full reactor decommissioning, it is a necessary exercise to learn lessons that may save time in the future. Most important is the study of the methods of measurement and calculation that will be applied later during full decommissioning.

## Opsomming

Elke kernreaktor bereik eventueel die einde van sy leeftyd. Met meer as 60 nuwe kernkrag reaktore tans onder konstruksie, is die behoefte om die veilige ontmanteling van 'n kernreaktor te verstaan belangriker as ooit. Een van hierdie reaktore wat aan die einde van sy leeftyd gekom het, is die FiR 1 TRIGA Merk II Navorsingsreaktor van VTT in Espoo, Finland.

Die FiR 1 ontmantelingsprojek word as geheel nagegaan, asook die vereistes wat deur die regulerende owerhede ingestel is wat betrekking het op ontmantelingsafval en die omgewing. Spesiale fokus word geplaas op heel-terrein karakterisering in terme van aktiwiteitsmetings. Tydens hierdie deel van die prosedure word 'n aktiwiteitsopgawe van alle geaktiveerde komponente en strukture bepaal. Die aktiwiteitsopgawe is bereken deur van MCNP en ORIGEN-S gebruik te maak. Dit word in die algemeen verduidelik. Die resultate hiervan vereis egter bevestiging deur fisiese metings. Hierdie fisiese metings word deur middel van  $\gamma$  spektroskopie uitgevoer vir drie verskillende soorte monsters (beton, Flual en aluminium), deur gebruik te maak van die In Situ Voorwerp Tel Sisteem (ISVTS™). Daarbenewens word 13 dromme, bevattende ioon-uitruil hars, gekarakteriseer en met aanvaarbare vrylatingsvlakke vergelyk.

Metings word uitgevoer, en met behulp van die Genie™ 2000 sagteware ontleed, om aktiwiteits konsentrasies vas te stel vir die bekragtiging van die berekende aktiwiteite. Algoritmes wat in die Genie 2000 sagteware gebruik word, word uiteengesit om beter te verstaan hoe die aktiwiteits konsentrasies bepaal word.

Vir die beton monster stem gemete en voorspelde aktiwiteite vir  $^{60}\text{Co}$  en  $^{152}\text{Eu}$  ooreen met 'n gepaartgaande onsekerheid van 11% en 2%, onderskeidelik. Terwyl nie-sistematiese verskille aanvanklik vir die Flual en aluminium gevind is, word dit verstaan dat die waarskynlikste oorsaak die aangenome materiaal samestelling in die berekening is.

Na induksie-gekoppelde plasma massaspektrometrie (IKP-MS), wat tot meer akkurate kennis van die samestellings van die Flual en aluminium monsters lei, is daar baie beter ooreenkoms tussen gemete en berekende resultate. Die verskille is steeds groot, maar sistematies. Die berekende waardes is konsekwent een orde-grootte groter as die gemete waardes, behalwe vir  $^{59}\text{Fe}$  in die aluminium monster waarvoor die waardes tot dieselfde orde-grootte, ooreenstemmend.

Die 13  $\gamma$ -spektra vir die ioon-uitruil hars dromme lyk almal dieselfde, met sommiges meer aktief as ander, soos wat verwag kan word vir 'n nie-homogene monster.  $^{60}\text{Co}$  en  $^{137}\text{Cs}$  word in elke drom gevind, met  $^{137}\text{Cs}$  vermoedelik afkomstig van 'n lekkende brandstofstaaf.

Hoewel baie tyd en moeite aan die ontleding van 'n klein hoeveelheid monsters bestee is, in vergelyking met die hoeveelheid monsters in die volledige reaktor, is dit 'n noodsaaklike oefening om lesse aan te leer wat in die toekoms tyd kan spaar. Die belangrikste is die studie van die meet- en berekeningmetodes wat later tydens volledige ontmanteling toegepas sal word.

## Acknowledgments

First and foremost I would like to thank my supervisor, Dr Petri Kotiluoto. Your endless patience for my never-ending list of questions has made an invaluable contribution, not only to my thesis, but also to my future career in Physics. Despite your busy schedule, you left no email unanswered. I learned so much from you.

Thank you to my co-supervisor, Prof Richard Newman, for putting me into contact with Petri and VTT, and for working so hard to help me.

Tommi Kekki, thank you for all your help! Thank you for sharing all your experience with me, and for always being there when the ISOCS system wouldn't listen to me.

Antti Rätty, thank you for sharing your office with me. You did far more to help me than anyone could have expected of you. I cannot tell you how much I appreciate it.

Thank you to the rest of the Reactor Physics team, especially Merja Tanhua-Tyrkkö, Tuomas Viitanen, and Olli Vilkkamo. Thank you also to Emmi Myllykylä and Tiina Lavonen for performing the ICP-MS analysis. Thank you to VTT, for this amazing research opportunity!

Thank you to Prof Paul Papka for always saving the day. Despite being so busy, and the fact that I am not even one of your students, you still found the time to read my thesis and answer all my questions. I have so much admiration for you.

Thank you, Christine Ruperti, for going above and beyond what is expected of you. I don't think my thesis would ever have been submitted if it weren't for you.

Last but not least, thank you to the Harry Crossley Foundation for the generous financial assistance.

## Table of Contents

### Chapter 1: Introduction

1.1 Nuclear reactors.....	1
1.1.1 Key components of a nuclear reactor and their functions .....	1
1.1.2 Power reactors versus research reactors.....	2
1.1.3 Types of nuclear reactors .....	3
1.2 Decommissioning of Nuclear Reactors.....	5
1.2.1 Three approaches to decommissioning.....	5
1.2.2 An international look at decommissioning .....	6
1.3 VTT Technical Research Centre of Finland Ltd.....	7
1.3.1 The FiR 1 research reactor .....	7
1.3.2 The FiR 1 BNCT facility .....	12
1.3.3 The decision to decommission.....	15
1.3.4 Final disposal in Finland .....	16
1.3.4.1 Low- and Intermediate-Level Waste (LILW).....	16
1.3.4.2 High-Level Waste (HLW) in the form of SNF.....	16
1.4 Thesis aims and outline.....	17

### Chapter 2: Background and Theory

2.1 Classes of ionising radiation.....	19
2.2 Limitations set by regulatory guides .....	19
2.2.1 Regulatory authorities .....	19
2.2.2 Relevant STUK regulations regarding decommissioning.....	20
2.3 Gamma radiation.....	22
2.3.1 Gamma ray interaction with matter .....	22
2.3.2 Gamma attenuation .....	24
2.3.3 Radioactivity and radioactive decay .....	25
2.3.4 Gamma ray measurement techniques .....	28
2.4 Beta particles .....	29
2.4.1 Charged particle interaction with matter .....	29
2.4.2 General $\beta$ measurement techniques .....	30
2.4.3 Tritium measurement techniques .....	31

2.5 Neutrons .....	33
2.5.1 Neutron activation .....	33
2.5.2 Neutron interactions and cross sections.....	35
2.5.3 Neutron interaction mechanisms.....	36
2.5.4 Expected major activation products .....	37
2.5.5 Characterising activation products .....	38
2.6 The pre-measurement inventory report .....	40
2.6.1 Activity prediction using MCNP and ORIGEN-S .....	40
2.6.2 Expected activated structures and components .....	46
<b>Chapter 3: Experimental Methods</b>	
3.1 Requirements for measurement techniques at VTT for material characterisation.....	51
3.2 Sample description and preparation.....	53
3.3 Sample measurement .....	57
3.3.1 Measurement equipment .....	57
3.3.2 Energy calibration .....	58
3.3.3 Physical measurements .....	59
<b>Chapter 4: Analysis</b>	
4.1 Modelling the measurement set-ups.....	61
4.2 Efficiency calibration .....	63
4.3 Peak area determination .....	64
4.4 Nuclide identification and activity calculation .....	67
<b>Chapter 5: Results and Discussion</b>	
5.1 Concrete .....	70
5.2 FluentaI.....	71
5.3 Aluminium.....	72
5.4 Ion-exchange resin.....	72
5.5 Understanding the peak analysis performed by Genie 2000 .....	76

## **Chapter 6: Conclusion**

6.1 VTT's decommissioning procedure .....	77
6.2 ISOCS equipment .....	78
6.3 Recommendations for future work.....	78

## **Addendums**

Addendum A: Relevant STUK regulations regarding decommissioning .....	79
Addendum B: All spectra not shown in Chapter 5 .....	82
Addendum C: Gamma energies used in activity calculations .....	87
Addendum D: Results of the ICP-MS analysis .....	91

## **References**



## List of Figures

<b>Figure 1.1</b>	The dependence of cross section (barns) on neutron energy (eV) for nuclides of high mass numbers.....	3
<b>Figure 1.2</b>	Aluminium tank.....	8
<b>Figure 1.3</b>	Labelled diagram of the FiR 1 reactor core.....	9
<b>Figure 1.4</b>	Core and reflector assembly as modelled in MCNP.....	10
<b>Figure 1.5</b>	Reactor core consisting of 80 fuel elements, graphite elements, irradiation positions, and four control rods .....	10
<b>Figure 1.6</b>	Steel tube elements filled with heavy concrete surrounding BNCT irradiation room .....	11
<b>Figure 1.7</b>	FiR 1 reactor with BNCT unit.....	13
<b>Figure 1.8</b>	Neutron fluence rate [ $\text{cm}^{-2} \text{s}^{-1}$ ] as a function of Fluental thickness [cm].....	13
<b>Figure 1.9a</b>	Original structure of the reactor. Horizontal cross section at core level showing the thermal column .....	14
<b>Figure 1.9b</b>	Original structure of the reactor. Vertical cross section at core level.....	14
<b>Figure 1.10</b>	Detailed view of the BNCT structures .....	15
<b>Figure 1.11</b>	The decommissioning procedure used by VTT.....	18
<b>Figure 2.1</b>	Relative penetrating distances of different particles.....	19
<b>Figure 2.2</b>	Pair production .....	23
<b>Figure 2.3</b>	The energies at which the photoelectric effect, Compton scattering and pair production dominate .....	24
<b>Figure 2.4</b>	The Q-value for a general $\beta^-$ reaction .....	26
<b>Figure 2.5</b>	Range of energies exhibited by the $\beta$ particle following $\beta^-$ decay.....	26
<b>Figure 2.6</b>	The energy resolution, expressed as FWHM as a function of energy .....	29
<b>Figure 2.7</b>	Physical phenomena studied during NAA.....	33
<b>Figure 2.8</b>	Neutron flux as a function of neutron energy .....	34
<b>Figure 2.9</b>	Neutron interactions .....	35
<b>Figure 2.10</b>	A hypothetical set of events that is simulated in MCNP .....	41
<b>Figure 2.11</b>	Schematic view of the activity calculation .....	47
<b>Figure 2.12</b>	Horizontal and vertical cross sections of the MCNP geometry with the BNCT facility.....	49
<b>Figure 2.13</b>	The simulated total neutron fluence rate distribution (units: $\text{cm}^{-2}\text{s}^{-1}$ ) as shown on the horizontal and vertical cross section of the reactor .....	50

<b>Figure 3.1</b>	Example of a general characterisation procedure.....	52
<b>Figure 3.2a</b>	The concrete sample.....	54
<b>Figure 3.2b</b>	Diamond drilling of the biological concrete shield for construction of the BNCT facility.....	54
<b>Figure 3.3</b>	The dimensions [mm] of the concrete diamond drilling samples number 66, 71-74, and 81-84.....	55
<b>Figure 3.4</b>	The positions of the diamond drilling samples in the reactor geometry.....	56
<b>Figure 3.5</b>	The Flualtal sample.....	57
<b>Figure 3.6</b>	Ion-exchange resin measurement set-up .....	60
<b>Figure 4.1</b>	Example of the modelled measurement set-up.....	61
<b>Figure 4.2a</b>	Model of the half full ion-exchange resin measurement set-up .....	62
<b>Figure 4.2b</b>	Model of the completely full ion-exchange resin measurement set-up.....	62
<b>Figure 4.3a</b>	The efficiency as a function of $\gamma$ -ray energy for the concrete geometry .....	65
<b>Figure 4.3b</b>	The efficiency as a function of $\gamma$ -ray energy for the Flualtal and aluminium geometries .....	66
<b>Figure 4.3c</b>	The efficiency as a function of $\gamma$ -ray energy for the full barrel ion-exchange resin geometry. ....	66
<b>Figure 4.4</b>	Interactive Peak Fit showing single wide peak being corrected to two peaks .....	66
<b>Figure 4.5</b>	Matrix of identified nuclides .....	67
<b>Figure 5.1</b>	The $\gamma$ -ray spectrum for concrete .....	73
<b>Figure 5.2</b>	The $\gamma$ -ray spectrum for Flualtal.....	73
<b>Figure 5.3</b>	The $\gamma$ -ray spectrum for aluminium .....	73
<b>Figure 5.4</b>	The $\gamma$ -ray spectrum for ion-exchange resin barrel 1091.....	74
<b>Figure B.1</b>	The $\gamma$ -ray spectrum for the concrete background measurement.....	82
<b>Figure B.2</b>	The $\gamma$ -ray spectrum for the Flualtal, Aluminium background measurement .	82
<b>Figure B.3</b>	The $\gamma$ -ray spectrum for ion-exchange resin barrel 1092.....	82
<b>Figure B.4</b>	The $\gamma$ -ray spectrum for ion-exchange resin barrel 1093.....	83
<b>Figure B.5</b>	The $\gamma$ -ray spectrum for ion-exchange resin barrel 1094.....	83
<b>Figure B.6</b>	The $\gamma$ -ray spectrum for ion-exchange resin barrel 1095.....	83
<b>Figure B.7</b>	The $\gamma$ -ray spectrum for ion-exchange resin barrel 1096.....	84
<b>Figure B.8</b>	The $\gamma$ -ray spectrum for ion-exchange resin barrel 1097.....	84

<b>Figure B.9</b>	The $\gamma$ -ray spectrum for ion-exchange resin barrel 1098.....	84
<b>Figure B.10</b>	The $\gamma$ -ray spectrum for ion-exchange resin barrel 1099.....	85
<b>Figure B.11</b>	The $\gamma$ -ray spectrum for ion-exchange resin barrel 1100.....	85
<b>Figure B.12</b>	The $\gamma$ -ray spectrum for ion-exchange resin barrel 1101.....	85
<b>Figure B.13</b>	The $\gamma$ -ray spectrum for ion-exchange resin barrel 1102.....	86
<b>Figure B.14</b>	The $\gamma$ -ray spectrum for ion-exchange resin barrel 1103.....	86
<b>Figure B.15</b>	The $\gamma$ -ray spectrum for the ion-exchange resin background measurement...	86

## List of Tables

<b>Table 1.1</b>	NPPs in commercial operation .....	4
<b>Table 1.2</b>	Status of nuclear facilities .....	7
<b>Table 2.1</b>	Waste clearance levels set by STUK according to nuclide group .....	21
<b>Table 2.2</b>	Expected major activation products .....	39
<b>Table 2.3</b>	Computed activities of various reactor components .....	48
<b>Table 3.1</b>	Sample information .....	53
<b>Table 3.2</b>	System specifications .....	59
<b>Table 4.1</b>	Dimensions of each of the measurement set-ups .....	62
<b>Table 4.2</b>	The maximum error associated with simplifying calibrations.....	63
<b>Table 5.1</b>	Activities of nuclides found in the concrete sample.....	74
<b>Table 5.2</b>	Activities of nuclides found in the Fluental sample.....	74
<b>Table 5.3</b>	Activities of nuclides found in the aluminium sample .....	75
<b>Table 5.4</b>	Activities of nuclides found in the ion-exchange resin .....	75
<b>Table 5.5</b>	Comparison of calculated activities to values reported by Genie 2000 .....	76
<b>Table C.1</b>	Concrete: $\gamma$ -ray energies used in activity calculation .....	87
<b>Table C.2</b>	Fluental 1: $\gamma$ -ray energies used in activity calculation .....	87
<b>Table C.3</b>	Aluminium 1: $\gamma$ -ray energies used in activity calculation .....	88
<b>Table C.4.1</b>	Ion-exchange resin barrel 1091: $\gamma$ -ray energies used in activity calculation ..	88
<b>Table C.4.2</b>	Ion-exchange resin barrel 1092: $\gamma$ -ray energies used in activity calculation ..	88
<b>Table C.4.3</b>	Ion-exchange resin barrel 1093: $\gamma$ -ray energies used in activity calculation ..	88
<b>Table C.4.4</b>	Ion-exchange resin barrel 1094: $\gamma$ -ray energies used in activity calculation ..	89
<b>Table C.4.5</b>	Ion-exchange resin barrel 1095: $\gamma$ -ray energies used in activity calculation ..	89
<b>Table C.4.6</b>	Ion-exchange resin barrel 1096: $\gamma$ -ray energies used in activity calculation ..	89
<b>Table C.4.7</b>	Ion-exchange resin barrel 1097: $\gamma$ -ray energies used in activity calculation ..	89
<b>Table C.4.8</b>	Ion-exchange resin barrel 1098: $\gamma$ -ray energies used in activity calculation ..	89
<b>Table C.4.9</b>	Ion-exchange resin barrel 1099: $\gamma$ -ray energies used in activity calculation ..	90
<b>Table C.4.10</b>	Ion-exchange resin barrel 1100: $\gamma$ -ray energies used in activity calculation ..	90
<b>Table C.4.11</b>	Ion-exchange resin barrel 1101: $\gamma$ -ray energies used in activity calculation ..	90
<b>Table C.4.12</b>	Ion-exchange resin barrel 1102: $\gamma$ -ray energies used in activity calculation ..	90
<b>Table C.4.13</b>	Ion-exchange resin barrel 1103: $\gamma$ -ray energies used in activity calculation ..	91
<b>Table D.1</b>	Results of the ICP-MS analysis .....	91

## Chapter 1: Introduction

The FiR 1 reactor is Finland's first nuclear reactor. Commissioned in 1962, it was designed for the purpose of research on neutron physics and activation analysis. Following this, Finland built two nuclear power plants (NPPs), one at Olkiluoto and one at Loviisa, each having two reactor units. Now, as the small FiR 1 reactor has reached the end of its lifetime, an opportunity has arisen to learn as much as possible about the process of decommissioning in Finland (in terms of environmental impact or transport safety analysis, for example) before the two larger facilities reach the end of their lifetimes.

### 1.1 Nuclear reactors

#### 1.1.1 Key components of a nuclear reactor and their functions

Ordinarily,  $^{238}\text{U}$  constitutes more than 99% of natural uranium, the remainder being fissile  $^{235}\text{U}$ . The percentage of fissile  $^{235}\text{U}$  can be increased to generate more suitable nuclear fuel. A fuel rod may consist of enriched  $\text{UO}_2$  pellets in fuel cladding. The percentage of enrichment indicates the percentage of  $^{235}\text{U}$  present in the pellets. These fuel rods are housed in cladding, which acts as a form of containment of the fission products. Fuel rods are packed together to form fuel assemblies, and many fuel assemblies may be packed together in the reactor core depending on the type of reactor. Some other fuel geometries and materials exist too, like metallic plates, uranium-zirconium-hydride fuel of TRIGA reactors, or even some liquid fuels (molten salt reactor). There is also the neutron source which is installed in the core (Sb-Be, for example). Neutrons from the neutron source strike  $^{235}\text{U}$  and form  $^{236}\text{U}^*$ , which then breaks into 2 fragments, 2-3 new neutrons, and heat. Various possible fission fragments may be formed, although the most probable mass numbers are close to 95 and 135.[1] The new neutrons can go on to strike other  $^{235}\text{U}$  nuclei, which in turn produces more neutrons and heat. A chain reaction is created that is controlled through the use of control rods. Control rods are made from materials that have a high probability of absorbing neutrons, such as boron or cadmium. When inserted, the rods capture neutrons, reducing the number of neutrons available to produce more fission products. Removing the rods allows the neutrons to multiply again.[2]

Neutron cross sections depend on neutron energy. Neutron energy regions are described as thermal ( $\leq 0.5$  eV), epithermal (0.5 eV - 100 keV), and fast (100 keV - 25 MeV).[3] In most materials, thermal neutrons have a higher probability of being absorbed or captured than fast neutrons. Figure 1.1 shows the dependence of the cross section on neutron energy for

nuclides of high mass numbers, with three distinct regions. In the first region, the cross section decreases with the inverse of the velocity of the neutron. In the second region, there are resonance peaks corresponding to the discrete quantum energy levels of the nucleus. Neutrons with a combined kinetic and binding energy matching these resonance energies have a higher probability of absorption or capture. In the last region, the cross section decreases more gradually with an increase in neutron energy, and the probability for neutron absorption or capture is very low.[4] This indicates the need for a neutron moderator, to shape the neutron energy spectrum to the desired energy range.[5]

In addition to fuel elements, the core also contains reflector elements to reflect neutrons back to the core.[4] There is also the coolant for which a popular choice is water, both light and heavy. In a power reactor, the coolant is used to capture the heat generated through fission so that it may be used in electricity production, as well as to control the pressure in the core.[6]

Many shielding structures should be in place to protect from the escape of fission products, but also to protect the core or the whole reactor from damage or outside threats. The fuel cladding is the first barrier. The second barrier is the pressure vessel, a thick vessel made of steel that contains the reactor core.[7] The final barrier is the containment structure. It might just house the reactor in the case of a research reactor, but it can also be designed to offer protection against unforeseen accidents such as a plane crash. In the improbable case of a reactor malfunction, it should prevent the leakage of radiation to the environment.[8] However, not all research reactors have this pressure vessel or containment structure. For example, the FiR 1 reactor in Finland is a TRIGA type reactor without such structures. Types of research reactors are discussed further in section 1.1.3.

For power reactors, there are additional important components relating to the production of electricity, such as turbines, generators, steam generators and cooling towers.

### 1.1.2 Power reactors versus research reactors

In a power reactor, the heat from the chain reaction described in section 1.1.1 is used to generate electricity by converting the heat to steam in steam turbines. In a research reactor, the neutrons produced are used for research, medical and industrial purposes.[9]

When comparing research and power reactors for the purpose of decommissioning, it is important to remember that since the main purpose of research reactors are to produce neutrons and not power, research reactors are simpler and have lower operating temperatures than power reactors. Research reactors often use highly enriched uranium fuel, although there are some exceptions. For example, a Finnish research reactor, the FiR 1

reactor, has low enriched (20%  $^{235}\text{U}$  enriched) fuel. Power reactors also use Low Enriched Uranium (LEU) fuel; however, the fuel required and fission product build up is far less for a research reactor. The spent fuel from a research reactor may be classed as intermediate-level waste.[10] However, the specific activity (discussed in section 2.3.3) is high and the research reactor fuel includes some of the same fission products as power reactor fuel.[11]

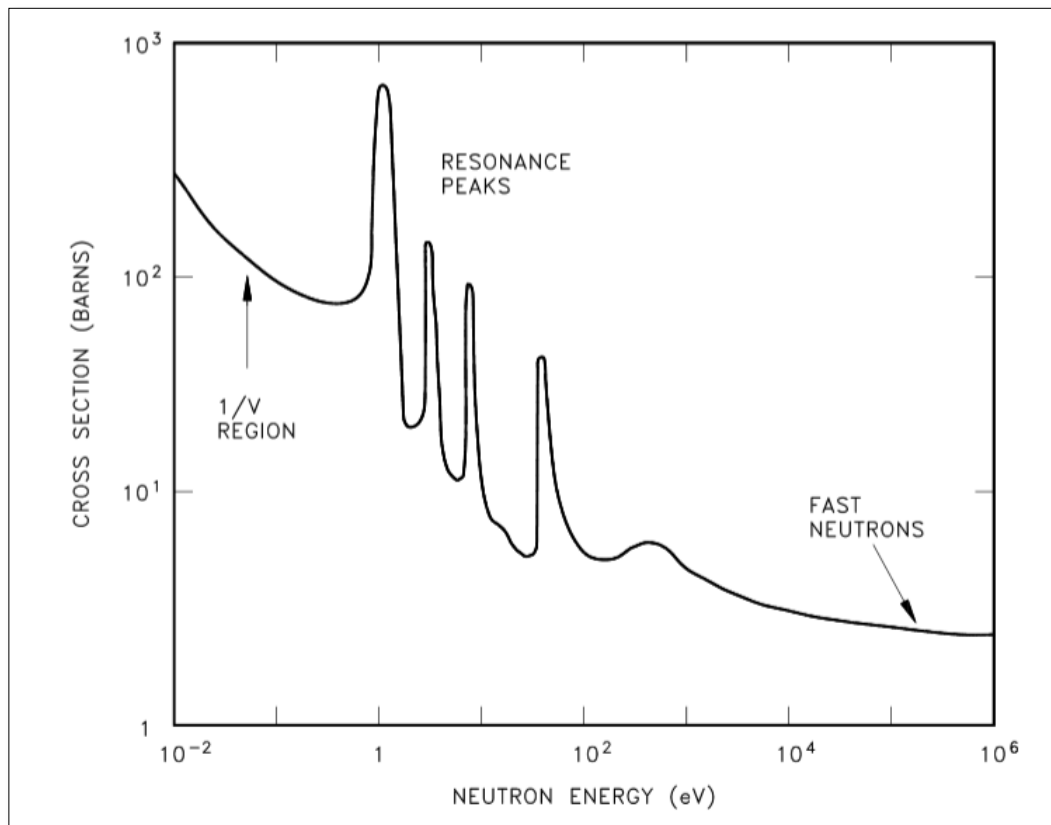


Figure 1.1 The dependence of cross section (barns) on neutron energy (eV) for nuclides of high mass numbers.[3]

### 1.1.3 Types of nuclear reactors

There are many types of reactors that differ according to fuel, moderator, and coolant. The six main types of reactors are summarised in table 1.1 in terms of their use in commercial NPP's.

The pressurised water reactor (PWR) is water moderated. The core could contain up to 250 fuel assemblies, with each fuel assembly consisting of 200-300 fuel rods. Water is kept under very high pressure (approximately 155 bar) to prevent water in the core from boiling. Water only boils in the secondary circuit for the purpose of steam generation which drives the turbine for electricity production. The boiling water reactor (BWR) differs from the PWR in that water boils in the core, and there is only one circuit. The core could contain as many as

750 fuel assemblies, with each fuel assembly consisting of about 100 fuel rods. The pressurised heavy water reactor (PHWR) uses heavy water as moderator because of the very low enriched uranium fuel. Fuel moves in pressure tubes through the calandria, which is a tank that contains the moderator. High pressure heavy water also acts as a coolant. Water boils in the secondary circuit for steam generation. The advanced gas-cooled reactor (AGR) is moderated by graphite and cooled by CO<sub>2</sub>. The CO<sub>2</sub> coolant runs from the core and passes parts of the steam generator tubes, but remains inside the pressure vessel. The light water graphite reactor (RBMK) is moderated by graphite and water-cooled. Water boils in the core as in BWR. However, excess steam does not slow fission and only reduces cooling, which is one of the problems with this design. FNRs are an expensive but important design. They make use of fast neutrons and no moderator. Power is generated from plutonium, which is also produced in a reaction with <sup>238</sup>U in the nuclear fuel.[13]

There are also different designs for research reactors. The TRIGA (Training, Research, Isotopes, General Atomics) reactor is discussed in section 1.3.1. There is the pool type reactor that is moderated and cooled by water. Typical reflector materials include beryllium or graphite. Similar to this design is the tank type reactor, with the main difference arising from the method of cooling. Other possible designs include research reactors moderated by heavy water, or even graphite. Fast reactors use a higher enriched fuel rather than a moderator.[9]

Table 1.1 NPPs in commercial operation.[12]

Reactor Type	Main Countries	Number	GWe	Fuel	Coolant	Moderator
Pressurised water reactor (PWR)	US, France, Japan, Russia, China	277	257	enriched UO <sub>2</sub>	water	water
Boiling water reactor (BWR)	US, Japan, Sweden	80	75	enriched UO <sub>2</sub>	water	water
Pressurised heavy water reactor (PHWR)	Canada, India	49	25	natural UO <sub>2</sub>	heavy water	heavy water
Gas-cooled reactor (AGR & Magnox)	UK	15	8	natural U (metal), enriched UO <sub>2</sub>	CO <sub>2</sub>	graphite
Light water graphite reactor (RBMK & EGP)	Russia	11 + 4	10.2	enriched UO <sub>2</sub>	water	graphite
Fast neutron reactor (FBR)	Russia	2	0.6	PuO <sub>2</sub> and UO <sub>2</sub>	liquid sodium	None
	TOTAL	438	376			



## 1.2 Decommissioning of Nuclear Reactors

Nuclear reactors are designed to have a specified life time, after which they are permanently shut down. Reasons for shutdown can be divided into three categories, the first of which is simply when the reactor reaches the end of its design life (~40 years). The limiting factor is usually material aging such as embrittlement of the pressure vessel. There is regular maintenance during annual outages, as it is possible to replace some aging components. However, there are some aging components that are much more difficult to replace. Extension of the lifetime can be approved by regulatory bodies, if it is possible to show that all the components still fulfil their safety function. Otherwise, the reactor is shut down. The second category includes those reactors that are closed following an accident, and the last category consists of those reactors that are closed early because of a political decision.[14] Permanent shutdown involves multiple stages, from the removal of highly radioactive nuclear spent fuel to the final clean-up of the site.[15]

Decommissioning, as defined by the Radiation and Nuclear Safety Authority of Finland (STUK), is the process by which a permanently closed nuclear facility is dismantled, such that no special measures are further required at the facility site because of residual radioactive materials.[16]

Decommissioning will form part of the life-cycle of every nuclear reactor in existence, and involves the collection, segregation, characterisation, treatment, storage and disposal of radioactive waste. During decommissioning, the aim is to minimise radioactive waste and maximise the recovery of valuable materials.[17]

### 1.2.1 Three approaches to decommissioning

There are three strategies [18] for decommissioning, the choice of which depends on:

- national policy;
- availability of waste routes;
- occupational, public and environmental safety;
- skills resources;
- cost considerations;
- technology requirements;
- structural deterioration; and
- interdependence with other on-site activities.

The first strategy is referred to as Immediate Dismantling. Any part of the facility, buildings or equipment that contain radioactive contaminants are removed or decontaminated to such a

level where regulatory control is no longer required. Dismantling occurs shortly after the operations at the facility have ceased.[19] This approach makes it possible for the same staff that has been working at the facility to form part of the decommissioning team, and to bring with them experience and familiarity with procedures of the reactor. This option may also be more cost effective.[20]

The second strategy is referred to as Safe Enclosure or Deferred Dismantling. There is no dismantling during this period but the facility must be left in a stable condition. This period of safe enclosure allows for the decay of radionuclides, which reduces radiation hazard, before dismantling and decontamination to such a level where regulatory control is no longer required.[19]

The final strategy to consider is Entombment. All radioactive components, structures and contaminants are entombed in a structurally sound substance such as concrete. The entire structure must then be monitored until the radionuclides have decayed to such a level where regulatory control is no longer required.[19] This method is most commonly applied in the case of major accidents, such as the Chernobyl disaster.

### 1.2.2 An international look at decommissioning

Decommissioning has taken place using various strategies all over the world. There are six reactors currently undergoing decommissioning in Russia, most of which had been shut down in the 1980s and are awaiting dismantling. In the United Kingdom, there are 29 reactors currently undergoing decommissioning. An extended period of safe storage has been chosen at the Berkeley NPP, following defueling and the draining, cleaning and filling of the cooling pool. Eventually the remaining structures will be dismantled and levelled. The Berkeley NPP is one of the first to begin the decommissioning procedure in the United Kingdom, and others are following similar procedures. Germany chose immediate dismantling for 11 of their 19 decommissioned reactors, but the strategy for the remaining eight is not yet known. Decommissioning of the Gundremmingen A reactor began in 1983 strategically at the parts of the facility with the lowest level of contamination, working towards the highest levels in 1990. This showed that safe, economic, and relatively fast decommissioning is possible. In contrast, France chose to partially dismantle 3 of their NPPs and deferred full dismantling for 50 years. However, this choice is explained by the fact that there are other reactors in operation on the same site which reduces monitoring costs.

Table 1.2 provides a general idea of the status of all nuclear facilities. These numbers vary slightly between sources because of technical differences in what is considered operational, and when precisely the construction phase begins.[21]

Table 1.2 Status of nuclear facilities.

	Commercial NPPs	Research reactors
Operating	442 [22]	253 [24]
Under construction	66 [22]	8 [24]
Retired (shutdown, undergoing decommissioning or decommissioned)	110 [23]	250 [23]

Square brackets indicate references.

### 1.3 VTT Technical Research Centre of Finland Ltd

VTT Technical Research Centre of Finland Ltd is a government, non-profit research organisation founded in 1942 that engages in applied technology research. VTT is planning the decommissioning of the FiR 1 TRIGA reactor. The reactor was built for Aalto University, formerly Helsinki Technical University, but its operating licence was transferred to VTT in 1972. Most recently, the main functions of the FiR 1 reactor included Boron Neutron Capture Therapy (BNCT) and industrial isotope production. The decision to decommission was made because it is no longer economically feasible to keep the reactor running, and nuclear medical technology or other reactor applications are not VTT's main businesses.

#### 1.3.1 The FiR 1 research reactor

There are currently five nuclear reactors in Finland: two units at Olkiluoto, two units at Loviisa, and Finland's first nuclear reactor, FiR 1 research reactor.[25] The Olkiluoto and Loviisa reactors are both light water reactors, Olkiluoto having boiling water reactors and Loviisa having pressurised water reactors (more specifically, VVER-440).

FiR 1 is a 250 kW TRIGA Mark II open pool reactor with graphite reflector, and it was in operation from 1962 until 2015. The reactor consists of a 6.4 m deep aluminium tank (figure 1.2), 2 m in diameter, with the reactor core (figure 1.3) and reflector assembly (figure 1.4) near the bottom. The core consists of 80 fuel elements, four boron carbide control rods, graphite elements and irradiation positions (figure 1.5).[26] The tank is surrounded by a concrete structure (figure 1.6), and filled with 4.9 m of demineralised water above the core for shielding purposes. There is a bitumen coating around the aluminium tank before the concrete because of the difference in thermal expansion coefficients of aluminium and concrete. There are four beam tubes that join the reflector assembly to the outer face of the

shield structure. The fuel is U (uranium) + ZrHx (zirconium hydride) with the enrichment level of uranium being 20 % U-235. In 1967, the power was increased from 100 kW to 250 kW. The beam tubes have not been in use since the late 1980s and were plugged in the year 1990.[27]



Figure 1.2 Aluminium tank, 6.4 m deep, 2 m in diameter.[27]

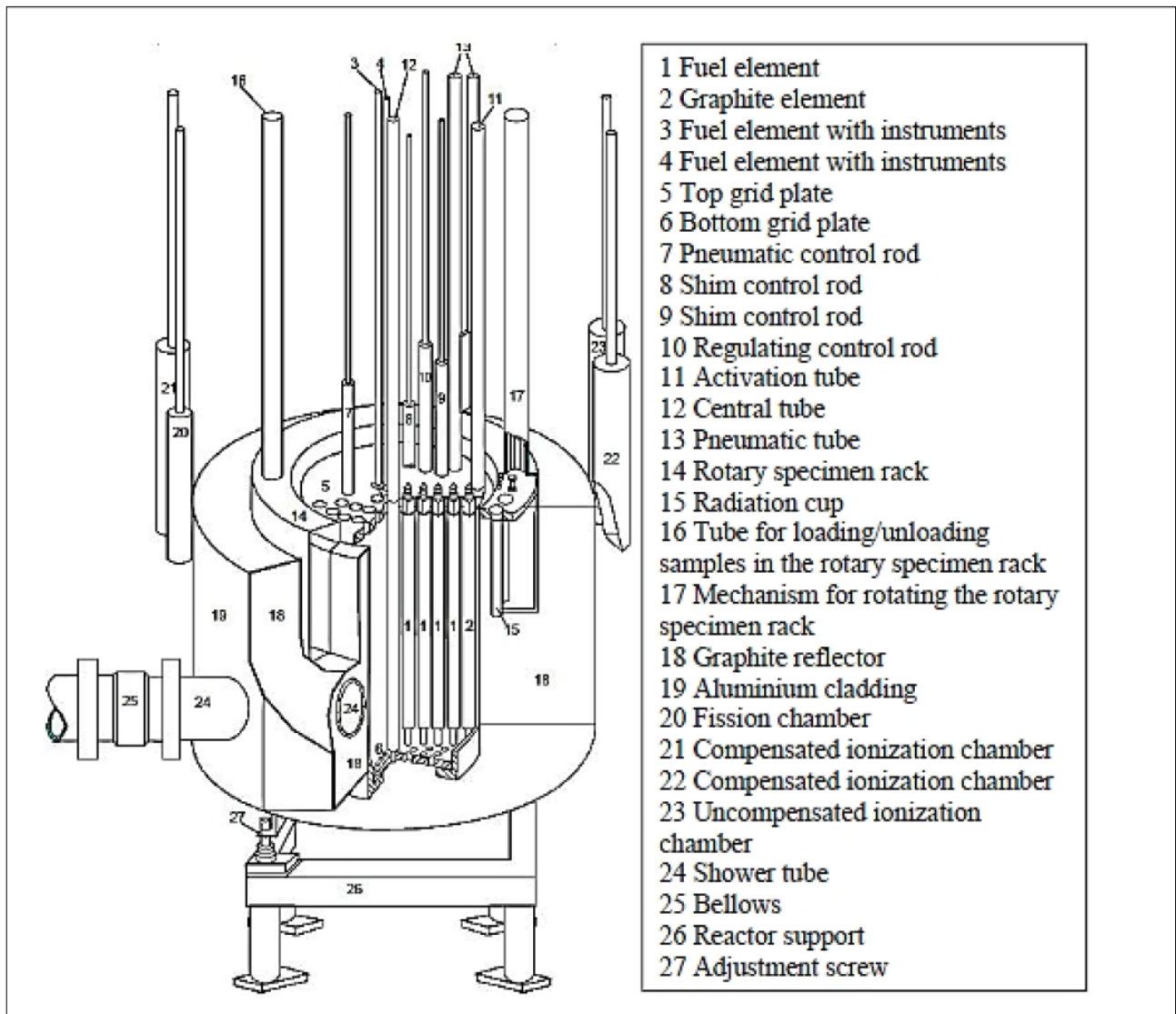


Figure 1.3 Labelled diagram of the FiR 1 reactor core.[27]

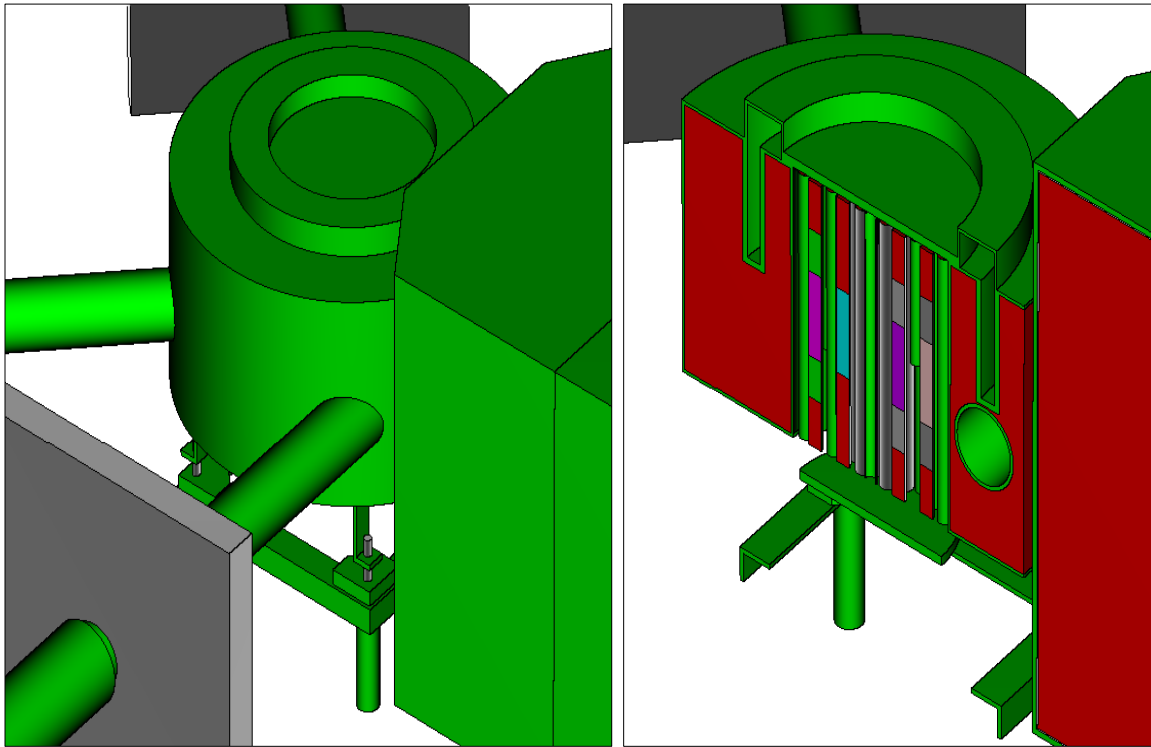


Figure 1.4 Core and reflector assembly as modelled in MCNP. A vertical cross section is shown on the right.[27]

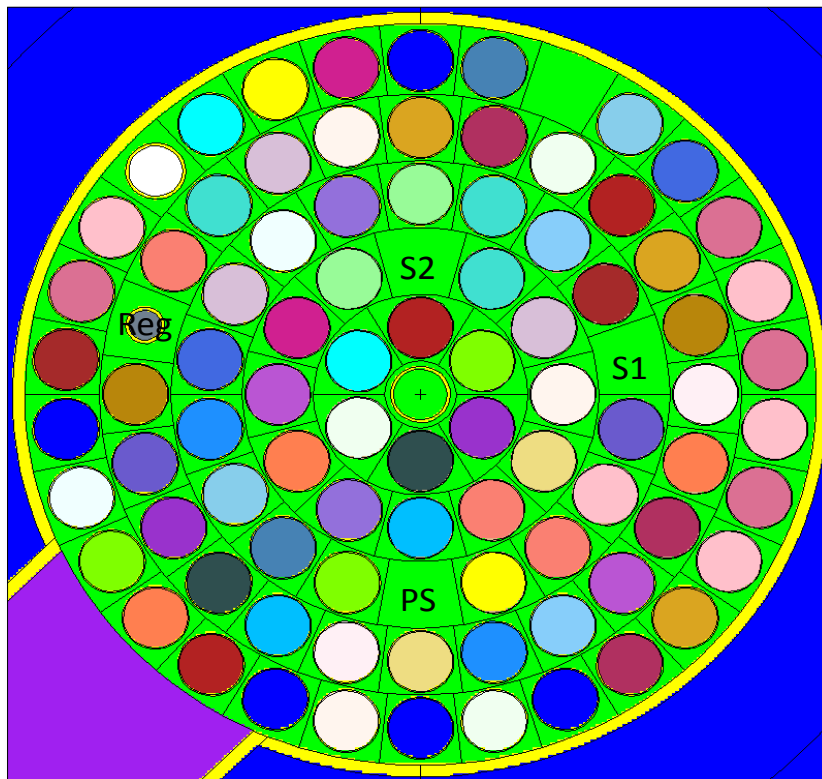


Figure 1.5 Reactor core consisting of 80 fuel elements, graphite elements, irradiation positions, and four control rods. The control rods are labelled S1, S2, Reg, and PS.[27]



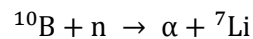


Figure 1.6 Steel tube elements filled with heavy concrete surrounding BNCT irradiation room.[27]

### 1.3.2 The FiR 1 BNCT facility

In 1993, work began to modify the reactor to include a Boron Neutron Capture Therapy (BNCT) facility (figure 1.7) for the treatment of malignant brain tumours, and later head and neck tumours where the best results were achieved.

In this treatment, stable  $^{10}\text{B}$  is administered to the patient intravenously before it targets tumour cells. The precise location of the tumour is irradiated through the following reaction with  $^{10}\text{B}$ :



Both particles are high energy transfer particles which destroy the cancer cells with high probability.[28]

To moderate, or slow, a neutron with the fewest elastic collisions, the atomic weight  $A$  of the target nucleus should be kept small. This is because the average energy loss of a neutron is proportional to the inverse square of the atomic weight  $A$  of the target nucleus,

$$\text{Energy loss} \cong \frac{2EA}{(A + 1)^2} \quad (1.1)$$

where  $E$  is the kinetic energy of the neutron.[29] Neutron interactions are discussed fully in section 2.5. The neutron capture rate of  $^{10}\text{B}$  in BNCT treatment is highest in the thermal energy range, but in this energy range the neutrons are not penetrating enough for the treatment. Using neutrons in the epithermal energy range allows them to penetrate tissue before they are thermalized to the optimal thermal energy range for capture. Thus, for the treatment, the neutron energy spectrum was shaped to the suitable epithermal energy range for BNCT using a moderating material developed and manufactured at VTT called Flualtal.[28] Flualtal is a composite of aluminium fluoride, aluminium and lithium fluoride (69 w-%  $\text{AlF}_3$ , 30 w-%  $\text{Al}$  and 1 w-%  $\text{LiF}$ ). Due to the higher density of Flualtal compared with other common neutron moderators, the same neutron attenuation can be achieved with a smaller thickness.[30] Figure 1.8 shows how the neutron fluence rate is shaped by a given thickness of Flualtal.

The thermal column (figure 1.9) was replaced by an epithermal BNCT moderator and beam (figure 1.10).[27] The irradiation room was built out of heavy concrete blocks.[32] Gamma shielding is provided by bismuth and lead, and lithiated polyethylene provides the neutron shielding. A lithium carbonate paraffin composition (lithium carbonate, polyethylene powder and paraffin wax) encapsulated in 1mm thick polyethylene terephthalate (PET) shells [33] lines the inside of the irradiation room to shield against neutrons.[27]



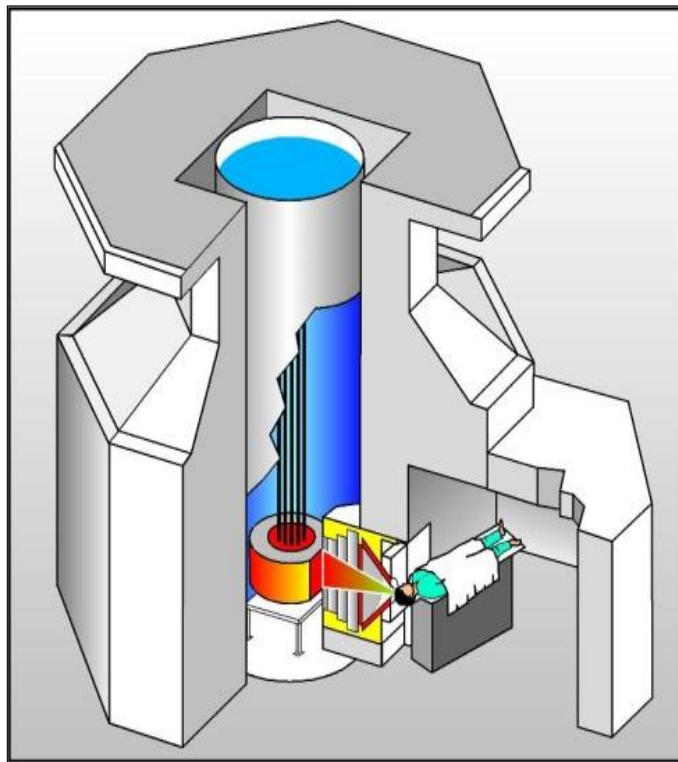


Figure 1.7 FiR 1 reactor with BNCT unit.[27]

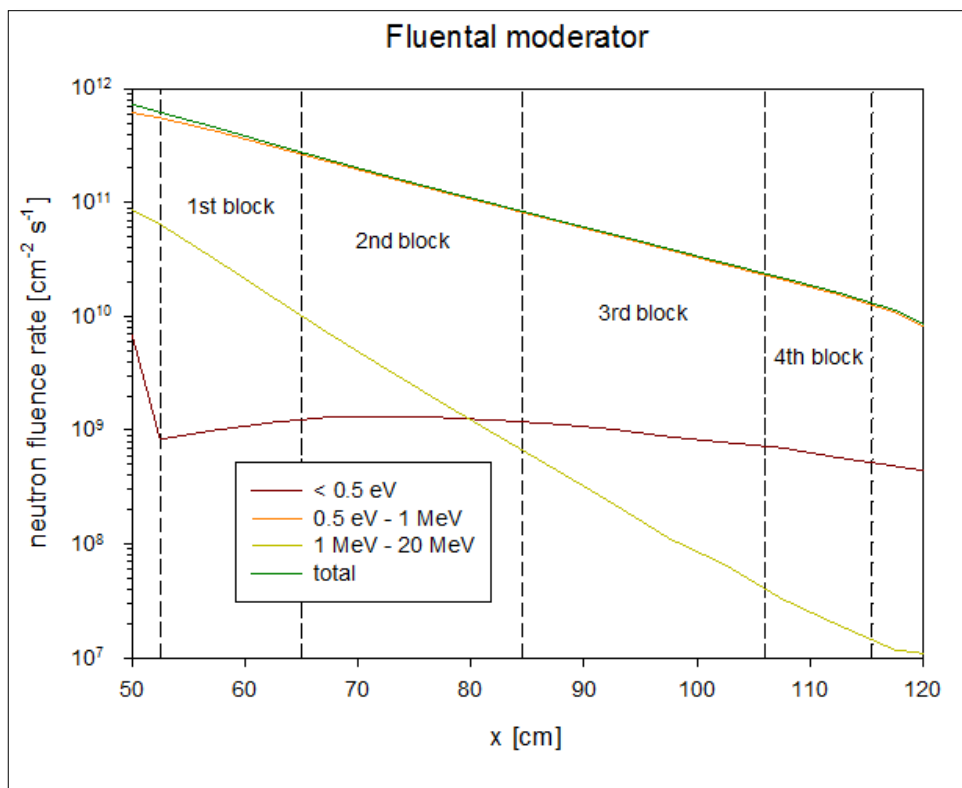


Figure 1.8 Neutron fluence rate [ $\text{cm}^{-2} \text{s}^{-1}$ ] as a function of Fluential thickness [cm].[31]  
Several different neutron energies are compared as indicated.

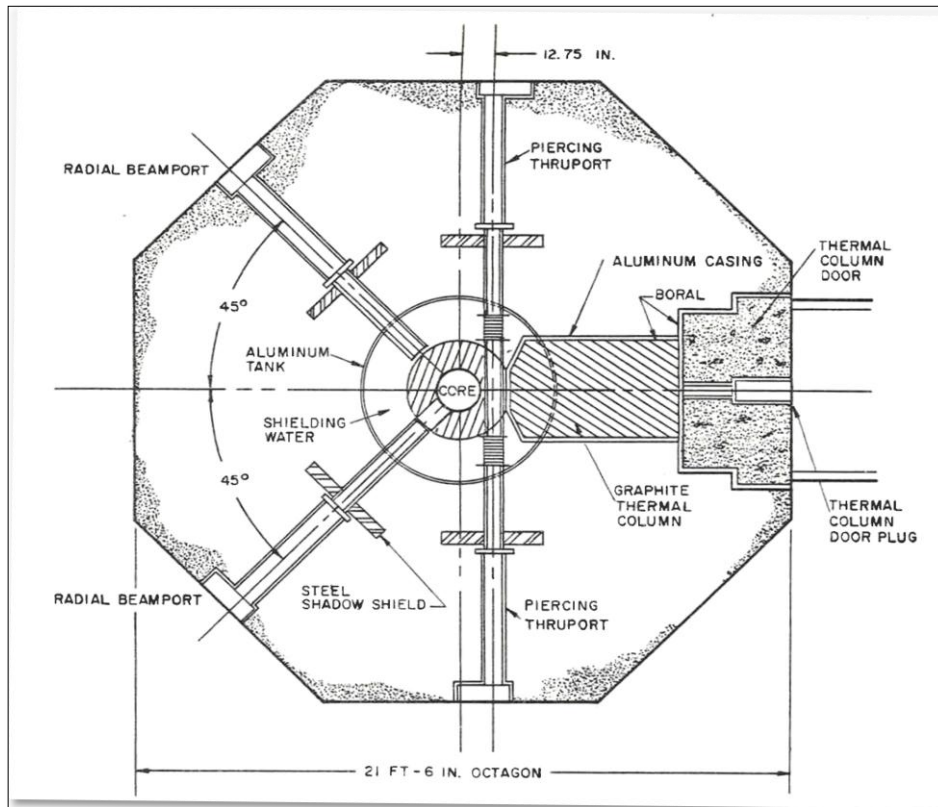


Figure 1.9a Original structure of the reactor. Horizontal cross section at core level showing the thermal column.[27]

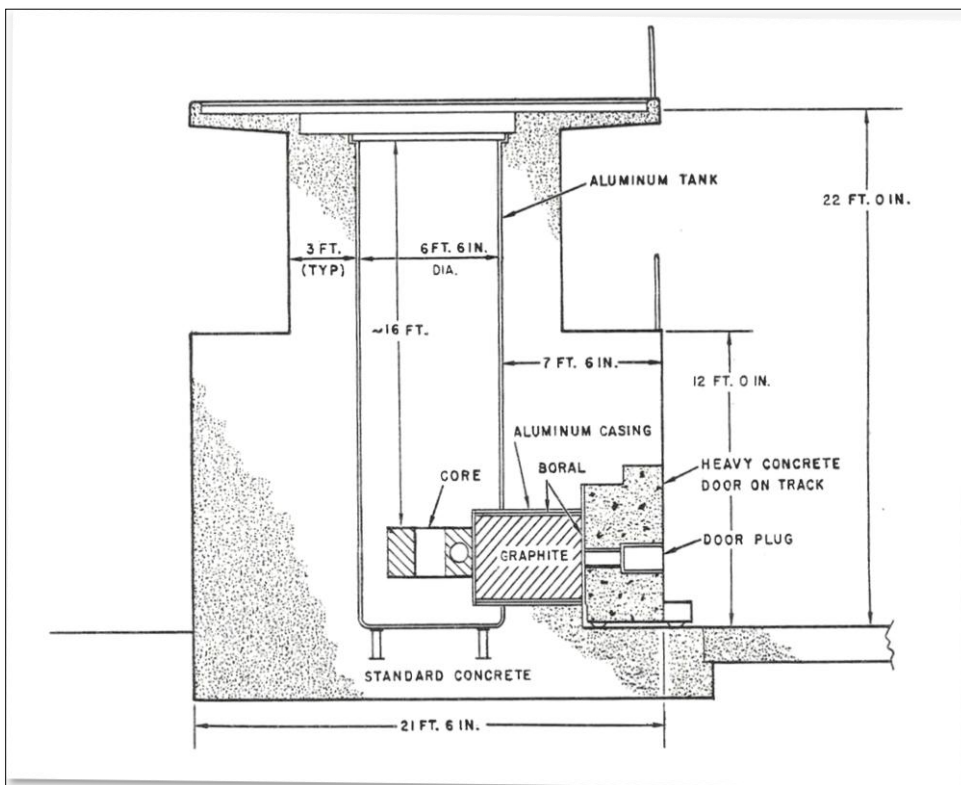


Figure 1.9b Original structure of the reactor. Vertical cross section at core level.[27]

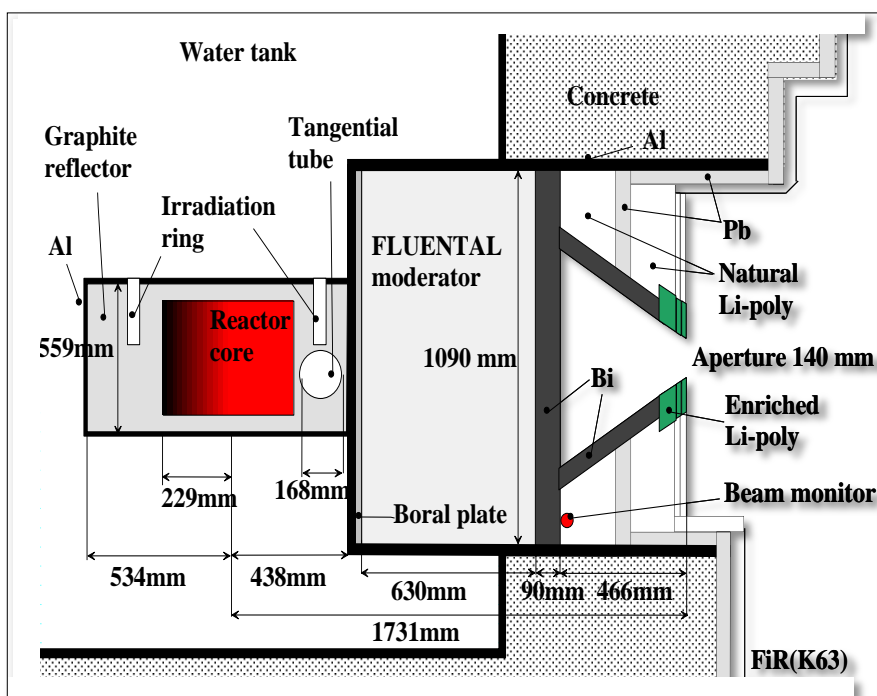


Figure 1.10 Detailed view of the BNCT structures.[27]

### 1.3.3 The decision to decommission

In the past, the reactor has been used for research in the national nuclear program, and in industry and health care. The reactor used to be operated daily in the 1970s and 1980s almost solely for the purpose of neutron activation analysis. It has also served the purpose of producing short lived isotopes.[34] Most recently, and since the completion of the treatment facility in 1997, BNCT formed the main reason for running the reactor. Over 200 patients were treated before the company running the treatments declared bankruptcy in 2012.[28]

The decision to decommission the reactor was made in July 2012, and the environmental impact assessment was completed in February 2015. The reactor was permanently shut down and the activity inventory report completed in June 2015.

In the decommissioning project, current work consists of verifying the results of the inventory report with physical measurements and planning of the storage facilities, dismantling methods, and safe transportation of radioactive waste and structures. There is also an application for a change of operational license underway. It involves updating documentation from operational procedures to decommissioning procedures. This licence is required before dismantling may begin. The dismantling of the reactor structures will start in 2018, following a period of safe enclosure.

#### 1.3.4 Final disposal in Finland

During the operation of a nuclear facility and following its decommissioning, radioactive waste materials are produced. Most of the radioactivity generated is in the fuel, and the rest comes from neutron activation products. There is typically also some surface contamination of the plant.[35] This waste will require final disposal according to its activity levels.

##### 1.3.4.1 Low- and Intermediate-Level Waste (LILW)

There are two NPPs in Finland, one in Olkiluoto, and one in Loviisa. These power companies have had disposal facilities for operational waste in use since 1992 and 1998, respectively. Expansion of these facilities will accommodate the low- and intermediate-level waste generated from the decommissioning of these plants. The final disposal procedures differ slightly at the Olkiluoto and Loviisa repositories. At Olkiluoto, the waste is disposed of at 60-95 meters in depth. A silo dedicated to low-level waste contains waste in concrete boxes. A silo dedicated to intermediate-level waste contains concrete boxes, in which liquid waste is mixed with bitumen. At Loviisa, the waste is disposed of at 110 meters depth. Steel drums in final disposal tunnels are used for low-level waste. A separate tunnel is allocated for the liquid intermediate-level waste, which is solidified in concrete containers.[36]

Before any waste is accepted by the repository, there are certain criteria that must be met. In addition to this, the average surface dose rate for bituminised waste should not exceed 0.8 Sv/h, with a maximum dose rate of 3 Sv/h. The average surface dose rate for other waste should not exceed 0.1 Sv/h. However, some waste need not enter the repositories at all, provided the activity is low enough. Metal scrap, for example, may be cleared provided the  $\gamma$  and  $\beta$  activities do not exceed 1 kBq/kg, and the  $\alpha$  activity does not exceed 100 Bq/kg. For surface contamination, the limits become 4 kBq/m<sup>2</sup> for  $\gamma$  and  $\beta$  activity, and 400 Bq/m<sup>2</sup> for  $\alpha$  activity.[37]

##### 1.3.4.2 High-Level Waste (HLW) in the form of Spent Nuclear Fuel (SNF)

At the end of 2012, Posiva applied for a construction license for an encapsulation and final disposal facility for SNF, and the application was approved in 2015. The encapsulation facility will be built above ground, and it will receive spent fuel that has been in storage for 30 to 50 years. The SNF will be dried and repackaged in final disposal canisters. The final disposal facility will be built underground at a depth of 450 meters, and be connected to the encapsulation facility.[38] This provides a second option for the disposal of the FiR 1 SNF, although the aim is to return the fuel to Idaho according to the United States Department of Energy Foreign Research Reactor Spent Nuclear Fuel Acceptance Programme (DOE FRR SNF AP).

#### 1.4 Thesis aims and outline

Figure 1.11 shows a flow diagram of the decommissioning procedure used by VTT, specifically in the case of the FiR 1 reactor. It is not, however, a general procedure required by Finnish law. While most of the steps are required, there are some additional steps (indicated in green) that are not required. The box outlined in red indicates where this thesis fits into the overall picture of decommissioning the FiR 1 reactor.

The thesis shall describe the work done with the aim to plan, execute and document the following endeavours:

- plan for representative samples to be taken from the reactor structures, including the aluminium tank, biological shield, the Fluental moderator and the ion-exchange resin from the cooling circuit.
- prepare the samples for radiometric analysis;
- $\gamma$  spectroscopy measurements of the taken samples;
- perform data analysis and determine the activity concentration in samples; and
- compare the activity concentrations in samples with inventory predictions, which were performed using Monte Carlo N-Particle Transport code (MCNP) [68] for 3D neutron flux calculations and ORIGEN-S [69] for point depletion and decay calculations.

In the following chapter, radiation regulatory authorities are discussed and a review is made of the regulatory guides set by these authorities related to the decommissioning of nuclear facilities. Beta and  $\gamma$  radiation, as well as neutron activation and analysis are discussed in detail. The activity prediction using MCNP and ORIGEN-S used in VTT's activity inventory report is, and the resulting predictions are shown for various reactor components. Experimental methods are covered in Chapter 3, including general information about detectors. The In Situ Object Counting System (ISOCS<sup>TM</sup>) is introduced, as well as the samples to be studied and their method of measurement. Chapter 4 details the use of Genie<sup>TM</sup> 2000 software, including modelling of measurements in the Geometry Composer, efficiency calibration, peak area determination, and nuclide identification and activity calculations. Results are presented and discussed in Chapter 5 before final conclusions are presented in Chapter 6.

# VTT's Decommissioning Procedure

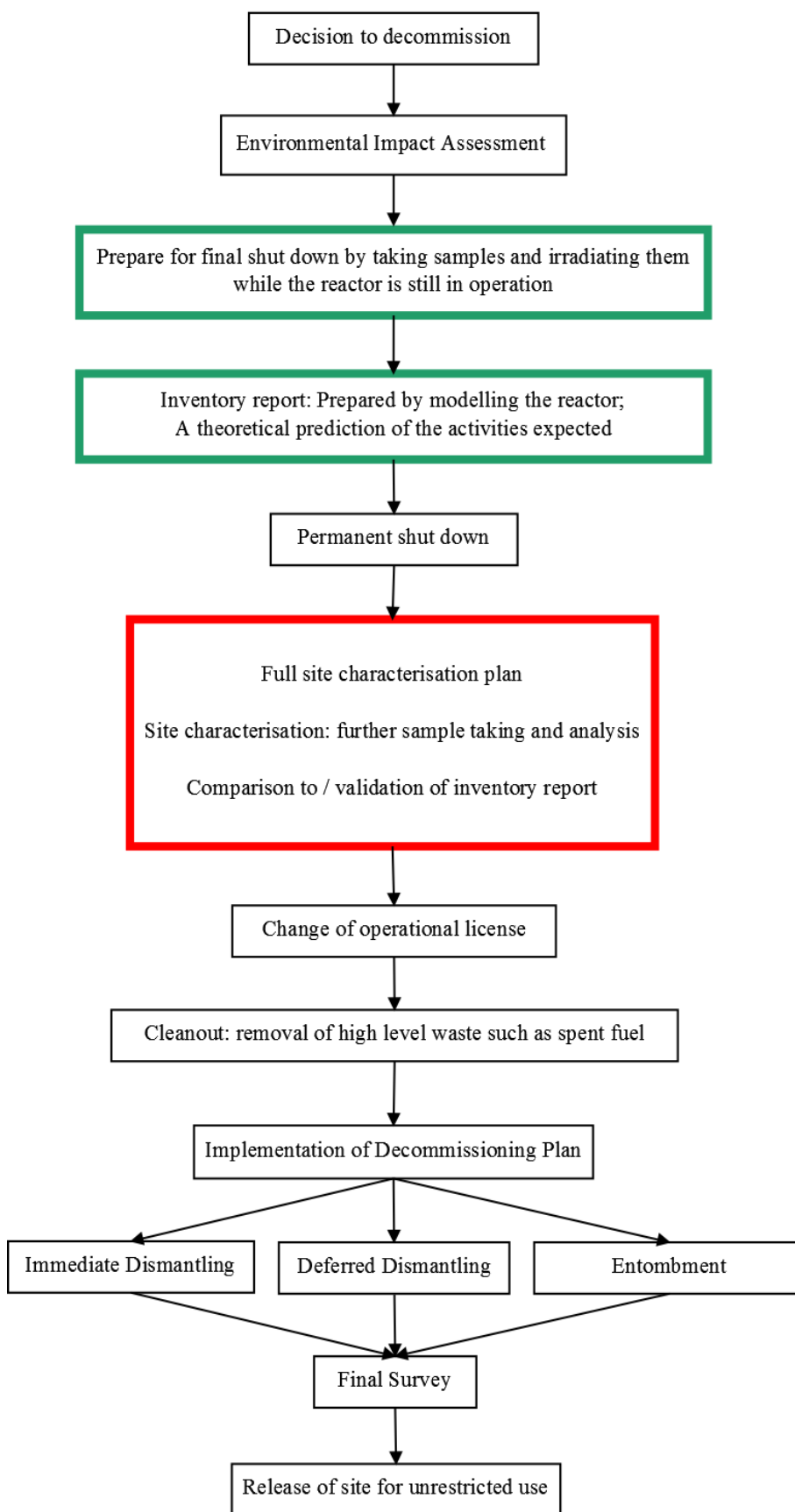


Figure 1.11 The decommissioning procedure used by VTT.[18]

## Chapter 2: Background and Theory

There are various kinds of ionising radiation that differ in penetrability, hazardousness, uses, and manner of interaction with matter (and consequently method of measurement). It is important to consider each class of ionising radiation and their differences in the process of decommissioning, as radioactive waste is generated during the operation of a nuclear facility. Regulatory authorities are in place to govern safe practices in all arenas of generating and disposing of radioactive waste.

### 2.1 Classes of ionising radiation

Types of ionising radiation include  $\alpha$  particles,  $\beta$  particles,  $\gamma$ -rays and X-rays, neutrons and cosmic radiation. According to the type of radiation, different shields are required (see figure 2.1). Alpha particles are positively charged, comprise two neutrons and two protons, and are the least penetrating. Beta particles are electrons or positrons, and are more penetrating. Next are  $\gamma$ -rays and X-rays, which differ according to whether they were produced in the nucleus or orbital shells of the atom, and are greatly penetrating. Lastly, there is neutron radiation which is the most penetrating.

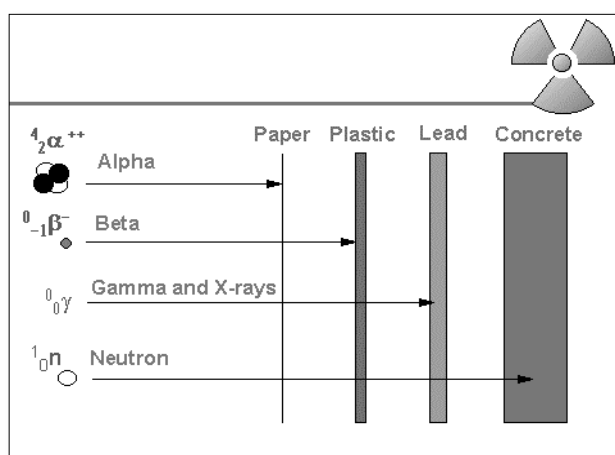


Figure 2.1 Relative penetrating distances of different particles.[39]

### 2.2 Limitations set by regulatory guides

#### 2.2.1 Regulatory authorities

International authorities such as the International Commission on Radiological Protection (ICRP), the International Atomic Energy Agency (IAEA), and the Nuclear Energy Agency (NEA) implement radiation safety through the formulation of regulations and recommendations for protection against radiation. They provide constraints for release levels and allowed doses to the public and radiation workers. Euratom plans safety standards, stress tests, directives and policies for use of nuclear power in the European Union. These include safety, security and safeguards issues relating to both fission and fusion reactors.[17]

The Radiation and Nuclear Safety Authority of Finland (STUK) provides strict regulatory guides (YVL guides) on nuclear safety in Finland.[35] When it comes to the decommissioning of the FiR 1 TRIGA Mark II research reactor, the waste management requirements set in YVL D.4 need to be fulfilled.

These guides are designed for all nuclear facilities, including both NPPs and research reactors. The guides may seem excessive in the case of research reactors because of the more stringent guides necessary for power reactors.[9]

### 2.2.2 Relevant STUK regulations regarding decommissioning

The relevant regulations are stated explicitly in Appendix A and summarised below.[35]

Essentially, the fact that the reactor will have to be decommissioned at the end of its life time should be kept in mind throughout the entire process of building and commissioning the reactor. The decommissioning process can be made easier if the facility is built with the necessary consideration for decommissioning. Factors such as the volume of waste that will require final disposal, the volume of waste produced during dismantling, the exposure of radiation workers during dismantling, and the environmental impact of decommissioning should all be considered. All these factors should be optimised.

Operational waste should be processed and stored in such a way that it does not lead to an average annual exposure exceeding 0.01 mSv (regulation 302). Any operational occurrence or Class 1 accident should not lead to an exposure exceeding 0.1 mSv or 1 mSv, respectively. This limit is increased to 5 mSv for Class 2 accidents (regulation 303). According to the YVL D.4 guide,[35] a Class 1 accident is an accident that is assumed to take place less than once in 100 years, but at least once in 1000 years. A Class 2 accident is assumed to take place less than once in 1000 years. This classification is per reactor unit. Nuclear waste resulting from the operation or dismantling of a nuclear facility may be considered cleared when it can be handled by members of the public without leading to an annual exposure exceeding 0.01 mSv (regulation 308). Buildings and sites related to a nuclear facility may be considered cleared when the use of the premises does not result in an annual dose exceeding 0.01 mSv, although this annual limit may be extended to 0.1 mSv if access to the premises is restricted. Even in the case of failed restrictions, it should be shown with high certainty that use of the premises should not result in an annual dose exceeding 1 mSv.

During operation, any information that will be relevant during decommissioning should be recorded. Such information may include the maintenance history of the reactor, or any spills.



Following permanent shutdown, a detailed inventory should be performed to characterise all activity and contamination on site. Following the completion of the decommissioning process, a final activity survey must be performed to ensure the site meets all clearance requirements. According to regulation 415,[35] buildings that will not be demolished can be considered cleared without restriction if the average surface activity contamination on all inside surfaces is less than 4000 Bq/m<sup>2</sup>, and no more than 10 000 Bq per any one metre squared.

Waste clearance levels according to nuclide groups are listed in table 2.1. Each nuclear facility is limited to 100 tonnes per year. The activity concentration limits should not be exceeded for waste averaged over at most 500 kg, while the surface activity contamination should not be exceeded for waste averaged over an area of at most 0.1 m<sup>2</sup>.

Alpha particles, although able to carry a large amount of energy, can easily be stopped with very little shielding. The amount of shielding required to stop  $\beta$  particles depends on the half-lives, as well as the amount of energy the particle is carrying, but it exceeds the amount of shielding required to stop  $\alpha$  particles. Gamma rays are the most penetrating of the three classes of radiation. The clearance levels for strong  $\gamma$  and  $\beta$  emitters are less than those for weak  $\gamma$  and  $\beta$  emitters and this is related to biological hazardousness.[35]

Pure  $\beta$  emitters such as  $^3\text{H}$  and  $^{14}\text{C}$  are difficult to measure, but relevant from a dismantling and final disposal perspective, as discussed in more detail in section 2.4.2, 2.4.3 and 2.5.4. For  $^3\text{H}$ , the clearance level activity concentration is 100 Bq/g, and for  $^{14}\text{C}$ , it is 1 Bq/g.

Table 2.1 Waste clearance levels set by STUK according to nuclide group.[35]

Nuclide group	Activity concentration Bq/g	Surface activity contamination Bq/cm <sup>2</sup>
$\alpha$ emitters	0.1	0.4
Strong $\gamma$ and $\beta$ emitters	1	4
Weak $\gamma$ and $\beta$ emitters	10	40

## 2.3 Gamma radiation

### 2.3.1 Gamma ray interaction with matter

Gamma rays interact with matter through a complete or partial transfer of their energy to the electrons of the atoms constituting the material. Many important interactions exist, although the three most important mechanisms are discussed.[40]

The photoelectric effect:

In this interaction, a photon is completely absorbed by an atom. The resulting energy transfer causes a photoelectron to be ejected. A portion of the energy from the  $\gamma$ -ray photon equal to the binding energy is transferred to the orbital electron, releasing it. The remainder is shared between the photoelectron and the recoil atom, but the energy of the recoil atom is comparatively negligible.[40]

When the photoelectron is released, it leaves behind a bound shell vacancy that is filled by the cascading of electrons that may result in characteristic X-ray emission or Auger electrons. The characteristic X-rays can also undergo photoelectric absorption. The photoelectric effect dominates at relatively low  $\gamma$ - and X-ray energies,  $E$ , or in absorber atoms with high  $Z$ . The probability of the photoelectric effect across all values of  $E$  and  $Z$  is roughly proportional to  $Z^n/E_\gamma^{3.5}$ , where  $n$  fluctuates between four and five depending on the energy region. This strong  $Z$  dependence explains why high  $Z$  materials are chosen for  $\gamma$  shields.[41]

Compton scattering:

A  $\gamma$ -ray photon strikes an electron, and the  $\gamma$ -ray is scattered by the electron through some angle  $\theta$ . This angle is measured relative to the original direction of the  $\gamma$ -ray photon. The electron receives a portion of the energy from the  $\gamma$ -ray photon, and recoils by some angle  $\phi$ . The portion of the energy received by the scattered photon,  $E'$ [MeV], varies greatly, and depends on the scattering angle  $\theta$ :

$$E' = \frac{E}{1 + \frac{E}{0.511}(1 - \cos \theta)} \quad (2.1)$$

where  $E$  [MeV] is the energy of the incident  $\gamma$ -ray photon, and 0.511 comes from the electron rest mass energy in  $\text{MeV}/c^2$ . This equation arises due to energy and momentum conservation laws. Substituting  $\theta = 0$  and  $\theta = \pi$  gives the maximum and minimum energy of the scattered photon, respectively. All angles in between are possible, and the scattered photon energy decreases with an increase in scattering angle. Since the energy received by the recoil electron is just the difference in energy between the incident and scattered

photon, the recoil electron can receive a full range of energies.[41] The probability of a Compton scattering event occurring is linearly proportional to  $Z$ , because there are more electrons to scatter from as  $Z$  increases.

Pair production:

This process only occurs if an incident  $\gamma$ -ray photon has energy greater than 1.022 MeV, i.e. twice the rest mass energy of an electron-positron pair, and it occurs in the Coulomb field of the nuclei of the absorbing material. The incident  $\gamma$ -ray photon is absorbed and an electron-positron pair is formed.

The excess photon energy is that which is left over after the 1.022 MeV has been subtracted from the incident energy, and is shared between the positron and electron as kinetic energy. The positron slows, comes to rest, and combines with an electron to form two annihilation photons (0.511 MeV) which are emitted in opposite directions in order to conserve momentum (see figure 2.2). However, the electron-positron pair can annihilate in more than two photons, even though this is the largest decay branch.[42]

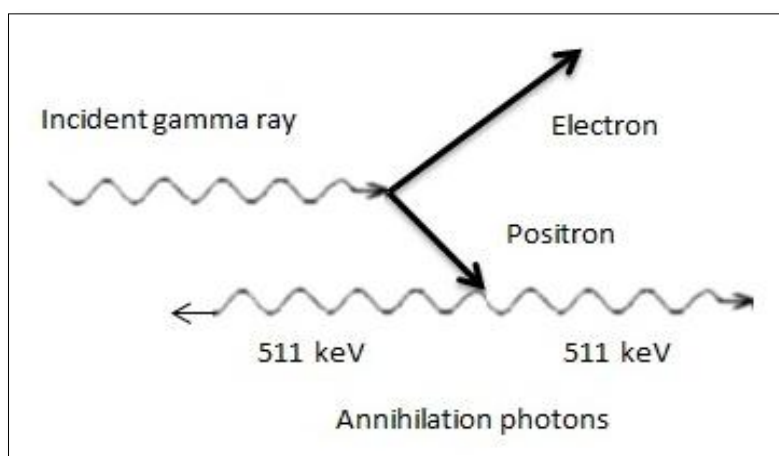


Figure 2.2 Pair production.[42]

Figure 2.3 shows how the three processes dominate at different photon energies for different absorbing materials. The two lines in the figure represent border line energies at which two adjacent processes are equally probable. Pair production dominates at high  $\gamma$  energies.

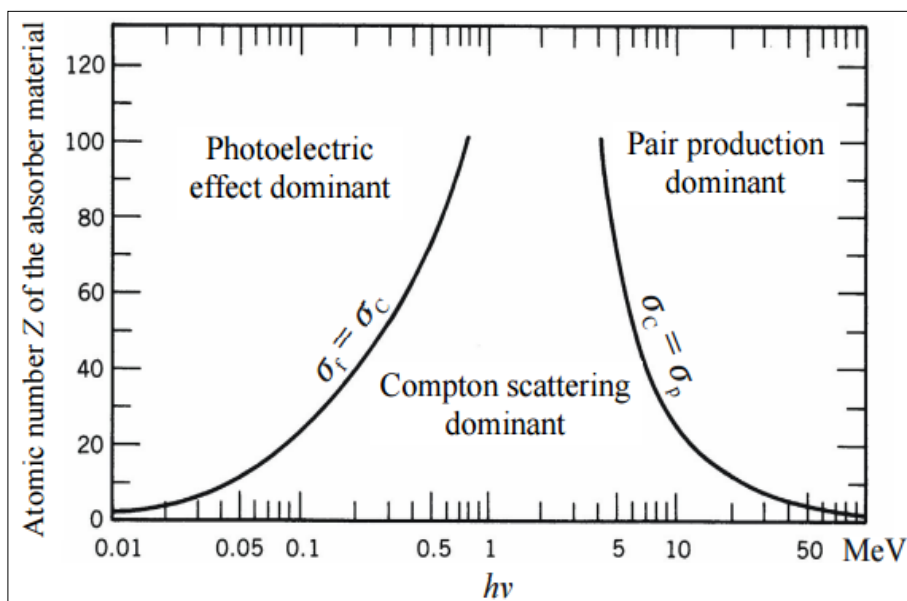


Figure 2.3 The energies at which the photoelectric effect, Compton scattering and pair production dominate.[41]

### 2.3.2 Gamma attenuation

By definition,  $\gamma$  attenuation is the fraction of  $\gamma$ -rays that pass through an absorber without interaction. Gamma rays either interact with the absorbing medium or they do not. Higher rates of attenuation are associated with more probable interaction with the absorbing medium.[43]

If a monoenergetic narrow  $\gamma$  beam is fired through an absorber, the beam should be exponentially attenuated because every time a  $\gamma$ -ray photon interacts with the absorbing medium it is removed from the beam. These interactions each have an associated probability per unit path length that can be summed to find the total probability of interaction per unit path length:

$$\mu = \tau + \sigma + \kappa \quad (2.2)$$

where  $\mu$  is the linear attenuation coefficient,  $\tau$  is the probability of the photoelectric effect occurring per unit path length,  $\sigma$  is the probability of Compton scattering per unit path length, and  $\kappa$  is the probability of pair production per unit path length. If  $I_0$  is the number of transmitted photons without an absorber present, and  $I$  is the number of transmitted photons with an absorber present, then the attenuation of the beam is equal to:

$$\frac{I}{I_0} = e^{-\mu t}. \quad (2.3)$$

The linear attenuation coefficient is dependent on the absorber density, despite the fact that the absorbing material has not changed. The mass attenuation coefficient takes the absorber density into account by dividing the linear attenuation coefficient by the absorber density. The absorber mass thickness,  $\rho t$ , is introduced to bring the mass attenuation coefficient into the attenuation equation:[41]

$$\frac{I}{I_0} = e^{-\left(\frac{\mu}{\rho}\right)\rho t}. \quad (2.4)$$

These coefficient values can be found tabulated from databases for different elements or compounds and mixtures.[44]

### 2.3.3 Radioactivity and radioactive decay

Activity is the measure of a source disintegration rate. The fundamental law of radioactive decay is given:

$$\frac{dN}{dt} = -\lambda N. \quad (2.5)$$

In this equation,  $\lambda$  is a decay constant which can also be said to be the probability of a decay per unit time, or a decay rate.  $N$  is the number of not yet decayed nuclei. The product of these terms, the activity, has a unit of disintegrations per second. The Becquerel, equal to one disintegration per second, is the SI unit for activity. The specific activity is the activity per unit mass. The solution to equation 2.5 is

$$N(t) = N_0 e^{-\lambda t} \quad (2.6)$$

where  $N_0$  is the initial number of nuclei.

Since

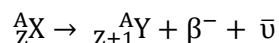
$$A = \lambda N, \quad (2.7)$$

the activity at a given time per second is given by the equation:

$$A(t) = A_0 e^{-\lambda t} \quad (2.8)$$

The half-life,  $t_{1/2}$  is the amount of time it takes for the activity to reduce to one half of its initial value and can be found from equation 2.6 or 2.8 to be  $t_{1/2} = \frac{\ln 2}{\lambda}$ . It is characteristic to the nuclide.

There are a number of modes through which a radioactive nucleus can decay. The reaction for  $\beta^-$  decay is given by:



where  $A$  is the mass number,  $Z$  is the atomic number,  $X$  is the initial nucleus,  $Y$  is the recoil nucleus and  $\bar{\nu}$  is the antineutrino. The  $\beta^-$  particle produced is the only considerably ionising particle in this reaction. The amount of energy released by a reaction is called the  $Q$ -value, and is shown for this reaction schematically in figure 2.4. It is the difference in energy between the initial and final states. The energy of each of the particles produced in the reaction ( ${}^A_{Z+1} Y$ ,  $\beta^-$ , and  $\bar{\nu}$ ) adds up to the  $Q$ -value. Thus the  $\beta$  particle can be emitted with any energy ranging from 0 to the  $Q$ -value, as there is an infinite number of energy sharing solutions in 3-body kinematics.[41] See figure 2.5.

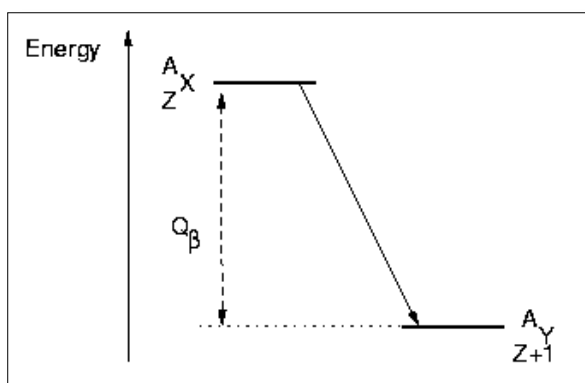


Figure 2.4 The  $Q$ -value for a general  $\beta^-$  reaction.[45]

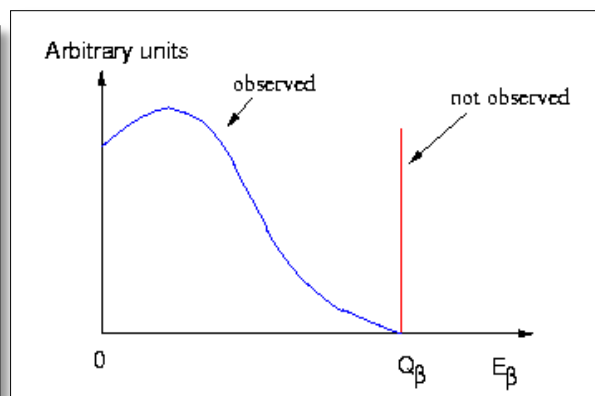
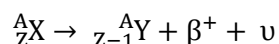
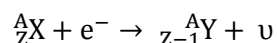


Figure 2.5 Range of energies exhibited by the  $\beta$  particle following  $\beta^-$  decay.[45]

Similarly for  $\beta^+$  decay, with reaction:



In competition with  $\beta^+$  decay, also electron capture is possible:

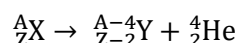


In electron capture, the nucleus absorbs an inner atomic electron from an electron shell, reducing the atomic number of the element by 1. As with  $\beta^+$  decay, a neutrino is emitted. This process occurs far less often than  $\beta^+$  decay because of the large difference in radii of the nucleus and electron shells. However, it dominates at lower  $Q$ -value energies, for example when the energy difference between the parent and daughter atom is less than 1.022 MeV.[46]

Certain nuclear processes, such as  $\beta$  decay, can produce excited nuclei that will then de-excite, often through the emission of  $\gamma$ -rays. An alternative process to  $\gamma$  emission is internal conversion. During internal conversion, an orbital electron of the excited atom directly receives the nuclear excitation energy, and is emitted with an energy equal to that excitation energy minus the energy binding the electron to the atom. The probability of this process occurring at energies greater than 100 keV is very low.

During internal conversion, an electron is emitted with energy that comes from the excited nucleus. Certain nuclear processes can produce an atom with a missing inner shell electron. When an outer shell electron fills the vacancy, this electron transition can be accompanied by a characteristic X-ray. An Auger electron may be emitted if the energy released during the electron emission is enough to eject an outer shell electron.[41]

The reaction for  $\alpha$  decay is given by:



where A is the mass number, Z is the atomic number, X is the initial nucleus, and Y is the recoil nucleus. The Q-value again represents the difference in energy between the initial and final states. The energy of the recoil nucleus and  $\alpha$  particle add up to the Q-value, but the energy of the  $\alpha$  particle is always:

$$E_\alpha \cong \frac{Q(A-4)}{A}. \quad (2.9)$$

Spontaneous fission is another possible nuclear decay process. During fission, a nucleus is promoted to an excited state through the absorption of energy which deforms the nucleus to the transition state configuration. The deformation increases the proton separation, thus decreasing the nuclear Coulomb energy. The deformation also increases the nuclear surface area, increasing the nuclear surface energy. In this transition state configuration, the Coulomb energy and the nuclear surface energy change at the same rate. If the nucleus deforms further after the transition state configuration, fission will occur and the nucleus breaks into two deformed, charged fragments. The point at which the nucleus breaks is called the scission point. Coulomb repulsion sends the two fragments flying apart, allowing them to achieve a more spherical shape. This loss of deformation involves a conversion from potential energy to excitation energy, which is lost through the fragments emitting neutrons and  $\gamma$ -rays once they have reached their full acceleration. There is also some emission of  $\beta$  particles, but this does not occur as promptly as the neutron emission. These  $\beta$  particles can excite a daughter resulting in further, “delayed” neutron emission. Most of the energy in fission goes to the kinetic energy of the fission fragments.[47]

### 2.3.4 Gamma ray measurement techniques

Gamma ray photons interact strongly with matter and these interactions allow their detection. They have a high penetrating ability and are very difficult to stop, making it an important type of radiation. The  $\gamma$ -rays ionise atoms, liberating electrons along their path, thereby transferring energy to the electron. The maximum energy that can be received by the electron is the energy with which the photon is incident. Each of the liberated electrons causes further ionisations. The fast electrons that are produced in these interactions transfer information to the detector about the  $\gamma$ -ray photons. In a proportional counter or semiconductor detector, the charges caused by ionisations are collected directly, while a scintillator detector collects these charges through indirect methods. Light is first produced that strikes a cathode, releasing electrons that are multiplied before being collected. In this way, the presence of the  $\gamma$ -ray is determined, and its energy measured.[48]

In  $\gamma$ -ray spectrometry, the detector is required to provide a good probability of interaction between the  $\gamma$ -ray photons and the detection medium, so that fast electrons are produced. It is also required to be able to detect the fast electrons produced. There should also not be significant escape of the fast electrons. The dimensions of the absorbing medium should match the range of the fast electrons so that they are completely stopped in the detector. Gas-filled detectors generally have a poor efficiency for  $\gamma$  detection, unless it is under very high pressure or the energy of the incident photon is very low.

The resolution of the detector is a measure of how well the detector is able to distinguish between two close lying energy peaks. High resolution corresponds to a small Full Width at Half Maximum (FWHM) (figure 2.6) and is necessary when the spectrum is complex. A large FWHM reflects a large fluctuation in the energy recorded for each event, even though the same energy was deposited each time.[41] The achievable resolution depends on statistical variations that come with the formation of the total charge that the detector measures. The resolution improves as the number of charge carriers increases. High resolution is typically achievable with Ge semiconductor detectors because of the large number of charge carriers produced per unit of energy lost by the incident radiation. It also only takes  $\leq 1$  eV to promote an electron to the conduction band, whereas scintillation detectors require  $\sim 30$  eV to produce a scintillation photon. There are also other factors affecting the resolution, such as electronic noise and pulse-pileup.[41,48]

Another detector commonly used is a scintillator detector as they can be inexpensive and they have good efficiency, but resolution is low.[48] High- and low-resolution  $\gamma$  spectroscopy involve producing energy spectra of  $\gamma$ -rays present in a radioactive sample. Following this, information about the sample can be deduced, such as the type and amount of each nuclide



present.[17] Depending on the requirements of the work,  $\gamma$ -rays can be detected with varying degrees of efficiency and quality of resolution by gas-filled detectors, scintillation detectors and solid-state detectors.

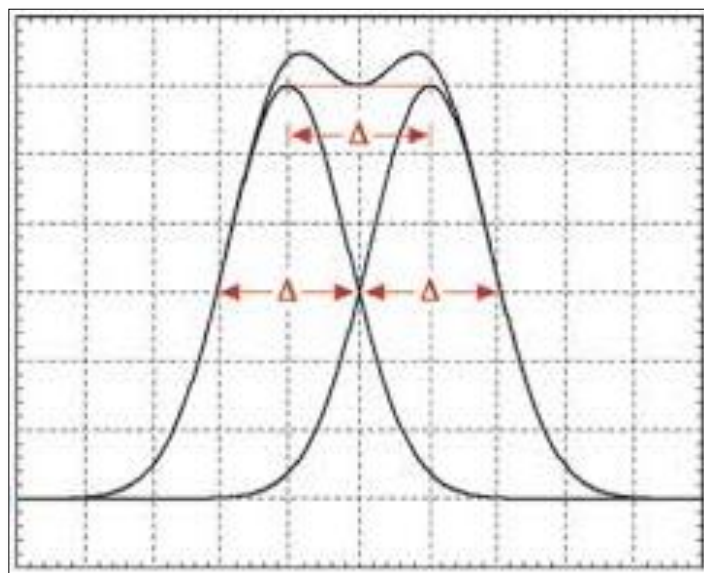


Figure 2.6 The energy resolution, expressed as FWHM (which has units of eV/keV/MeV) as a function of energy.[49]  $\Delta$  represents the FWHM and is a measure of the peak separation.

## 2.4 Beta particles

### 2.4.1 Charged particle interaction with matter

In general, the transport of charged particles is described with the Boltzmann-Fokker-Planck equation. The so called continuous slowing down approximation (CSDA) is done and the equation is reduced to the Boltzmann equation with an additional CSDA term. Electrons and positrons are particles with mass and a specific range in material. Due to their charge, they interact via the Coulomb force. The Monte Carlo method is discussed in detail in section 2.6.1. Charged particles continuously interact with the Coulomb force, so there is an infinite number of small interactions that would need to be simulated in the Monte Carlo method. Instead, the CSDA is also made, and in a way, these small interactions are grouped together to a finite set of energy losses with associated scattering angles.[50]

## 2.4.2 General $\beta$ measurement techniques

Beta particles are charged particles and thus lose energy through interactions with other charged particles in the absorbing medium. They are stopped more easily by matter than  $\gamma$ -rays because of their charge. Beta particles are detected by gas-filled detectors and scintillator based detectors. Samples containing pure  $\beta$  emitters often need to be prepared for analysis by chemical separation, after which time a measurement can be made using proportional counters or by X-ray spectrometry. However, depending on how much the continuous energy spectra of different  $\beta$  emitting radionuclides overlap, it is sometimes possible to separate the overlapping spectra of different radionuclides in the analysis afterwards. For the use of a proportional counter, a  $\beta$  emitter energy greater than 150 keV is required. Low background is possible with proper shielding. Where liquid samples are used, liquid scintillation counting can be performed, and this means a few  $\beta$  emitters may be present due to the high sensitivity of the technique.[17] For liquid scintillation, the threshold energy required for the  $\beta$  particle to be detected is very low (below 1 keV). This is because the  $\beta$  particle should have enough energy to produce a minimum of two photons that will strike each of the two photomultiplier tubes in coincidence.[51]

Beta particle detectors usually have a reduced sensitivity to the lower energy  $\beta$  particles because of the detector threshold to avoid system electronic noise. Beta backscattering is also a prominent effect for surfaces with high atomic number and incident angles close to  $90^\circ$ , which can induce a false high reading. The large range of  $\beta$  energies encountered induces different efficiencies and requires an accurate efficiency calibration.[17]

Various methods are detailed in literature for  $\beta$  counting. Hoepfener-Kramer [52] measured  $\beta$  activity for clearance measurements of nuclear facility decommissioning materials by using a gas-flow proportional counter. There is also an IAEA publication [17] that describes direct measurement in the form of thin walled Geiger detectors and thin plastic scintillators, but low efficiency and fragility of the detector make this method unpractical.

One of the most important  $\beta$  measurement techniques found in literature is the scaling factor method. The scaling factor method is based on the inference of the  $\beta$  activity through its relation to an associated easy-to-measure  $\gamma$  transition, or daughter product  $\gamma$  emission.[17] This is because of the constant ratio of activity concentrations that exists between the difficult-to-measure nuclide and the key nuclide.[53] The relationship is given by the following equation:

$$A_d = SF_{d,e}A_e \quad (2.10)$$

where  $A_d$  is the activity of the difficult-to-measure radionuclide  $d$ ,  $A_e$  is the activity of the easy-to-measure radionuclide  $e$ , and  $SF_{d,e}$  is the scaling factor.[54]

The scaling factor is obtained from sampling or a modelling calculation code. This ratio can be dependent on the similarity of the two nuclides' production mechanisms or transport behaviours. However, if a constant ratio is found to exist between two nuclides that do not exhibit the above mentioned similarities, the scaling factor method is still applicable.[55]

The scaling factors should be determined from facility to facility. For activated metals,  $^{60}\text{Co}$  is a typical key nuclide due to its ease of measurability and relatively long half-life. For the same reasons,  $^{137}\text{Cs}$  is often used for fission products and actinides. Sometimes, where chemical separation of  $^{144}\text{Ce}$  is possible,  $^{144}\text{Ce}$  is also used to measure actinides because of the chemical similarity between them.[56]

#### 2.4.3 Tritium measurement techniques

The rate at which  $^3\text{H}$  is released during disassembly of equipment depends on the  $^3\text{H}$  trapped in the materials. The amount of  $^3\text{H}$  trapped in a metal depends on temperature, gas pressure, exposure time, type of metal, chemical form of the  $^3\text{H}$ , as well as other factors that are discussed by Perevezentsev.[57] Even at room temperature,  $^3\text{H}$  permeates deep into metals. Tritium measurements are made difficult by the fact that when  $^3\text{H}$  decays, it emits very low energy  $\beta$  particles (average energy 5.6 keV) that can easily be absorbed by materials. Perevezentsev showed that even under controlled conditions, different methods for  $^3\text{H}$  concentration determination can give greatly varying results, perhaps due to the non-uniform  $^3\text{H}$  distribution present on the surface of the metals.

If  $^3\text{H}$  is to be measured according to its  $\beta$  emission, only  $\beta$  particles within a surface layer of approximately 1  $\mu\text{m}$  can be detected in organic materials and 0.1  $\mu\text{m}$  for metals.[58] This means most of the  $^3\text{H}$  will go undetected in the layer beyond the first 1  $\mu\text{m}$ .

Hoeppener-Kramer [52] measured  $^3\text{H}$  for clearance measurements of nuclear facility decommissioning materials by counting the  $\beta$  activity of the  $^3\text{H}$  through liquid scintillation. The liquid scintillation spectrometer is well suited for  $^3\text{H}$  measurements as the sample can be mixed into the scintillation liquid.[17]

Perevezentsev [57] describes 5 methods to attempt to achieve  $^3\text{H}$  depth profiles in different metals under various conditions. One method involved detecting the emitted  $\beta$  particles by radiography methods such as high sensitivity photo film or magnetic microscope. Another method involved measuring the bremsstrahlung and characteristic X-rays produced by electron interactions with atoms of a  $^3\text{H}$  containing metal. Although this is easier to detect than  $\beta$  particles, the method is very time consuming. The method was performed using a Ge

semi-conductor detector. A third method is a chemical procedure involving metal dissolution in acid and measuring the  $^3\text{H}$  in the water distillate by liquid scintillation counting. Electrochemical layer-by-layer etching was also considered which showed that only a very small amount of  $^3\text{H}$  was released into the gas phase. Radioluminography was the final method discussed.

The bremsstrahlung counting method is covered in more detail in reference 58 for a thermonuclear fusion reactor. Two disks were produced - one of high atomic number, and one of low atomic number - and a small amount of  $^3\text{H}$  was absorbed by the disks. The energy distributions were measured using a Si avalanche photodiode detector, but it is also possible to use a High Purity Germanium (HPGe) detector. However, any material of interest from the reactor will not only be emitting X-rays due to the bremsstrahlung reactions of the  $^3\text{H}$   $\beta$ 's, and so the presence of other radioactive elements will influence the precision of this method.

Hou [59] states that one of the most important sources of  $\beta$  activity in reactor nuclear waste comes from  $^3\text{H}$ , and that  $^3\text{H}$  is a pure, low energy  $\beta$  emitter. Therefore, the individual  $^3\text{H}$  radionuclide needs to be separated from the sample in order to measure its radioactivity using liquid scintillation counting. Methods for decomposition include combustion and acid digestion, but these methods are both time consuming. Hou describes a method in which a steel sample is scraped, mixed with cellulose powder and combusted. In a different article Hou [60] describes graphite to be an important radioactivity source during dismantling and states that  $^3\text{H}$  is one of the main contributors.

Warwick [61] first states two routinely used techniques for  $^3\text{H}$  measurements, namely leaching the sample with water, and sample decomposition either by oxidation or combustion, before providing a very detailed methodology for  $^3\text{H}$  measurement and its application to analysis of decommissioning materials. Warwick provides a study of the temperature dependence of  $^3\text{H}$  released from materials commonly surveyed during decommissioning.

Zweben et al [62] describes three techniques including direct  $\beta$  detection with magnetic steering,  $\beta$  detection using a Tokamak Fusion Test Reactor (TFTR) as an ionisation chamber and scintillator detector using a fill gas.

## 2.5 Neutrons

### 2.5.1 Neutron activation

Neutron activation provides the most prominent contribution to the radioactive inventories of a reactor.[56] It is not only the components in the reactor core that undergo neutron activation. Neutron streaming leads the activation of other components, such as concrete structures surrounding core and beam tubes.

#### Neutron activation analysis

Figure 2.7 shows the physical phenomena studied during Neutron Activation Analysis (NAA). An incident neutron strikes a target nucleus thereby forming a compound nucleus in an excited state. De-excitation occurs quickly. Prompt Gamma Neutron Activation Analysis (PGNAA) involves the measurement of the de-excitation radiation. The new nucleus might still be radioactive and will also de-excite with characteristic radiation until a stable nucleus is reached.

The majority of neutrons in a reactor come from fission. Initially the neutrons are considered fast with energies in excess of 100 keV, but collisions cause them to slow down until they reach the thermal energy range ( $\approx 0.5$  eV).

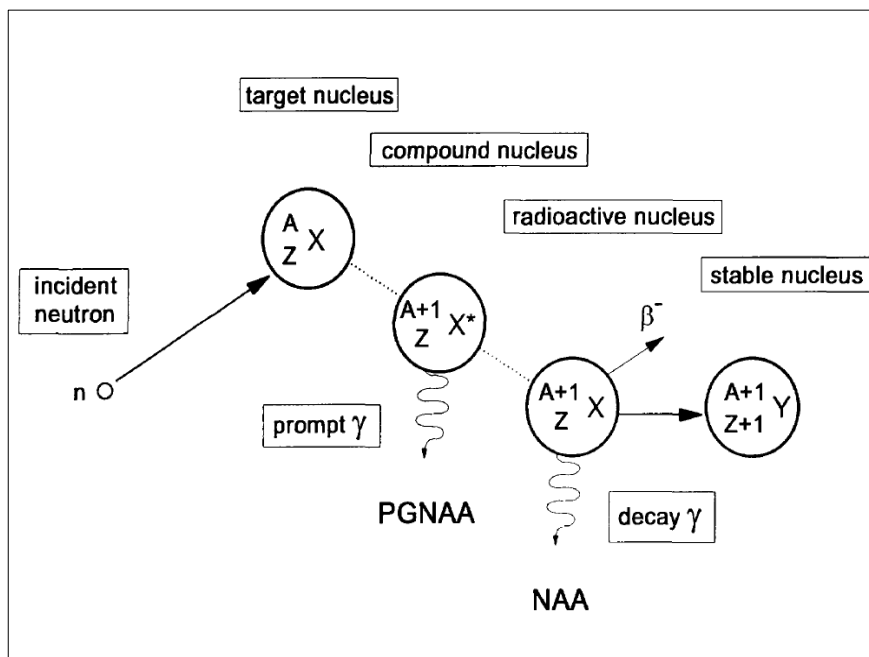


Figure 2.7 Physical phenomena studied during NAA.[63]

The neutron energy spectrum takes a different shape for the three defined neutron energy regions: fast, epithermal, and thermal. Superimposing these three regions gives the total neutron energy spectrum, which can be described semi-empirically as:

$$\begin{aligned}\varphi(E) &= [\varphi_f(E)] + [\varphi_e(E)] + [\varphi_t(E)] \\ &= 0.484 \cdot \Phi_f \cdot e^{-E} \cdot \sinh(\sqrt{2E}) + \frac{\Phi_e(E)}{E^{1+\alpha}} \cdot \left[ \left( 1 - e^{-\frac{E^2}{(0.1 \text{ eV})^2}} \right) \cdot e^{-\frac{E}{300 \text{ keV}}} \right] + \Phi_t \cdot \frac{E}{(kT)^2} \cdot e^{-\frac{E}{kT}}\end{aligned}\quad (2.11)$$

where the subscripts f, e, and t represent fast, epithermal and thermal, respectively;  $\varphi$  is the neutron flux per eV with units  $\text{cm}^{-2}\cdot\text{s}^{-1}\cdot\text{eV}^{-1}$ ;  $\Phi$  is the total neutron flux with units  $\text{cm}^{-2}\cdot\text{s}^{-1}$ , k is the Boltzmann constant, and T is the temperature with units K.  $\varphi_f(E)$  is the Watt representation, and  $\varphi_t(E)$  is the Maxwell-Boltzmann distribution. The neutron flux per unit energy is shown as a function of neutron energy in figure 2.8 including all three energy regions.

For a certain isotope exposed to a neutron flux per unit energy,  $\varphi(E)$ , the reaction rate per nucleus R is given in units of  $\text{s}^{-1}$ :

$$R = \int_0^{\infty} \varphi(E) \cdot \sigma(E) \, dE \quad (2.12)$$

where  $\sigma(E)$  is the reaction cross section in units of  $\text{cm}^2$ . It can also be expressed in terms of neutron velocity instead of energy:

$$R = \int_0^{\infty} \varphi(v) \cdot \sigma(v) \, dv \quad (2.13)$$

where v is the neutron velocity.[63]

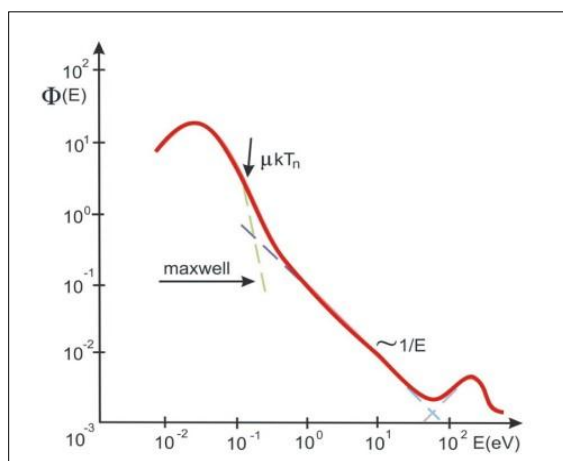


Figure 2.8 Neutron flux as a function of neutron energy.[3]

## 2.5.2 Neutron interactions and cross sections

There are a number of types of interactions that a neutron can undergo when it encounters a target nucleus. These interactions are summarised in figure 2.9. In neutron scattering, an incident neutron is scattered by the target nucleus, causing the neutron to undergo a change in velocity. The target nucleus remains unchanged in terms of the number of protons and neutrons, but it may acquire some energy that will later be released during de-excitation. When a neutron is absorbed, a number of outgoing particles may be produced as shown in figure 2.9.

Alternatively; a neutron need not interact with the target material at all. Each of these events is governed by a particular probability that is expressed in terms of a cross section  $\sigma$ . A subscript on  $\sigma$  differentiates the types of possible interactions. For example, the absorption cross section  $\sigma_a$  is given by:

$$\sigma_a = \frac{\text{probability of neutron absorption}}{\text{number of target atoms per unit area}} = \frac{1}{\left[\frac{1}{\text{cm}^2}\right]} = [\text{cm}^2] \quad (2.14)$$

Thus, it is effectively a cross sectional area for the reaction. As mentioned in section 1.1.1, neutron cross sections depend on neutron energy.[29]

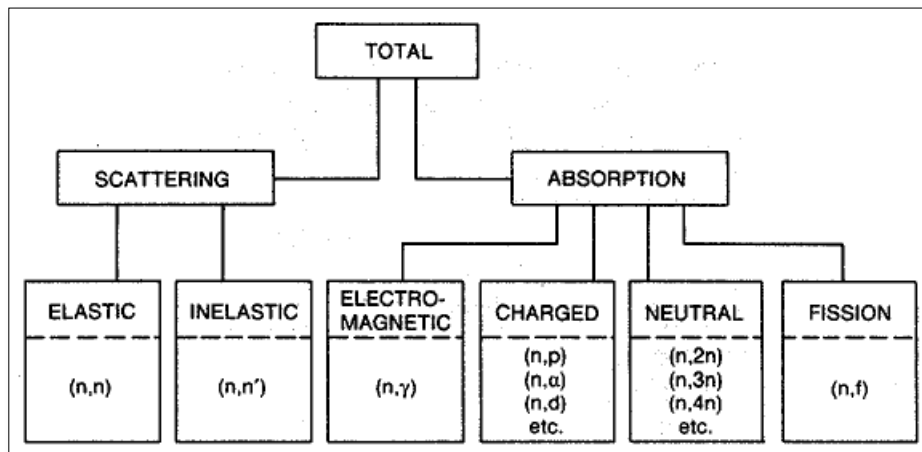


Figure 2.9 Neutron interactions.[29]

Elastic scattering is highly probable for slow neutrons, but because of the smaller kinetic energies associated with these interactions, these interactions are harder to detect. Rather, these elastic collisions serve to bring the neutrons to an equilibrium thermal energy, at which point these thermal interactions become more important. Here, secondary radiation is produced that is easier to detect. Fast neutrons can transfer more energy per collision than slow neutrons, producing a recoil nucleus that can be detected immediately. At high enough energies, inelastic scattering is also possible. An excited recoil nucleus is produced that de-excites by  $\gamma$  emission, thereby causing the recoil nucleus to lose even more energy.[41]

### 2.5.3 Neutron interaction mechanisms

Three neutron interaction mechanisms are discussed.[64]

#### Compound nucleus formation

When an incident neutron is absorbed by a nucleus it forms a compound nucleus whose mass number is one greater than the original nucleus. Upon the formation of the compound nucleus, the internal energy of the compound nucleus is then the sum of the kinetic energies of the neutron and the original nucleus. However, the compound nucleus is formed at an energy above the ground state that includes both the internal energy of the compound nucleus as well the binding energy of the neutron with the original nucleus. The compound nucleus can return to its ground state through emission of one (a proton or a neutron) or multiple nucleons (an  $\alpha$  particle) if that nucleon has enough energy to escape the system.

If a neutron is emitted then the process is known either as compound inelastic scattering or compound elastic scattering, depending on whether or not that nucleus is left in an excited state.

Another possibility for the decay of the compound nucleus is the emission of capture  $\gamma$ -rays.

Compound nucleus formation is probable when there exists an excited state for the compound nucleus that has an energy close to the sum of the internal energy of the compound nucleus and the binding energy of the added neutron. Cross sections for interactions that involve the formation of the compound nucleus as an intermediate step, are strongly dependent on the energy of the incident neutron.

#### Potential scattering

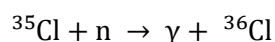
This type of elastic scattering is independent of neutron energy and does not involve compound nucleus formation. The neutron is simply scattered off the nucleus. Potential scattering thus only depends on the forces the incident neutron experiences as it approaches the nucleus.



## Direct interaction

This interaction is typical for higher energy neutrons. When a neutron collides with a nucleon in the nucleus, it may result in an ejected proton and the retention of the neutron (direct interaction (n,p) interaction). This is less important for reactor physics.

Long lived radionuclides may be formed as a result of these interactions. For example, in the following reaction,



the  $\gamma$ -ray is released promptly, leaving the radionuclide  $^{36}\text{Cl}$ . Chlorine-36 will continue to decay (see following section) through  $\beta^-$  emission or electron capture with a half-life of 301 000 years. This continued emission is known as delayed emission, whereas the  $\gamma$ -ray that was produced alongside the  $^{36}\text{Cl}$  radionuclide is known as prompt emission.

### 2.5.4 Expected major activation products

The relative percentage of present nuclides is time dependent. Initially, the major activation products expected to be present in steels are  $^{39}\text{Ar}$ ,  $^{55}\text{Fe}$ ,  $^{59}\text{Ni}$ ,  $^{60}\text{Co}$ ,  $^{63}\text{Ni}$ , and  $^{94}\text{Nb}$  (See table 2.2). The activation products initially expected in reinforced concretes are  $^3\text{H}$ ,  $^{14}\text{C}$ ,  $^{41}\text{Ca}$ ,  $^{55}\text{Fe}$ ,  $^{60}\text{Co}$ ,  $^{152}\text{Eu}$  and  $^{154}\text{Eu}$ ; and  $^3\text{H}$ ,  $^{14}\text{C}$ ,  $^{152}\text{Eu}$  and  $^{154}\text{Eu}$  in graphite. After this, the half-lives of the nuclides determine which nuclides dominate at which time. For example,  $^{60}\text{Co}$  has a half-life of 5.26 years, which allows it to die off during a period of interim storage.[18]

Table 2.2 contains the major activation products expected,[19] along with their corresponding half-life, formation mechanism, emission type, and method of measurement. More details about the methods of measurement are provided in sections 2.3.4, 2.4.2, and 2.4.3.

The most important of the activation products in table 2.2 in the context of the FiR 1 reactor are  $^3\text{H}$  and  $^{14}\text{C}$ . Tritium consists of one proton and two neutrons. It is a radioactive form of hydrogen with a half-life of 12.32 years, and it decays purely through the emission of a very low energy  $\beta$  particle.[65] Due to its very small size,  $^3\text{H}$  is extremely mobile. Tritium in the water vapour phase can exchange with the water in human skin. Tritium is problematic because of the large amount present in the FiR 1 decommissioning waste, according to calculations.

In concrete and graphite, as well as most other construction materials used in reactors,  $^{14}\text{C}$  is generated through the activation of nitrogen. It is difficult to measure because, like  $^3\text{H}$ ,  $^{14}\text{C}$  is a low energy pure  $\beta$  emitter.  $^{14}\text{C}$  is problematic owing to its very long half-life of 5730 years. Carbon is also part of organic compounds so there is a risk it will arrive in the

biosphere through ground water contamination of a geological repository and cause some internal dose to humans.

#### 2.5.5 Characterising activation products

A radioactive inventory should be determined from a characterisation survey throughout the facility. This will involve the taking of material samples that can also be used to verify activation estimate calculations, or to investigate the migration of contamination into structural materials.[66]

The IAEA outlines the following points in the characterisation procedure that should be addressed.[56]

1. A study of the historical operations documentation to determine what kind of radionuclides might be present. This documentation should include the operational history of the reactor, the maintenance history (including repairs done and materials replaced), spills or leaks, or accidental contamination of anything beyond expected areas. Where little documentation is available such as in the cases of older reactors, experienced staff should compensate for the information deficit. In any case, this information should not be trusted absolutely and its validity should be tested.
2. Theoretical calculations, even if performed by the most state-of-the-art computer codes and software, should be supplemented by a sampling and measurement plan.

The sampling and measurement plan should set out how the characterisation objectives will be achieved. Details, such as the type, number, location and analysis of samples required to fully characterise the sample area, should be set out.

Table 2.2 Expected major activation products.[18]

Activation Product	Half-life [67]	Formation Mechanism	Emission Type	Method of Measurement
$^3\text{H}$	12.32 y	Neutron capture in the neutron moderator, and in the concrete biological shield ( $^6\text{Li}(n,\alpha)^3\text{H}$ , $^2\text{H}(n,\gamma)^3\text{H}$ and $^3\text{He}(n,p)^3\text{H}$ )	Pure $\beta$ emitter No $\gamma$ emission	Discussed in section 2.4.3.
$^{14}\text{C}$	5700 y	$^{14}\text{N}(n,p)^{14}\text{C}$ , $^{13}\text{C}(n,\gamma)^{14}\text{C}$ and $^{17}\text{O}(n,\alpha)^{14}\text{C}$ , and through indirect reactions	Pure $\beta$ emitter	LSC; similar to $^3\text{H}$
$^{22}\text{Na}$	2.602 y	$^{23}\text{Na}(n,2n)^{22}\text{Na}$ and $^{23}\text{Na}(\gamma,n)^{22}\text{Na}$	$\beta^+$ and $\gamma$ emission	$\gamma$ spectrometry
$^{36}\text{Cl}$	$3.01 \times 10^5$ y	$^{35}\text{Cl}(n,\gamma)^{36}\text{Cl}$ and $^{39}\text{K}(n,\alpha)^{36}\text{Cl}$ , and indirectly through $^{34}\text{S}$	$\beta^-$ emission or EC with weak X-ray emission	$\gamma$ spectrometry
$^{39}\text{Ar}$	269 y	$^{39}\text{K}(n,p)^{39}\text{Ar}$ and $^{38}\text{Ar}(n,\gamma)^{39}\text{Ar}$	$\beta^-$ emission	Proportional $\beta^-$ counting or LSC
$^{41}\text{Ca}$	$1.02 \times 10^5$ y	$^{40}\text{Ca}(n,\gamma)^{41}\text{Ca}$	EC with weak X-ray emission	Chemical separation and LSC
$^{54}\text{Mn}$	312.2 d	$^{54}\text{Fe}(n,p)^{54}\text{Mn}$	EC with 835 keV $\gamma$ emission	$\gamma$ spectrometry
$^{55}\text{Fe}$	2.744 y	$^{54}\text{Fe}(n,\gamma)^{55}\text{Fe}$	EC with weak X-ray emission	Chemical separation and X-ray spectrometry - hard to measure and can be correlated to $^{60}\text{Co}$
$^{59}\text{Ni}$	$7.6 \times 10^4$ y	$^{58}\text{Ni}(n,\gamma)^{59}\text{Ni}$	EC with continuous bremsstrahlung spectrum	Hard to measure and can be correlated to $^{60}\text{Co}$ ; can be measured by the X-ray spectrometry of $^{60}\text{Co}$
$^{63}\text{Ni}$	101.2 y	$^{62}\text{Ni}(n,\gamma)^{63}\text{Ni}$	$\beta^-$ emission	Hard to measure and can be correlated to $^{60}\text{Co}$ ; measured by chemical separation followed by LSC
$^{60}\text{Co}$	5.274 y	$^{59}\text{Co}(n,\gamma)^{60}\text{Co}$	$\beta^-$ emission followed by emission of 2 major $\gamma$ rays (1.17 and 1.33 MeV)	$\gamma$ spectroscopy
$^{65}\text{Zn}$	243.9 d	$^{64}\text{Zn}(n,\gamma)^{65}\text{Zn}$	EC and $\beta^+$ emission	$\gamma$ spectrometry
$^{93}\text{Mo}$	$4.0 \times 10^3$ y	$^{92}\text{Mo}(n,\gamma)^{93}\text{Mo}$	EC	Detection of characteristic X-rays using an intrinsic Ge diode
$^{93}\text{Zr}$	$1.61 \times 10^6$ y	$^{92}\text{Zr}(n,\gamma)^{93}\text{Zr}$	$\beta^-$ emission, with low energy $\gamma$ emission of daughter	Chemical separation and $\beta^-$ counting
$^{94}\text{Nb}$	$2.03 \times 10^4$ y	$^{93}\text{Nb}(n,\gamma)^{94}\text{Nb}$	$\beta^-$ emission followed by $\gamma$ cascade	$\gamma$ spectrometry
$^{108\text{m}}\text{Ag}$	438 y	$^{107}\text{Ag}(n,\gamma)^{108\text{m}}\text{Ag}$	EC with weak X-ray emission, followed by $\beta^-$ emission	$\gamma$ spectroscopy
$^{110\text{m}}\text{Ag}$	249.8 d	$^{109}\text{Ag}(n,\gamma)^{110\text{m}}\text{Ag}$	$\beta^-$ emission, followed by $\beta^-$ emission of the daughter	$\gamma$ spectroscopy
$^{125}\text{Sb}$	2.759 y	$^{124}\text{Sb}(n,\gamma)^{125}\text{Sb}$	$\beta^-$ emission, followed by $\beta^-$ and $\gamma$ emission of the daughter	$\gamma$ spectroscopy
$^{133}\text{Ba}$	10.55 y	$^{132}\text{Ba}(n,\gamma)^{133}\text{Ba}$	EC and $\gamma$ emission	$\gamma$ spectroscopy
$^{134}\text{Cs}$	2.065 y	$^{133}\text{Cs}(n,\gamma)^{134}\text{Cs}$	$\beta^-$ emission or EC	$\gamma$ spectroscopy
$^{152,154,155}\text{Eu}$	13.52 y 8.601 y 4.753 y	Neutron capture in $^{151}\text{Eu}$ and $^{153}\text{Eu}$ , or by chain absorptions in Sm.	$^{152}\text{Eu}$ decays by $\beta^-$ emission, followed by $\alpha$ emission $^{154,155}\text{Eu}$ decays $\beta^-$ emission	$\gamma$ spectroscopy or $\beta^-$ counting
$^{166\text{m}}\text{Ho}$	$1.20 \times 10^3$ y	$^{165}\text{Ho}(n,\gamma)^{166\text{m}}\text{Ho}$	$\beta^-$ emission	Chemical separation and $\gamma$ spectroscopy

## 2.6 The pre-measurement inventory report

### 2.6.1 Activity prediction using MCNP and ORIGEN-S

The activity inventory has already been predicted computationally by Petri Kotiluoto and Antti Rätty.[27] By modelling the reactor structures in three dimensions (both before and after the addition of the BNCT facility), a Monte Carlo N-Particle Transport code (MCNP) [68] is used to calculate neutron fluence rates.

The Monte Carlo method can be used for neutrons, photons, electrons, or a combination of these. It is discussed briefly for the case of combined neutron and photon transport.

MCNP requires the user to specify the geometry, describe the materials, describe the neutron source, specify the tally (or scoring region) type, and specify any variance reduction techniques. Instead of solving the transport equation as with deterministic methods, each particle is simulated in the Monte Carlo method, and tallies are kept of the average particle behaviour. The simulated particle behaviour is averaged to infer information about the full physical system. The Monte Carlo method does not give as solution information about the entire phase space as deterministic methods would. Instead, the user has to specify for which tallies information is required.

Many processes in physics are statistical, such as particle interaction with matter. The Monte Carlo method simulates these statistical processes. To do this, each step in a statistical process is simulated according to sampling of associated probability distributions, through the use of a random number generator. These probabilities can be found from evaluated nuclear data files and they are based on extensive international experimental work and evaluation of the measurement results.

The Monte Carlo method follows each neutron from the neutron source along its path. The path ends either when the neutron escapes or when it is absorbed.

Assume a neutron travels through a fissionable material of known composition. The neutron undergoes various interactions with the target material, such as scattering or absorption. It could even escape the material without interaction. Each of these possibilities occurs with some probability, and the choice of the possibility is governed by the use of a random number generator that gives a value between 0 and 1. This is illustrated with an example (see figure 2.10).

At event 1, a neutron strikes the fissionable material and is scattered in a certain direction. This direction is randomly chosen from the scattering distribution. A photon is also produced in this interaction, but it will be retrieved later. Event 2 shows that once the neutron is

scattered, fission occurs. Thus, the neutron is absorbed, and two new neutrons and a photon are released. Event 3 shows the first neutron followed to its capture. At event 4, the second neutron is retrieved and followed to its escape from the material. The capture and escape are decided from random sampling. At event 5, the photon is retrieved and scatters in the material. The photon escapes at event 6. The procedure then returns to event 1, at which point the first photon generated is

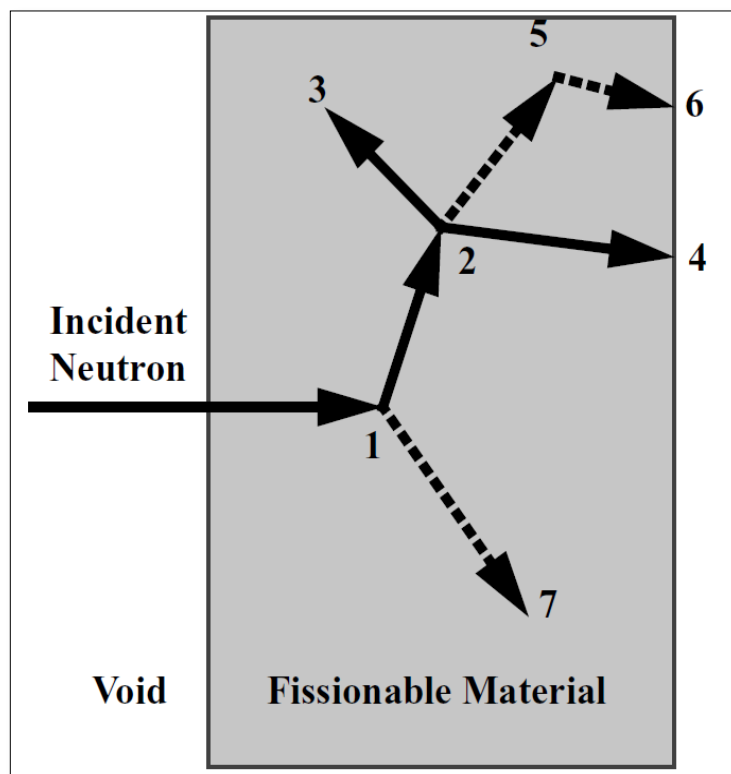


Figure 2.10 A hypothetical set of events that is simulated in MCNP.[68]

retrieved and followed to its capture. The most recent particle to be stored is the first to be retrieved. With every neutron followed, the neutron distribution becomes better understood. Tallies are kept of the user defined quantities of interest and an estimation of the associated uncertainty.

These quantities of interest are, for example, neutron flux or energy deposition. Fluxes can be requested across any surface or cell, a part of a surface or cell, or a combination of surfaces and cells. Fluxes can be requested at any point or detector. Energy depositions can be requested in particular cells. Energy distributions resulting from radiation deposited in a detector can be requested. Particles can be marked so that their contribution to a tally across a surface or within a cell can be seen separately.

Geometries are defined in MCNP in terms of cells and surfaces in a Cartesian coordinate system. To define a cell, cell cards are used that contain information about the number of the cell, the material and material density, as well as some information about surfaces that bind small geometrical cells of homogeneous material. Cells can be created by a combination of regions of space bound by surfaces through the use of intersections, unions and complements. Geometries are defined as a combination of cells.

Thus, the neutron flux is simulated with the Monte Carlo method in a model describing the actual geometry, material shielding and scattering properties, and the neutron source from the reactor core. This flux is homogenised for each single component or piece of structure e.g. 1 kg of concrete.

#### Monte Carlo Errors

In the MCNP simulation, the code tracks individual particles through a defined geometry. To estimate the average flux in a cell, a track length estimator is needed. As the name suggests, it tracks the length of the particle's track through the scoring cell. The use of the track length estimator makes the cell flux a statistical quantity, with an uncertainty dependent on how many tracks are recorded in the volume of the cell.

The estimated relative error  $R$  is defined as:

$$R \equiv \frac{S_{\bar{x}}}{\bar{x}} \quad (2.15)$$

where  $S_{\bar{x}}$  is the estimated standard deviation from the mean, and  $\bar{x}$  is the estimated mean.

$R \propto \frac{1}{\sqrt{N}}$  for a well-behaved tally, where  $N$  is the number of histories.

Assuming the full phase space is sampled, the result can be interpreted as generally reliable for values of  $R$  less than 0.1. For  $R$ -values greater than 0.1, the results become questionable. For values of  $R$  in excess of 0.5, results are considered meaningless.

For some structures of the reactor, there is a high uncertainty associated with the fluence rate, with values of  $R$  greater than 0.1. The high uncertainty in a particular scoring cell is explained by low fluence rates, making that scoring cell less significant in terms of contribution to the neutron activation.

In addition to this  $R$  value, a figure of merit (FOM) is also calculated to inform the user when  $R$ -values cannot be trusted. This happens, for example, when important paths are not sampled enough in the defined region of the problem. If  $T$  is the computer time,

$$\text{FOM} \equiv \frac{1}{R^2 T} \quad (2.16)$$

$$R^2 \propto \frac{1}{N}, T \propto N.$$

Thus, a constant value of FOM is expected with an increase in number of histories for a well behaved tally. If FOM values drastically decrease with an increase in number of histories, values of  $R$  might not be accurate.

Since

$$R^2 \propto \frac{1}{N} \text{ and } T \propto N,$$

R is inversely proportional to  $\sqrt{T}$ . Thus, to reduce R, T should be increased, or the proportionality constant between R, and  $(T)^{-\frac{1}{2}}$  should be decreased. Variance reduction techniques are used to decrease this constant because of its dependence of choice of tally or sampling. The correct use of variance techniques is important not only because it can hugely improve the efficiency of the calculation, but incorrect use might produce a totally incorrect answer with no indication thereof.

The “weight cut-off” variance reduction technique was used in the activity inventory report for the concrete sample’s neutron flux calculation, because of the relatively low neutron flux at that sample position. To generate weights, MCNP’s automatic weight window generator is used. The weights are obtained after an iterative sequence of MCNP runs, optimised for the scoring region. In the first run, there are only a few hits in the scoring region. In the second run, the generated weights are used to achieve more hits in the scoring region by giving more weight to more important particle tracks. This continues until satisfactory results are obtained with low uncertainty and reasonable running time. For the remaining samples, no variance reduction techniques were applied.

The MCNP calculations make use of continuous energy cross section libraries as well as the newest available evaluated neutron data files. The evaluated neutron data files have some uncertainty, but it is low relative to other sources of uncertainty. A more important source of uncertainty would be the material definitions required by the code. Uncertainties also arise from the use of a slightly simplified reactor geometry.

Following the MCNP calculations for the neutron flux, the ORIGEN-S code [69] is used to calculate activity inventories, taking into account the operational history of the FiR 1 reactor. This operation history includes operating time on a day to day basis, as well as decay time in the evenings and over weekends.

ORIGEN-S is a point-depletion code. Point depletion means that the ORIGEN-S code is “0-dimensional”, so there is no geometry input. The entire geometry is treated as a homogeneous mass that is exposed to a constant (both in spectrum and magnitude) neutron flux.

The ORIGEN-S code takes as input the neutron flux, irradiation history and material data. The depletion and decay are calculated in ORIGEN-S by solving the Bateman equations.[70]

When a material is subjected to a particle flux, the concentration of the  $i^{\text{th}}$  isotope can be found from the Bateman equations,

$$\frac{dN_i}{dt} = - \sum_{j \neq i} \left[ \lambda_{ji}^d + \int \varphi(E, t) \sigma_{ji}^{\text{tr}}(E) dE \right] N_i + \sum_{j \neq i} \left[ \lambda_{ij}^d + \int \varphi(E, t) \sigma_{ij}^{\text{tr}}(E) dE \right] N_j \quad (2.17)$$

where  $i$  and  $j$  are isotope indices,  $N_i$  is the concentration of that isotope, the  $\lambda^d$ 's are decay constants,  $\varphi(E, t)$  is the particle flux magnitude at energy  $E$ , and  $\sigma_{ji}^{\text{tr}}(E)$  is the cross section induced by the particle when transmutation occurs.

A constant flux over  $dt$  can be assumed for a small fluence and transmutation cross section.

The transmutation cross section averaged across the spectrum is given by

$$\bar{\sigma}_{ij}^{\text{tr}} \equiv \frac{1}{\bar{\varphi}} \int \varphi(E) \sigma_{ij}^{\text{tr}}(E) dE \quad (2.17)$$

where

$$\bar{\varphi} = \int \varphi(E) dE. \quad (2.18)$$

Substituting this into the Bateman equations gives:

$$\frac{dN_i}{dt} = - \sum_{j \neq i} [\lambda_{ji}^d + \bar{\sigma}_{ij}^{\text{tr}} \bar{\varphi}] N_i + \sum_{j \neq i} [\lambda_{ji}^d + \bar{\sigma}_{ij}^{\text{tr}} \bar{\varphi}] N_j \quad (2.19)$$

This can be written in vector form:

$$\frac{d\mathbf{N}}{dt} = \mathbf{\Lambda} \mathbf{N} \quad (2.20)$$

where

$$\Lambda_{ij} \equiv \lambda_{ij}^d + \bar{\sigma}_{ij}^{\text{tr}} \bar{\varphi} \quad (2.21)$$

Solving this results in:

$$\mathbf{N}(t) = e^{\mathbf{\Lambda}t} \mathbf{N}(0) \quad (2.22)$$

where

$$e^{\mathbf{\Lambda}t} \equiv 1 + \mathbf{\Lambda}t + \frac{1}{2} \mathbf{\Lambda}^2 t^2 + \dots \quad (2.23)$$

is valid for small  $t$ .



This is called the matrix exponential method and is used for the calculation of activities and decay chains of nuclides. In Rätty's calculation,[28] group weighting factors are calculated according to three categories of neutron fluence rates:

0 - 0.625 eV:

$$\text{THERMAL} = \sigma \left( \frac{1}{v} \right)_{\text{th}} = \sqrt{\frac{\pi}{4} \cdot \frac{T_0}{T}}, T_0 = 293.15\text{K} \quad (2.24)$$

0.625 eV – 1 MeV:

$$\text{RES} = \sum_{E_g \geq 0.625\text{MeV}}^{E_g \leq 1\text{MeV}} \frac{\phi_g}{\phi_{\text{th}}} \quad (2.25)$$

1 MeV – 20 MeV:

$$\text{FAST} = \sum_{E_g \geq 1\text{MeV}} \frac{\phi_g}{\phi_{\text{th}}} \quad (2.26)$$

These weighting factors are needed in the equation for the effective cross section,  $\sigma_{\text{eff}}$ ,

$$\sigma_{\text{eff}} = \text{THERM} \times \sigma_0 + \text{RES} \times \sigma_{\text{res}} + \text{FAST} \times \sigma_{\text{MeV}} \quad (2.27)$$

In these equations, T represents the temperature in Kelvin, v represents the velocity of the neutrons, the subscript g means group in neutron energies, the subscript th refers to the thermal energy range,  $\phi$  is the neutron flux with units  $\text{s}^{-1}\text{cm}^{-2}$ ,  $\sigma_0$  is the cross section for neutrons in the THERMAL category,  $\sigma_{\text{res}}$  is the cross section for neutrons in the RES (i.e. resonance) category, and  $\sigma_{\text{MeV}}$  is the cross section for neutrons in the FAST category. The effective cross section is then used to calculate reaction rates.

The minor impurities in the material compositions do not strongly influence the MCNP flux calculation, because minor impurities do not cause many absorption or scattering reactions. Most of the compositions in activity calculations are based on material specifications obtained at the time of construction. However, because activating elements are the minor impurities in materials, it is important to know them well when calculating the activation reaction in ORIGEN-S. The calculation model is so simple that uncertainty is practically directly proportional to the uncertainty of impurities.

A schematic view of the calculation is shown in figure 2.11. The activity prediction is then verified using physical measurements. In compiling an inventory report, the method of comparing measured activities with computationally predicted activities is, of course, not

unique to VTT. Studsvik, a nuclear analysis company headquartered in Sweden, has used codes developed at Studsvik to perform waste characterisations for all nuclear facilities in Sweden. These calculations are performed with a combination of codes, including MCNP, IndAct, and FISPACT, and compared to real measurements.[71]

In Canada, ORIGEN has been used in combination with the SAS2H control module (needed for time dependent cross sections) to characterise used fuel from a Pickering CANDU reactor prior to disposal. Comparisons with real measurements show very good element-wise agreement in activity concentrations.[72]

The activity inventory is very important in the planning process because it gives information about, and helps with the planning of the required waste packaging, interim storage and final disposal of decommissioning waste.[27] The inventory report is also important for the radiation safety of the workers performing the dismantling.

#### 2.6.2 Expected activated structures and components

A summary of the predicted activities of various reactor components is given in table 2.3. In the last column of the table, critical radionuclides predicted by the calculation are shown.

Horizontal and vertical cross sections of the MCNP geometry with the BNCT facility are shown in figure 2.12 and an illustration of the simulated total neutron fluence rate distribution is shown in figure 2.13.

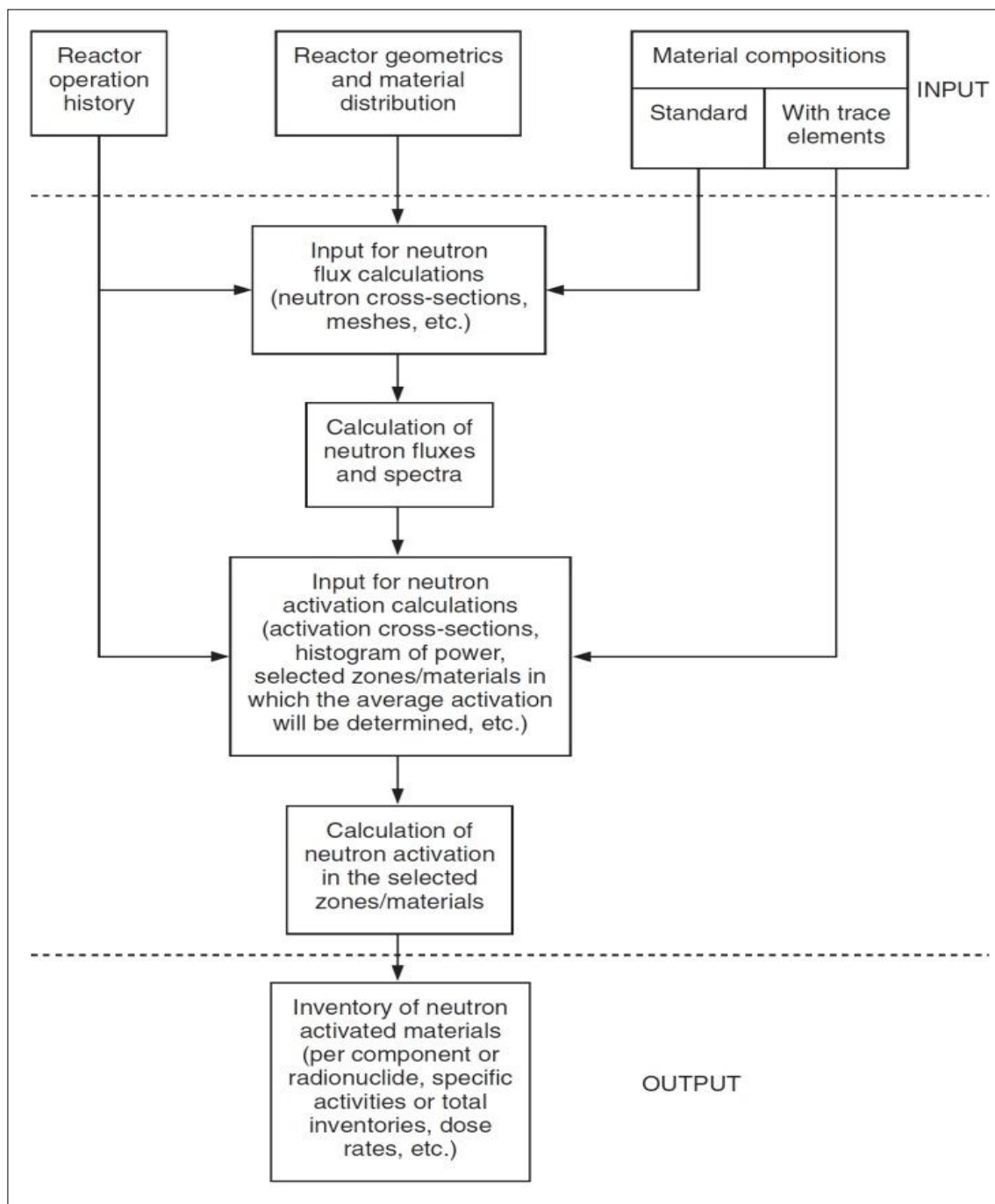


Figure 2.11 Schematic view of the activity calculation.[18]

Table 2.3 Computed activities of various reactor components.

Component or structure	Material	Specific activity (Bq/g)	Relevant critical radionuclides [28]
Biological shield around the core	Concrete	1.54E+05	<sup>3</sup> H, <sup>55</sup> Fe, <sup>60</sup> Co, <sup>152</sup> Eu, <sup>40</sup> K
Biological shield around the beam tubes	Concrete	2.42E+03	<sup>3</sup> H, <sup>55</sup> Fe, <sup>60</sup> Co, <sup>152</sup> Eu, <sup>40</sup> K
Tank	Aluminium	2.19E+00	<sup>55</sup> Fe, <sup>65</sup> Zn, <sup>63</sup> Ni, <sup>60</sup> Co, <sup>54</sup> Mn, <sup>59</sup> Fe
Structures inside the tank (tubes etc.)	Aluminium	1.49E+05	<sup>55</sup> Fe, <sup>65</sup> Zn, <sup>63</sup> Ni, <sup>60</sup> Co, <sup>54</sup> Mn, <sup>59</sup> Fe
Bitumen around tank	Bitumen *	6.44E+02	<sup>14</sup> C, <sup>63</sup> Ni, <sup>59</sup> Ni, <sup>3</sup> H
Reflector	Graphite and aluminium	1.15E+06	<sup>55</sup> Fe, <sup>65</sup> Zn, <sup>63</sup> Ni, <sup>60</sup> Co, <sup>54</sup> Mn, <sup>59</sup> Fe, <sup>3</sup> H, <sup>14</sup> C, <sup>133</sup> Ba, <sup>152</sup> Eu
Irradiation ring	Aluminium and steel	2.99E+07	<sup>55</sup> Fe, <sup>65</sup> Zn, <sup>63</sup> Ni, <sup>60</sup> Co, <sup>54</sup> Mn, <sup>59</sup> Fe, <sup>59</sup> Ni, <sup>14</sup> C
Beam ports	Aluminium	8.65E+03	<sup>55</sup> Fe, <sup>65</sup> Zn, <sup>63</sup> Ni, <sup>60</sup> Co, <sup>54</sup> Mn, <sup>59</sup> Fe
Beam port bellows and clamps	17-4-PH steel **	3.42E+06	<sup>63</sup> Ni, <sup>55</sup> Fe, <sup>60</sup> Co, <sup>59</sup> Ni, <sup>14</sup> C
Beam port plugs	Boral, steel, lead, heavy concrete	1.37E+02	<sup>108</sup> Ag, <sup>59</sup> Ni, <sup>63</sup> Ni, <sup>10</sup> Be, <sup>14</sup> C, <sup>60</sup> Co, <sup>55</sup> Fe, <sup>121</sup> Sn, <sup>113</sup> Cd, <sup>39</sup> Ar, <sup>41</sup> Ca, <sup>40</sup> K, <sup>36</sup> Cl, <sup>3</sup> H, <sup>10</sup> Be
Shadows around beam ports	Carbon steel ***	4.90E+03	<sup>63</sup> Ni, <sup>55</sup> Fe, <sup>60</sup> Co, <sup>59</sup> Ni, <sup>14</sup> C
Fluental moderator	Fluental	9.77E+05	<sup>3</sup> H, <sup>14</sup> C
Other parts in BNCT station	Bismuth, lead, lithiated plastic, aluminium	1.86E+05	<sup>108</sup> Ag, <sup>206</sup> Tl, <sup>55</sup> Fe, <sup>36</sup> Cl, <sup>208</sup> Bi, <sup>210</sup> Po, <sup>63</sup> Ni, <sup>3</sup> H, <sup>65</sup> Zn, <sup>60</sup> Co, <sup>54</sup> Mn, <sup>59</sup> Fe
Thermal column graphite (removed in 1995)	Graphite	3.14E+04	<sup>3</sup> H, <sup>14</sup> C, <sup>60</sup> Co, <sup>133</sup> Ba, <sup>152</sup> Eu

\*Bitumen: 85.0 w-% C, 9.08 w-% H, 4.10 w-% S, 1.22 w-% N, 0.58 w-% O, 0.01 w-% Ni, 0.01 w-% V.[73, 74]

\*\* 17-4-PH steel: 69.91 w-% Fe, 17.5 w-% Cr, 5 w-% Ni, 5 w-% Cu, 1 w-% Si, 1 w-% Mn, 0.225 w-% Nb, 0.225 w-% Ta, 0.07 w-% C, 0.04 w-% P, 0.03 w-% S.

\*\*\* Carbon steel: 65.134 w-% Fe, 17.635 w-% Cr, 9.559 w-% Ni, 6.170 w-% Mn, 0.742 w-% Si, 0.178 w-% N, 0.150 w-% Mo, 0.129 w-% C, 0.090 w-% Co, 0.079 w-% Ti, 0.046 w-% P, 0.029 w-% Nb, 0.027 w-% S, 0.024 w-% Al, 0.004 w-% Cu, 0.004 w-% Se, 0.001 w-% V.

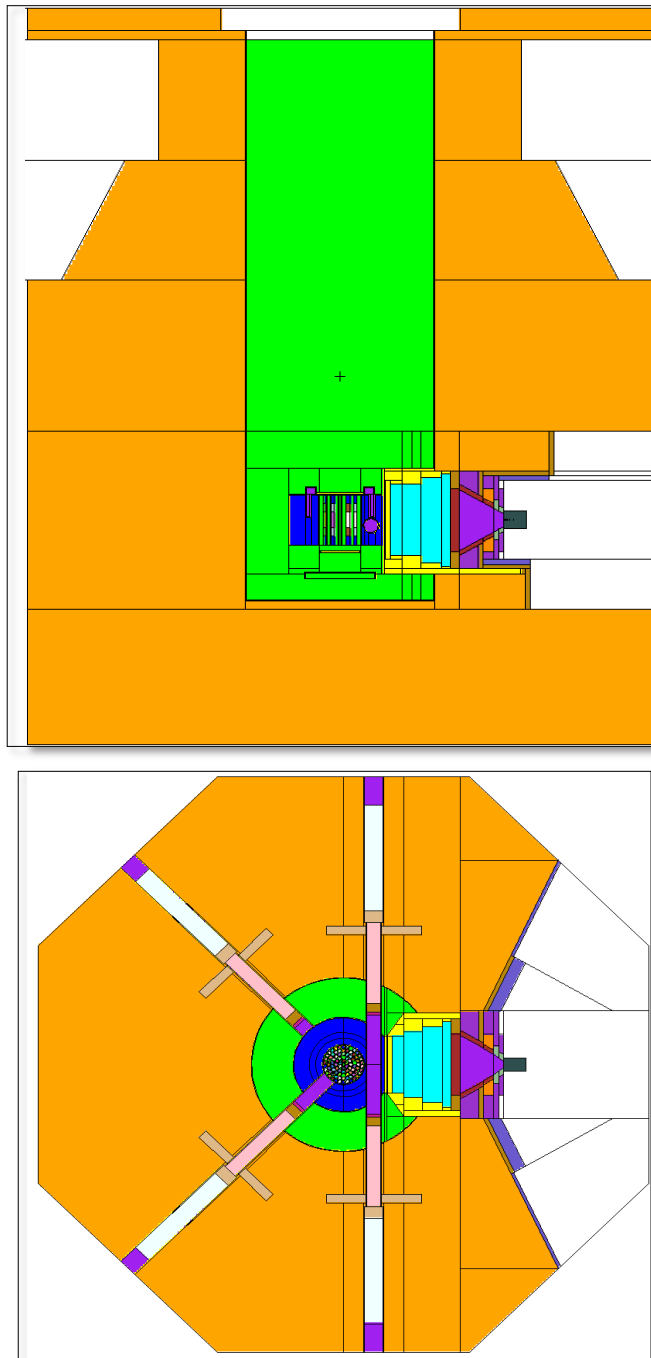


Figure 2.12 Horizontal and vertical cross sections of the MCNP geometry with the BNCT facility.[27]

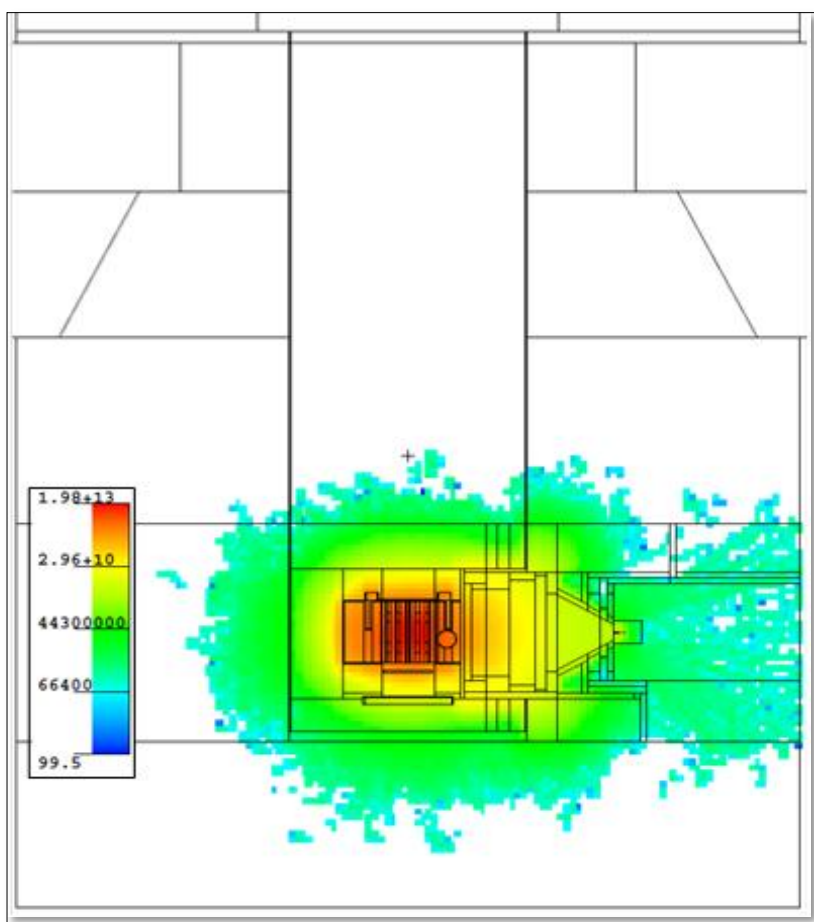
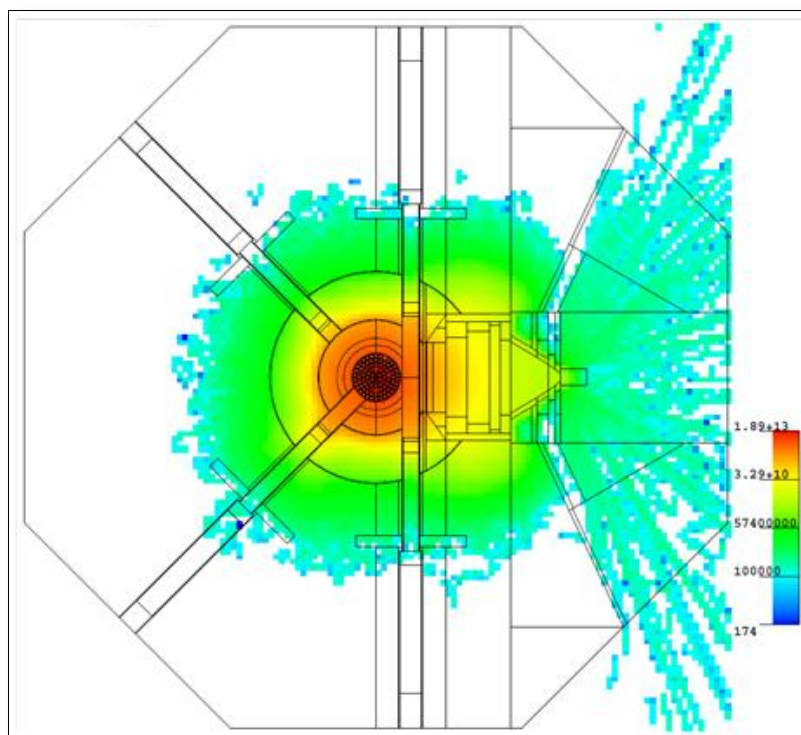


Figure 2.13 The simulated total neutron fluence rate distribution (units:  $\text{cm}^{-2}\text{s}^{-1}$ ) as shown on the horizontal and vertical cross section of the reactor.[27]

## Chapter 3: Experimental Methods

Much of the equipment required for characterising materials related to decommissioning are already owned by VTT, including a range of detectors and software. There is added convenience in that in situ measurements are possible with the In Situ Object Counting System (ISOCS) equipment available for use. A preliminary set of samples are available for measurement to test all systems and software before actual dismantling begins. In this chapter, the samples, their preparation and their characterisation are discussed. But first it is important to consider the requirements that must be met for material characterisation measurements at VTT.

### 3.1 Requirements for measurement techniques at VTT for material characterisation

According to the Nuclear Energy Act [75] radioactive waste may not be moved out of Finland, but there is an exception in the case of the research reactor for the spent fuel. The dismantling procedure requires the U.S. origin fuel to be removed from the core and returned to Idaho National Laboratory in the U.S. DOE FRR SNF AP.[76] Alternatively, it could be stored in Finland.

The IAEA requires the fuel to be removed as soon as possible, although it depends on many factors such as the type of reactor, the fuel condition, and the transport and offsite management of the fuel. The fuel should remain in the reactor for a few months after final shut down to allow highly active short-lived nuclides to decay. The IAEA requires that the fuel needs to be stored safely while it is still in the reactor installation, controlling any risk to staff and members of the public.[77] Specifically in the case of the TRIGA fuel used in the FiR 1 reactor, the activity is low enough that excess heat does not require any cooling. For the shutdown FiR 1 reactor, no primary water cooling was necessary. Part of the spent fuel is stored in dry storage pits. In transportation casks, the heat transfer does not pose a problem either, although there is a three month waiting period following the termination of use before transportation occurs because of short lived nuclides.

The main restriction to sample taking is that the samples have to be taken without compromising the structural integrity of the reactor, because the reactor will not be dismantled before 2018 - 2019.

The measurements should also be accurate enough to fulfil all official regulations, but also be simple and cost effective enough to be performed later systematically for dozens of waste packages during dismantling. For now, the emphasis is not on taking as many samples as

possible, but rather on performing the measurements as carefully as possible, and using the results and experiences to develop a practical measurement system. This sampling and measurement plan should be logically optimised through consideration of unique factors, such as symmetry of the measurement area and the distance from the core or other key radioactive components. For example, more measurements should be performed closer to the core. An initial set of low statistics measurements can be performed to first obtain information to guide further measurements, and to determine which samples require higher statistics. The number of measurements performed is also determined by the required accuracy of the results.[77]

Figure 3.1 shows a flow diagram of a general characterisation procedure.

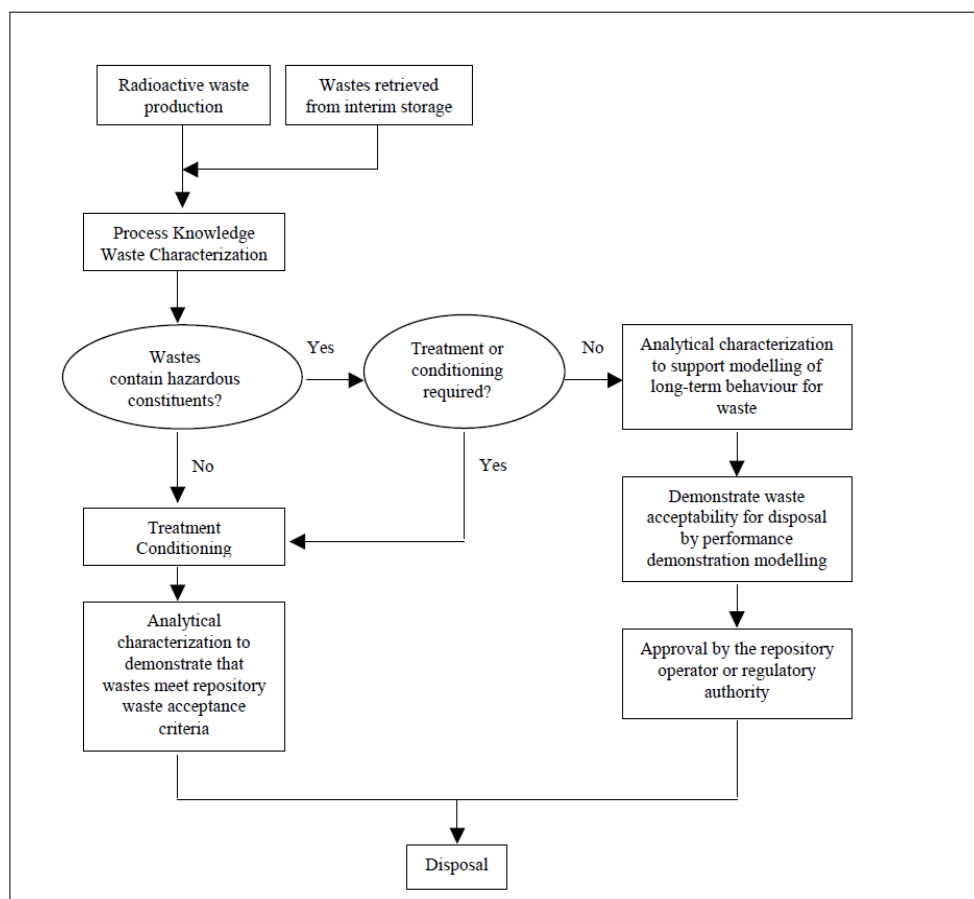


Figure 3.1 Example of a general characterisation procedure.[78]



### 3.2 Sample description and preparation

Measurements were performed on four different types of samples. The first sample is concrete drilled from the biological shield of the reactor, the second is aluminium from the reactor tank, the third is Flualtal from the moderator, and the last is the ion-exchange resin from the cooling circuit. Information about these samples is summarised in table 3.1.

Table 3.1 Sample information.

Sample Name	Sample Type	Measurement date	Measurement duration (sec)	Measurement dead time	Sample mass (g)
Concrete	Concrete	9.11.2015 - 13.11.2015	343489.1	0.10 %	14885
Flualtal 1	Flualtal	21.10.2015	58579.3	0.03 %	3.455
Flualtal 2	Flualtal	22.10.2015	25951.4	0.03 %	3.863
Aluminium 1	Aluminium	20.10.2015	60868.6	0.04 %	0.7244
Aluminium 2	Aluminium	21.10.2015	28407.3	0.04 %	0.626
IER 1091	Ion-Exchange Resin	17.12.2015	3600	0.42 %	45400
IER 1092	Ion-Exchange Resin	16.12.2015	3600	0.08 %	47600
IER 1093	Ion-Exchange Resin	16.12.2015	3600	0.12 %	43600
IER 1094	Ion-Exchange Resin	17.12.2015	3600	0.57 %	52400
IER 1095	Ion-Exchange Resin	17.12.2015	3600	1.06 %	40000
IER 1096	Ion-Exchange Resin	17.12.2015	3600	0.07 %	35000
IER 1097	Ion-Exchange Resin	16.12.2015	3600	0.12 %	39200
IER 1098	Ion-Exchange Resin	9.12.2015	3600	0.5 %	40800
IER 1099	Ion-Exchange Resin	15.12.2015	3600	0.06 %	44200
IER 1100	Ion-Exchange Resin	14.12.2015	3600	0.63 %	40200
IER 1101	Ion-Exchange Resin	15.12.2015	3600	0.28 %	22200
IER 1102	Ion-Exchange Resin	14.12.2015	3600	0.15%	43000
IER 1103	Ion-Exchange Resin	15.12.2015	3600	0.54 %	23400

The concrete used in the construction of the reactor is inhomogeneous (figure 3.2a) . The inhomogeneity might introduce uncertainties, but due to the size of the sample, the average activity is expected to represent the concrete well. These samples were drilled (figure 3.2b) in the location indicated in figure 3.3 through horizontal and vertical cross sections of the reactor structures, in 1996 when the BNCT facility was built. The diamond drill cores with measurement positions and dimensions [mm] are shown in figure 3.4. Before measurement, the samples were weighed.



Figure 3.2a The concrete sample.



Figure 3.2b Diamond drilling of the biological concrete shield for construction of the BNCT facility.[27]

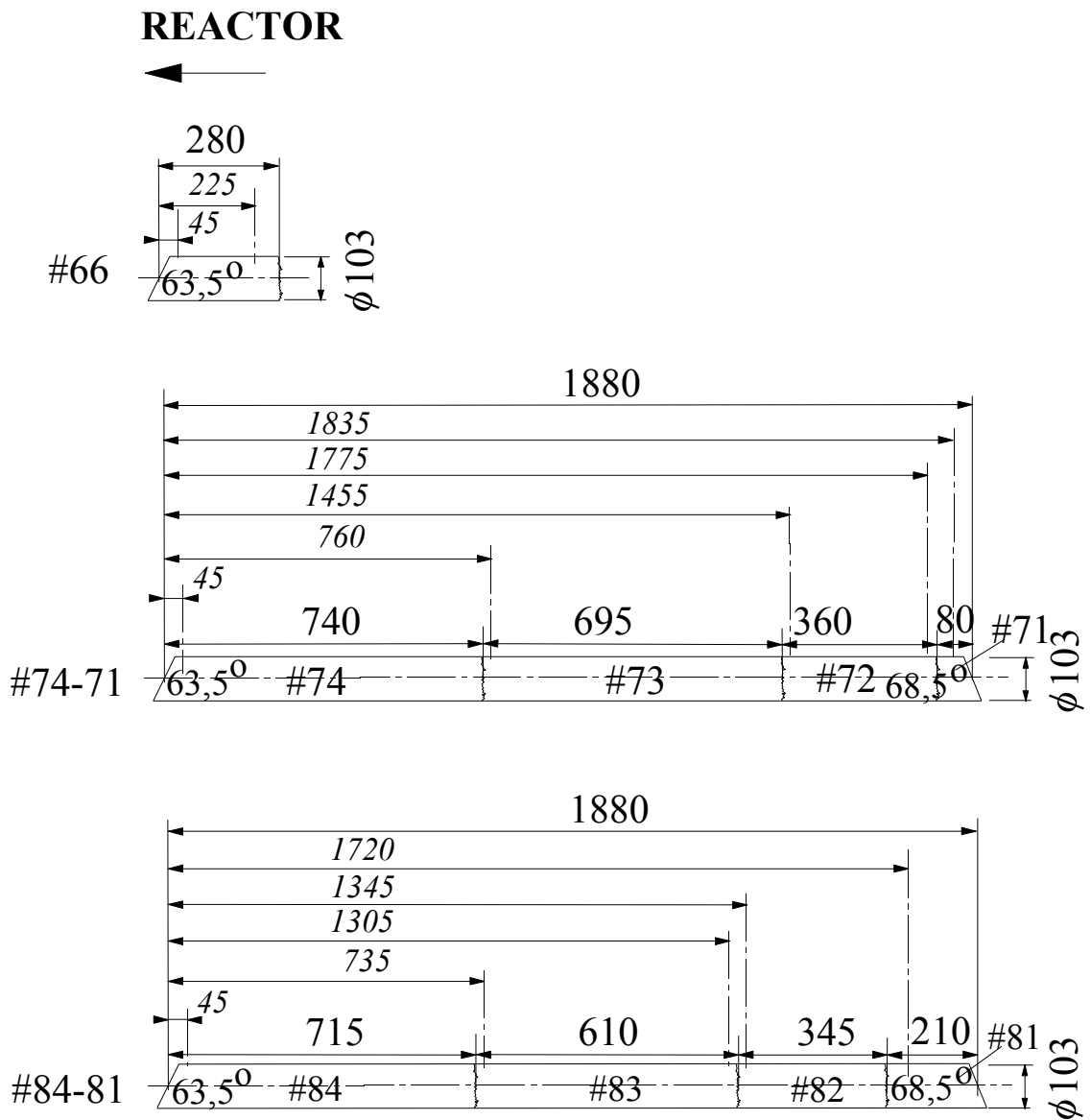


Figure 3.3 The dimensions [mm] of the concrete diamond drilling samples number 66, 71-74, and 81-84.[79]

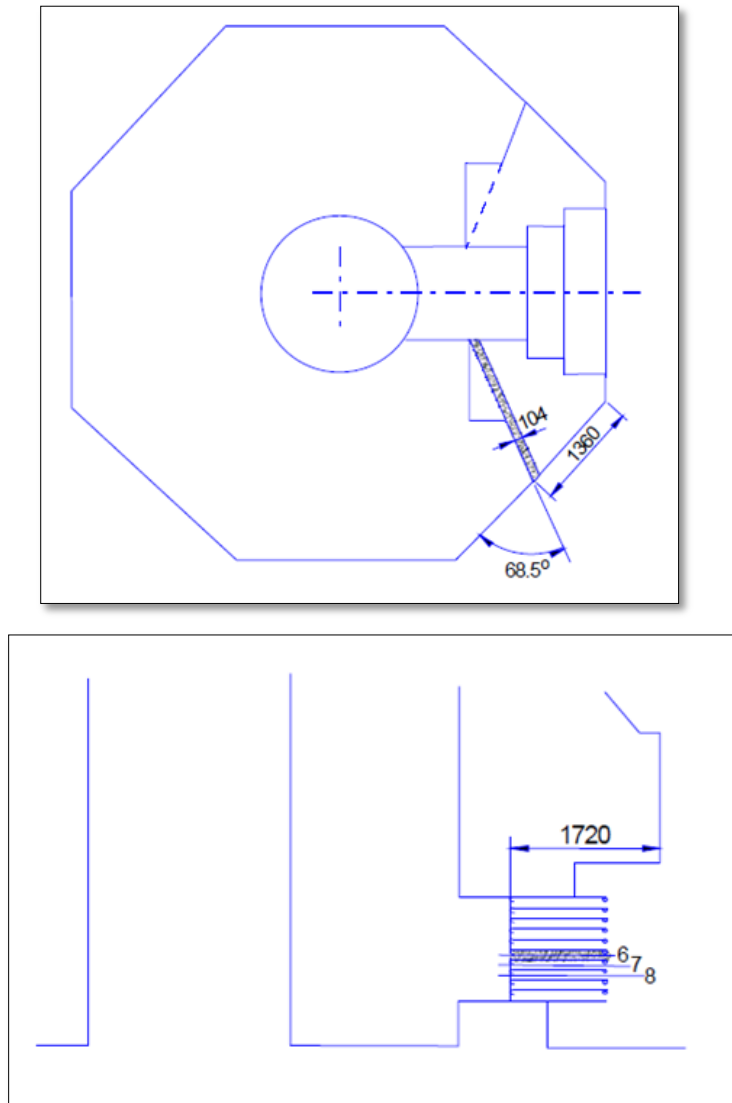


Figure 3.4 The positions of the diamond drilling samples in the reactor geometry.[27]

Fluental samples (figure 3.5) were irradiated for 4 hours in June of 2015 by placing them in the reactor core irradiation positions. The samples were then weighed and placed in small plastic canisters. Since physical dismantling of the reactor may not yet begin, aluminium samples were taken from the top of the tank, above the water level, and



Figure 3.5 The Fluental sample.

irradiated in the reactor core irradiation positions to mimic the conditions the rest of the tank would experience during the operation of the reactor. As with Fluental, samples were irradiated for 4 hours in June of 2015, weighed, and placed in small plastic canisters.

The ion-exchange resin is used in the cooling circuit of the FiR 1 research reactor to purify the water. In order to minimise corrosion and radioactivity during reactor operation, the reactor tank water conductivity has been kept below  $1.5 \mu\text{S}/\text{cm}$ , since any impurities in the water could become activated in the neutron interactions. The nuclear grade resin used is AMBERLITE™ IRN150 resin [80] with a density of 690 g/L.

### 3.3 Sample measurement

#### 3.3.1 Measurement equipment

To perform measurements for each of these samples, a wide range of detectors are available, including gas-filled, scintillation and semi-conductor detectors. Because of their high density, semi-conductor detectors, such as HPGe detectors, are well suited for the measurement of  $\gamma$ -rays. Although  $\beta$  and  $^3\text{H}$  measurements are discussed in detail in the previous chapter, this thesis will focus on  $\gamma$ -ray spectrometry using a HPGe detector.

When ionising radiation interacts within the semi-conductor absorbing medium, it causes excitations of electrons from the valence band to conduction band above the band gap. Electrons leave holes behind in the valence band, forming electron-hole pairs. In an applied electric field, the electrons move in the conduction band, and holes move in the valence band. A hole moves in the same direction as the field when an electron leaves a normal valence site to fill an existing hole.[41] These currents are collected by electrodes producing a pulse dependent on the energy deposition of the ionising radiation in the semi-conductor.[17]

Sample measurements were performed using In Situ Object Counting System (ISOCS) equipment supplied by CANBERRA. It is a measurement tool designed specifically for in situ measurements. It offers high resolution, high sensitivity measurements with short measurement times. The cryostat and mounting station allow the HPGe detector to be pointed in any direction. Efficiency calibrations are easily performed with this system for almost any geometry, with no radioactive sources required for the calibration. It is also battery powered, greatly improving mobility. The field of view can be adjusted using 30°, 90°, or 180° collimators.[81] In addition to the detector, ISOCS components include:

- shields and collimators
  - adjustable shielding and collimation capabilities;
- portable workstation
  - provides a portable mounting base for the ISOCS system;
  - includes a pivoting detector holding mechanism;
  - includes a battery powered Digital Signal Processor;
- laptop with Genie 2000 software
- ISOCS calibration software
  - allows for accurate efficiency calibration

The ISOCS system specifications and settings for these measurements are shown in table 3.2.

### 3.3.2 Energy calibration

A typical point source calibration was performed using the sources  $^{241}\text{Am}$ ,  $^{54}\text{Mn}$ , and  $^{60}\text{Co}$ . With the 59.54 keV transition from  $^{241}\text{Am}$ , the 834.83 keV transition from  $^{54}\text{Mn}$ , and the 1173.2 and 1332.5 keV transitions from  $^{60}\text{Co}$ , both high and low energies are represented. Energy calibration in general is performed with a calibration standard through the use of certificate files created by the user. The certificate files contain information regarding the calibration standard. Once the calibration standard has been counted, the resulting spectrum is compared to the information in the certificate files, including the energies of the nuclides in the standard. The user is able to select peaks in the spectrum and match it to its corresponding energy listed in the certificate file.

Table 3.2 System specifications.

ISOCS version	Version 4.3
Laptop specifications	HP Compaq nc6220, WIN XP, Genie 2000 version 3.3
Detector model	BE2020
Detector relative efficiency	20%
Detector HV settings	+3000V

### 3.3.3 Physical measurements

The concrete sample was placed at some distance away from the detector so that the full concrete sample was within the collimation solid angle of the detector. This reduces the efficiency, but produces a better representation of the sample since the uncertainty due to inhomogeneity is higher the closer the sample is to the detector. The efficiency in this case refers to the absolute efficiency: the number of counts actually detected over the number of counts emitted in all directions.[82] The measurement time is normally determined by considering some factors:

- the number of counts recorded in a measurement. There should be enough counts to produce a reasonably low uncertainty. This is limited by background counting.
- the activity of the sample. These samples were drilled in 1996 and have a low activity.
- the distance from the detector. Placing the sample closer to the detector improves efficiency.

A background measurement was performed using an inactive drill sample of similar geometry to the active one. This was done because concrete naturally contains U and Th radioactive nuclide series. Performing the background measurement in this way allows these background radioactive nuclides to be subtracted.

The Fluental and aluminium samples were characterised by placing them on top of the detector after nearly four months of cooling, with a measuring time determined according to the same factors as the concrete samples. A background measurement was performed for later subtraction.

Measurement of barrels containing the ion-exchange resin is shown in figure 3.6. The barrel was rotated using a motorised platform, and 1 rotation was completed every 56 seconds. This was done because the activity distribution is not known and could be inhomogeneous. The activity level is small, and so the detector was positioned close to the barrel. The collimator opening was set to the largest possible angle so that the whole barrel was within



the collimation solid angle of the detector. In this way, the efficiency was maximised and the measurement time was minimised. The overall weight of the contents was also measured and the average density was calculated and taken into account in the analysis as a self-shielding factor. This procedure was performed for 13 barrels, and a background measurement was performed for later subtraction.



Figure 3.6 Ion-exchange resin measurement set-up.



## Chapter 4: Analysis

Upon completion of the measurements, the analysis was performed using Genie 2000 software. Analysis begins with modelling each of the measurement set-ups for the purpose of determining an efficiency calibration without the use of calibration sources or further MCNP calculation. Following this, peak area determinations, nuclide identification and activity calculations were performed.

### 4.1 Modelling the measurement set-ups

A “simple cylinder” geometry template was chosen for each of the samples and modified to represent the real sample as closely as possible, by entering certain information about the sample. This information includes the source length, the source diameter, and the source to detector distance, as shown in figure 4.1. The dimensions are shown for the remaining cases in table 4.1. The material composition and density of the samples can be chosen from the library or defined by the user.

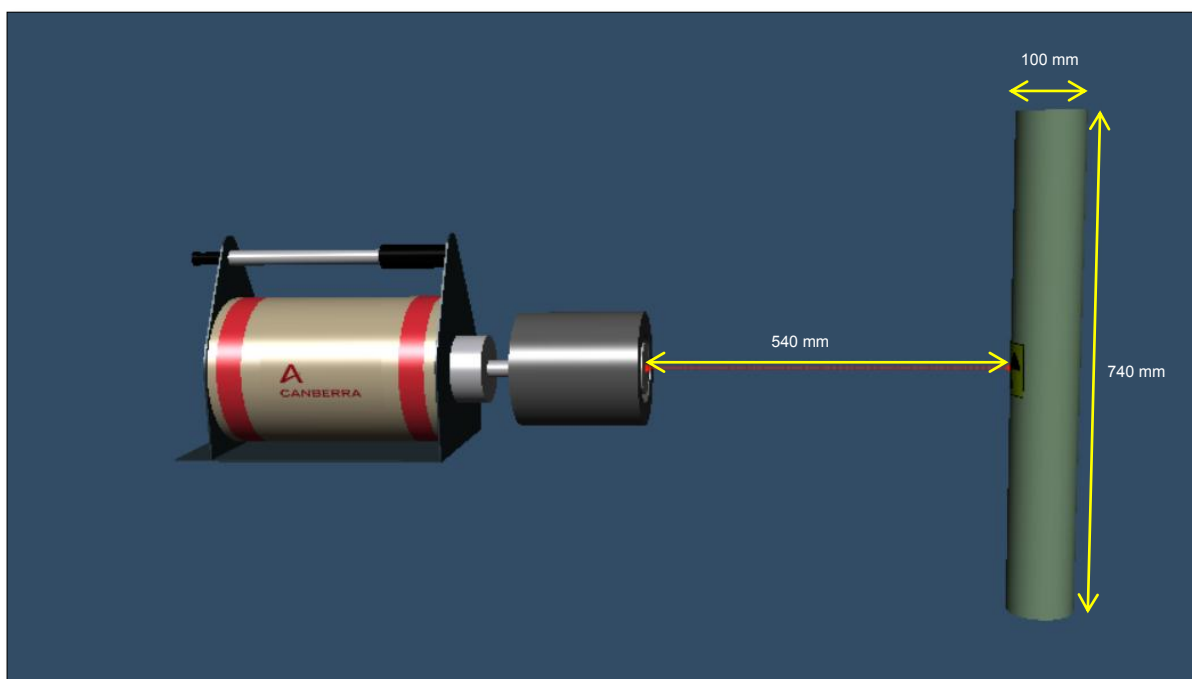


Figure 4.1 Example of the modelled measurement set-up, with dimensions shown for the concrete measurement set-up.

Table 4.1 Dimensions [mm] of each of the measurement set-ups.

	Source length [mm]	Source diameter [mm]	Distance from source to detector [mm]
Concrete	740	100	540
Fluental	10	10	3
Aluminium	4	10	3
Ion-exchange resin	620	400	465

Since it would be too time consuming to re-perform the calibration for each of the 13 barrels containing the ion-exchange resin, two calibrations are performed. The first calibration is done for barrels that are half full (figure 4.2a), and the second for completely full barrels (figure 4.2b). Each barrel is then classified as either half or completely full according to its weight and calibrated accordingly. The maximum error associated with this simplification is determined by calibrating the results from the same barrel using both calibrations and finding the difference, and shown in table 4.2.

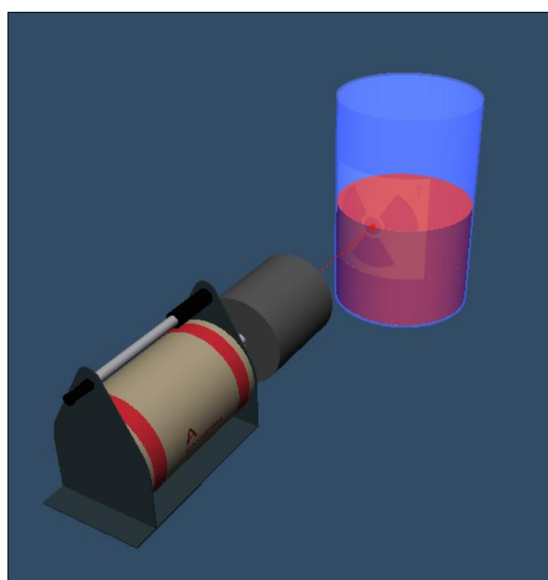


Figure 4.2a Model of the half full ion-exchange resin measurement set-up.

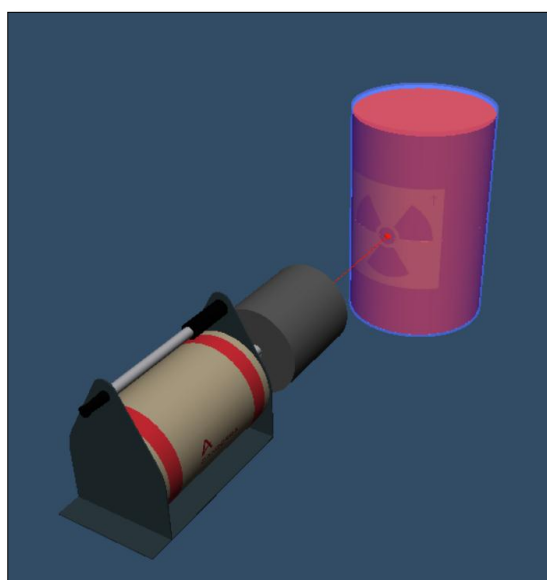


Figure 4.2b Model of the completely full ion-exchange resin measurement set-up.

Table 4.2 The maximum error associated with simplifying calibrations as either half full or completely full.

Nuclide Name	Half	Full	Maximum Error Bq/unit
	Mean Activity Bq/unit	Mean Activity Bq/unit	
<sup>60</sup> Co	2.10E+05	2.09E+05	7.35E+02
<sup>109</sup> Cd	5.67E+04	5.65E+04	2.20E+02
<sup>137</sup> Cs	6.60E+05	6.57E+05	2.46E+03
<sup>152</sup> Eu	5.63E+03	5.61E+03	2.49E+01
<sup>231</sup> Th	9.56E+04	9.52E+04	3.68E+02

#### 4.2 Efficiency calibration

Because the set-up is energy calibrated, the resulting spectra peaks indicate which nuclides are present. The present nuclides determine whether an efficiency calibration needs to be performed according to their half-lives. If all the nuclides present are short lived, they can be disposed of after an appropriate delay while waiting for the nuclide to decay sufficiently. The presence of long lived nuclides (relative to cooling time) requires an efficiency calibration so that the activity of the nuclides may be determined from the number of counts per second. This allows for the planning of their safe disposal. Knowing the activity allows comparison to regulatory levels, which will determine which of category radioactive waste it falls into.

Generally speaking, the efficiency calibration is done by determining the quantitative relationship between the response of the measurement system and a given quantity of the substance.[83]

The detector, collimators and source are modelled as close as possible to reality using a Geometry Composer. This is shown in section 4.1. The program first verifies the geometry definition before allowing an efficiency curve to be generated. Efficiency data points are automatically generated from the defined geometry. The input file that needs to be calibrated according to this geometry is selected and the calibration is completed. The efficiency curve and a report are generated, and the calibrated data source is ready for use.

Using ISOCS allows a relatively fast method for determining efficiency calibrations for a large variety of sample geometries. Ordinarily, a calibration source or some Monte Carlo modelling tool would be required, but calibration sources can be costly and Monte Carlo modelling tools can be time consuming because of the time to perform calculations and code running times. Although ISOCS actually uses a set of MCNP calculations performed at Canberra, the user is not required to use MCNP.

The peak detection efficiency  $\varepsilon$  is a function of energy (E), and is defined as

$$\varepsilon(E) = \frac{P}{T y A C_1 F}$$

where P is the net peak area of the calibration peak, T is the measurement live time, y is the branching ratio of the calibration nuclide at energy E, A is the activity of the source at certificate time,  $C_1$  is a correction factor to take the decay of the nuclide from certificate time to the time of measurement into account, and F is a factor to correct the units of the activity A.[84]

An efficiency curve is determined through the use of a peak search algorithm that matches located peaks to known emission rates for each line.[85] The efficiency as a function of  $\gamma$ -ray energy is given for the different geometries in figure 4.3a-c.

#### 4.3 Peak area determination

The library consists of a list of energies that is used by the algorithm to build a table of peak locations. A linear least squares fit is performed to verify the existence of each peak. Instead of this, the user can also define regions of interest. Next, net peak areas are calculated in one of two ways. Either a sum/non-linear least squares fit is performed, or a library (Gamma-M) method is used.[85]

The sum/non-linear least squares fit method begins by determining the limits of the peak region based on either the results of the peak locate algorithm, or the user defined regions of interest in the peak locate step. In the former case, it is necessary for the algorithm to determine whether adjacent peaks should be analysed as singlets or multiplets. This is done by comparing adjacent centroids. If

$$c_{i+1} - c_i < n_W \cdot FWHM_i$$

then the two adjacent peaks with centroid  $c_{i+1}$  and  $c_i$  form a multiplet. In this equation,  $n_W$  is the user defined separation parameter, and  $FWHM_i$  is the FWHM of the peak with centroid  $c_i$ . The analysis of singlets is simpler; the algorithm determines the total number of counts in the peak before removing the background, whereas the analysis of multiplets involves a non-linear least squares fit to determine peak areas. In this fitting technique, the mathematical model describing the peak region (which may include singlets or multiplets) is given by some function:

$$F(x_i, \alpha_1, \alpha_2, \dots, \alpha_m) = y_i \quad (4.1)$$

where  $y_i$  represents the counts corresponding to channel  $x_i$ . This function is then linearly approximated iteratively with each successive iteration improving the free parameters ( $\alpha$ ) of the model. The result is a set of linear equations that can be expressed in matrix form and solved. Tests are performed to make sure this matrix can be solved; otherwise peaks are deleted from the multiplet until it can be solved. Once the best fit has been achieved, individual peak areas are determined (whether the peak is within a multiplet or just a singlet) by integration.[84]

The library (Gamma-M) method fits the expected model to each peak in the table of peak locations. During this step, interfering peaks are identified and corrected by removing their contribution to other peaks.[85]

Interactive Peak Fit (IPF) is an option for the user to add to the analysis sequence to manually evaluate and adjust the peaks the program finds automatically. The user can influence the peak area calculation by adding peaks the program ignored for statistical reasons or deleting irrelevant peaks. The IPF window shows each multiplet or singlet in order of increasing energy. Figure 4.4 shows a peak that is considered too wide and separated into two peaks. A solid shaded region is shown below the peaks. This is the background continuum that needs to be subtracted. There are various possible ways in which this can be done, but initially the software will perform a simple linear interpolation between the values at either ends of the peak. For many purposes this is sufficient, but a slightly more complicated background subtraction technique is applied in a subsequent step in the analysis procedure and discussed in section 4.4. The plot shown below the peaks in figure 4.4 represents the difference between the fit and real data.[86]

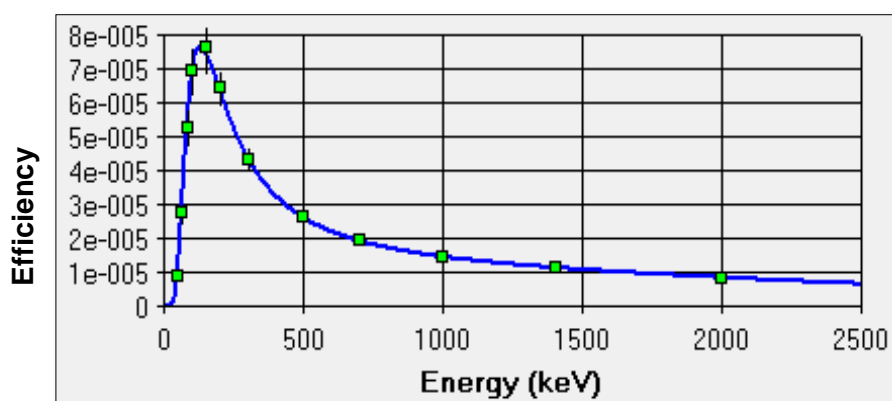


Figure 4.3a The efficiency as a function of  $\gamma$ -ray energy for the concrete geometry.

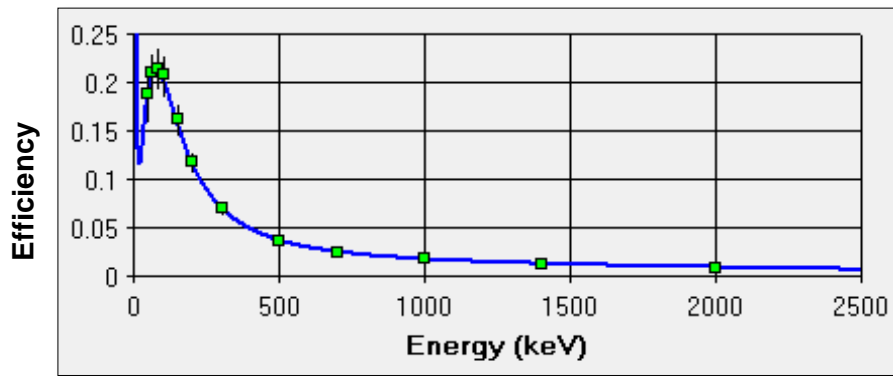


Figure 4.3b The efficiency as a function of  $\gamma$ -ray energy for the Fluntal and aluminium geometries.

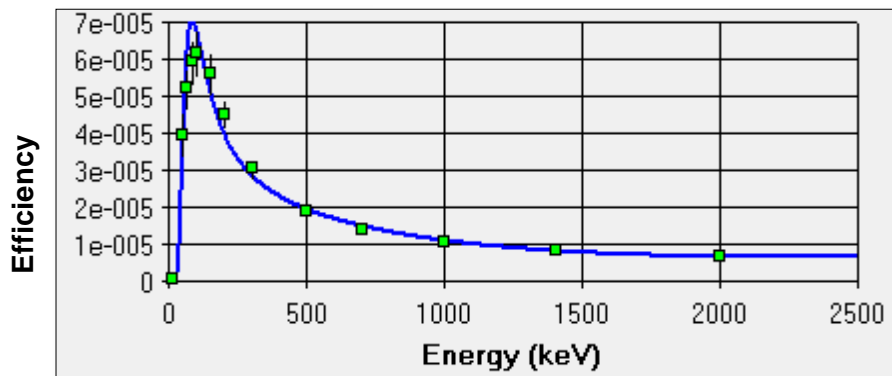


Figure 4.3c The efficiency as a function of  $\gamma$ -ray energy for the full barrel ion-exchange resin geometry.

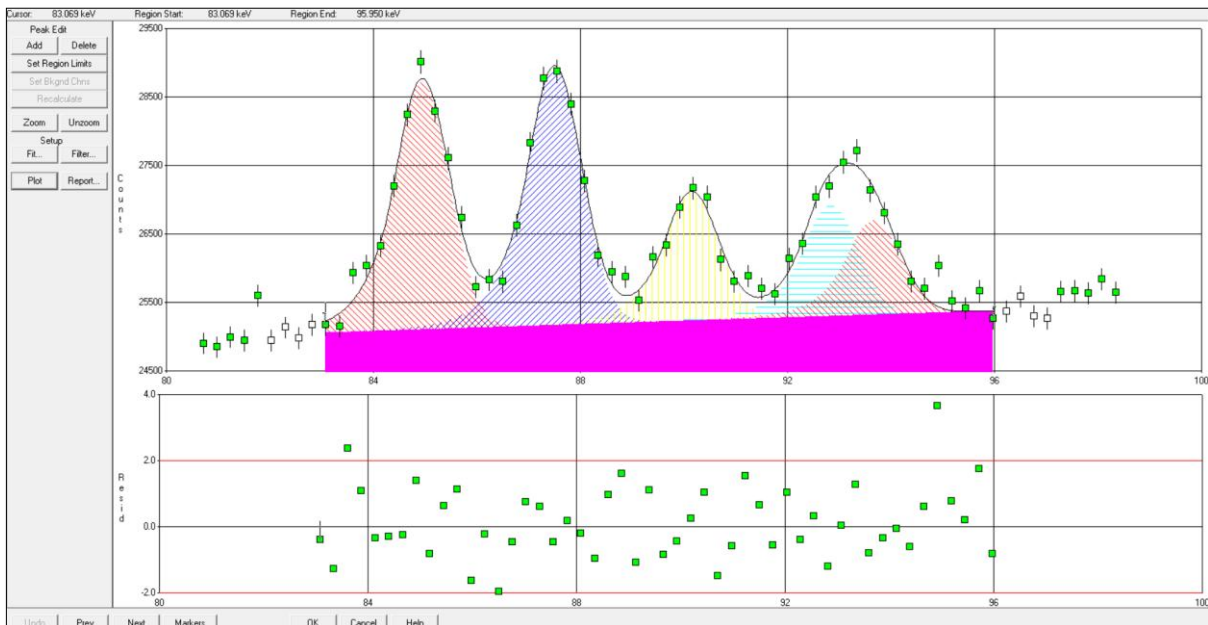


Figure 4.4 Interactive Peak Fit showing single wide peak being corrected to two peaks.

#### 4.4 Nuclide identification and activity calculation

The analysis library consists of many nuclides, along with some characteristic information about the nuclide. This includes all energy lines, half-lives and branching ratios. For the nuclide identification (NID) algorithm to identify a nuclide, it requires that one or more  $\gamma$ -ray transitions fall within a certain energy tolerance of a peak in the spectrum. This energy tolerance is defined by the user. For nuclides with multiple energies, the sum of the branching ratios of energies with corresponding peaks in the spectrum is compared to those without, in order to determine a positive identification of the

		NUCLIDES				
		1	2	3	4	5
PEAK ENERGIES	1					X
	2	X	X			
	3					
	4			X	X	
	5	X				
	6				X	
	7			X		
	8					
	9					X

Figure 4.5 Matrix of identified nuclides.[68]

nuclide. The algorithm also requires that the decay time of the spectrum be comparable to the nuclide's half-life.

The user defines a confidence index with which a nuclide must pass these tests in order to be considered as identified. This results in a matrix of nuclides and peak energies, an example of which is shown in figure 4.5. In this figure, the first peak energy has been found to correspond to the fifth identified nuclide. The second peak energy has been found to correspond to both the first and the second identified nuclide, etc.[84]

The algorithm then determines the specific activity for each energy with a corresponding spectrum peak, for every positively identified nuclide.[87]

The specific activity  $S$  is calculated by:

$$S = \frac{P}{m \varepsilon' y T F C_1 C_2} \quad (4.2)$$

where  $P$  is the net peak area of the calibration peak,  $m$  is the sample mass (this could also be volume),  $\varepsilon'$  is the attenuation corrected efficiency,  $y$  is the branching ratio of the

calibration nuclide,  $T$  is the measurement live time,  $F$  is a factor to correct the units of the activity,  $C_1$  is a correction factor to take the decay of the nuclide from certificate time to the time of measurement into account, and  $C_2$  is a correction factor to take into account decay during counting.

There is a random uncertainty  $\sigma_S$  associated with the specific activity  $S$ , determined by:

$$\sigma_S = S \sqrt{\left(\frac{\sigma_R}{100}\right)^2 + \left(\frac{\sigma_P}{P}\right)^2 + \left(\frac{\sigma_m}{m}\right)^2 + \left(\frac{\sigma_{\varepsilon'}}{\varepsilon'}\right)^2 + \left(\frac{\sigma_y}{y}\right)^2 + \left(\frac{\sigma_C}{C}\right)^2} \quad (4.3)$$

where  $\sigma_R$  is the random uncertainty selected by the user,  $\sigma_P$  is the peak area  $P$  uncertainty,  $\sigma_m$  is the sample mass  $m$  uncertainty,  $\sigma_{\varepsilon'}$  is the effective efficiency  $\varepsilon'$  uncertainty,  $\sigma_y$  is the yield  $y$  uncertainty, and  $\sigma_K$  is the uncertainty associated with a composite of the decay corrections  $C_1$  and  $C_2$ .

The total uncertainty of the specific activity is given by:

$$\sigma_{S(T)} = \sigma_S + \frac{\sigma_{sys} \cdot S}{100} \quad (4.4)$$

where  $\sigma_{sys}$  is the systematic uncertainty defined by the user.[84]

Decay correction is taken into account in the calculation of the specific activity, including correction for the decay during the time between sample taking and acquisition, the decay during the acquisition time, as well as any decay during sample taking. An additional decay correction is made for those nuclides not in equilibrium with their daughters. There is an algorithm for this correction based on the time at which the sample is taken, the time at which the acquisition begins, the acquisition time, and information about the parent and daughter nuclides in the nuclide library.[87]

Background spectra are acquired to determine exactly which peaks are as a result of the sample. In order to perform an adequate subtraction, peak location and area determinations should also be performed on these spectra. Peak area determination is discussed in section 4.3. The acquisition time of the background spectrum does not have to be the same as the sample spectrum, because the algorithm will scale the results of the background spectrum accordingly. Once again, a user defined energy tolerance is used to determine which peaks in the two spectra correspond to one another. A reference source of known count rate can be used to introduce a reference peak to the spectrum. This allows a correction to be made through the normalisation of all other peaks according to the reference peak. This can be performed in addition to the background subtract algorithm for the best results.[87]



The corrected peak areas following background subtraction  $P'$  is given by:

$$P' = R \cdot (G - B) - I \quad (4.5)$$

where  $R$  is a random summing correction factor which is set to 1 if the reference peak correction described above is not applied,  $G$  is the gross counts in the region of interest surrounding the peak,  $B$  is the continuum subtracted from the  $G$ , and  $I$  is the environmental background interference. The calculation for  $I$  is given by:

$$I = \frac{T_L}{T_b} \cdot I_b \quad (4.6)$$

where  $T_L$  is the spectrum live time, and  $T_b$  is the background spectrum live time.  $I_b$  is the peak area in the background spectrum, given by:

$$I_b = R_b \cdot (G_b - B_b). \quad (4.7)$$

The final peak area, once corrected for the continuum background as well, is given by:

$$P' = R \cdot \left( G - \frac{N}{2n} (B_1 + B_2) \right) - I \quad (4.8)$$

where  $N$  is the number of counts in the region of interest surrounding the peak in the background spectrum,  $n$  is the number of continuum channels,  $B_1$  is the total number of counts in the low energy continuum region, and  $B_2$  in the higher energy region.[84]

## Chapter 5: Results and Discussion

After efficiency calibration and nuclide identification analysis, the Gamma Acquisition and Analysis program provides a spectrum, which shows all nuclides that may be present. Alongside this, a report file is generated which provides the activity of each radionuclide present in Bq/unit. The final activity concentration is calculated by taking the weighted average of activity concentrations calculated using individual  $\gamma$ -ray lines associated with a particular radionuclide. The activity of each radionuclide can then be compared to the accepted release levels provided by radiation safety authorities in order to make decisions about disposal. The half-life of the radionuclide is also considered in this decision. All activities shown are at the time of measurement. The calculated activities have been corrected to the measurement time, while the measured activities involve no decay corrections.

### 5.1 Concrete

The  $\gamma$ -ray spectrum for the concrete measurement is shown in figure 5.1. The background spectrum is shown in addendum B. The software provides many possible nuclides which the user can then evaluate and decide which are realistic. All short living nuclides are eliminated, where a half-life of 100 days or less is used as the criteria for “short living”. Those nuclides with a relative uncertainty greater than 45% are found to coincide with those nuclides not predicted in the inventory report, and ignored. Other nuclides are ignored because they are found not to exist in the spectrum. The remaining nuclides are compared with the inventory calculations as shown in table 5.1. Also shown are the half-lives and peak confidences. The relative uncertainty is calculated by dividing the activity uncertainty provided by the program, by the activity (Bq/unit) (the algorithms for both of which are discussed in section 4.4). The  $\gamma$  energies used in the activity calculation are listed per radionuclide in Addendum C.

Comparing the last two columns of table 5.1 shows that major discrepancies exist between measured and predicted activities for  $^{22}\text{Na}$  and  $^{65}\text{Zn}$ . It is possible  $^{154}\text{Eu}$  has been misidentified as  $^{22}\text{Na}$  since both nuclides have the 1274.5 keV line. The required activating element for  $^{65}\text{Zn}$  to be formed is not present in the material composition in the ORIGEN-S calculation, and so the calculation is unable to accurately predict the  $^{65}\text{Zn}$  activity. Measured and predicted activities for  $^{60}\text{Co}$  and  $^{152}\text{Eu}$  agree with an uncertainty of 11% and 2.3%, respectively. These are the most important nuclides that will be used later for building the scaling matrix for hard-to-measure activities. Generally, when studying materials as large as the concrete biological shield, it is assumed that the material composition is homogeneous.

A small sample is taken and studied thoroughly with both  $\beta$  and  $\gamma$  measurements to find the fractions of activities per nuclide. When the rest of the biological shield is measured using  $\gamma$  techniques, the same fractions of nuclide-wise activities are assumed for the full biological shield, allowing the  $\beta$  measurements to be determined. This assumption is acceptable because the  $\beta$  and  $\gamma$  activities both result from the same neutron flux and both are linearly proportional to the density of the flux.

## 5.2 Flualtal

In the same way, a  $\gamma$ -ray spectrum from a Flualtal sample of mass 3.455 g was obtained (see figure 5.2). The background spectrum is shown in addendum B. All short-lived nuclides are eliminated, where this time a half-life of the order hours is used as the criteria for “short-lived” because the sample was irradiated in 2015. The remaining nuclides are compared with the inventory calculations, but no agreement is found between the measured and calculated results. There is not some systematic difference and it could be because the Flualtal composition is not known well enough. The inventory calculation is based on manufacturing specifications, and not measurements. The small activating impurities have no meaning from an operating perspective, so they are not specified in the manufacturing specifications. However, the small activating impurities are essential during decommissioning.

In an attempt to more accurately understand the Flualtal composition, the material composition of the Flualtal is measured by VTT using inductively coupled plasma mass spectrometry (ICP-MS), a highly accurate and sensitive technique for determining elemental compositions. Five measurements are performed and the results are averaged for the ORIGEN-S calculation. The ICP-MS results are shown in addendum D. The small activating impurities are thus taken into account in these calculations. The choice of irradiation position is also assumed in the first set of calculations, but updated to the exact position in the second set of calculations. This improves results because the thermal, epithermal and fast neutron fluxes differ slightly in each irradiation position. In the measurement analysis, a small change is made in the Geometry Composer. In the original model, the source to detector distance is set to 0 mm, as the source is placed on the detector. This distance is increased to 3 mm to account for the fact that there is a plastic cover in place to protect the detector. The efficiency calibration is re-performed and the results are shown in table 5.2. The half-lives and peak confidences are shown. The relative uncertainty (column 7) is calculated by dividing the activity uncertainty provided by the program (column 6), by the activity in Bq/unit (column 5). The  $\gamma$  energies used in the activity calculation are listed per radionuclide in Addendum C.

There is still a large difference in the results, but it is more systematic. The largest source of error is now that the position of the Fluental sample in the capsule (e.g. centre of capsule) is not known exactly. This could be avoided with a larger measuring distance, but the sample activity is too low.

### 5.3 Aluminium

The  $\gamma$ -ray spectrum obtained from a 0.7244 g aluminium sample is shown in figure 5.3. The background spectrum is shown in addendum B. Following the same process of elimination described for Fluental, the list of nuclides shown in table 5.3 remains for comparison with activity calculations. Again there is no agreement between the measured and calculated results, even though the aluminium composition was thought to be quite well understood. It is thought that perhaps there was some contamination with the drill core, but the sample was washed with acid before measurement. Even if there were some contamination, it would not explain differences to this extent. Further investigation is required to understand the large differences found.

The aluminium samples are also sent for ICP-MS to achieve a better understanding of the composition. Three measurements are performed and the results are averaged for the ORIGEN-S calculation. The same changes are made in the measurement analysis of the aluminium sample as for the Fluental sample and the results are shown in table 5.3. The half-lives and peak confidences are shown. The relative uncertainty (column 7) is calculated by dividing the activity uncertainty (column 6), by the activity in Bq/unit (column 5). The  $\gamma$ -ray energies used in the activity calculation is listed per radionuclide in Addendum C. The difference between measured and calculated results are once again much more systematic, but still large.

### 5.4 Ion-exchange resin

Measurements are performed on 13 barrels containing the ion-exchange resin. The spectra obtained from all of the barrels look very similar, although some barrels were more active than others, and some barrels had differences in the nuclides they contained. This is expected since the activity and nuclides do not spread themselves equally into 13 barrels. The  $\gamma$ -ray spectrum from barrel 1091 is shown in figure 5.4. The  $\gamma$  spectra for the remaining resin barrels are shown with the background spectrum in addendum B. Table 5.4 shows each barrel with its mass and calibration approximation, as well as the nuclides present in each. For each nuclide the average activity across all 13 barrels is determined and compared with the release levels. According to these results, if it was not for  $^{137}\text{Cs}$ , these barrels would be safe to release in less than 30 years. Perhaps there was some leaking fuel rod, but the activity is low.

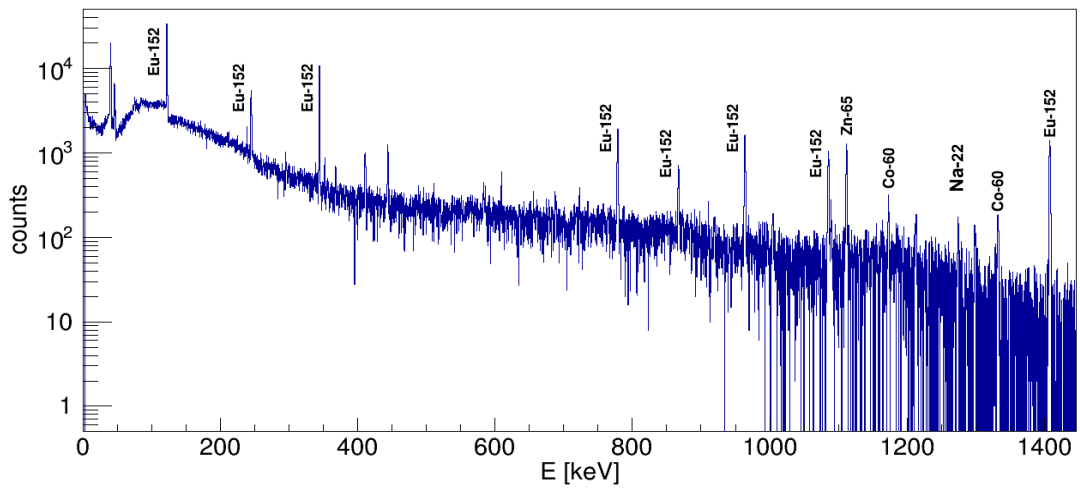


Figure 5.1 The  $\gamma$ -ray spectrum for concrete.

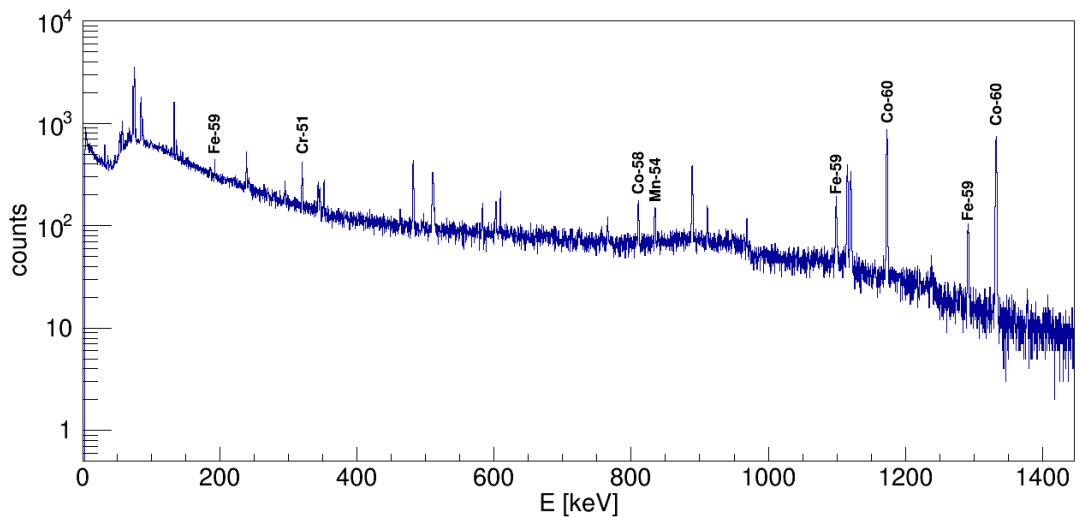


Figure 5.2 The  $\gamma$ -ray spectrum for Fluental.

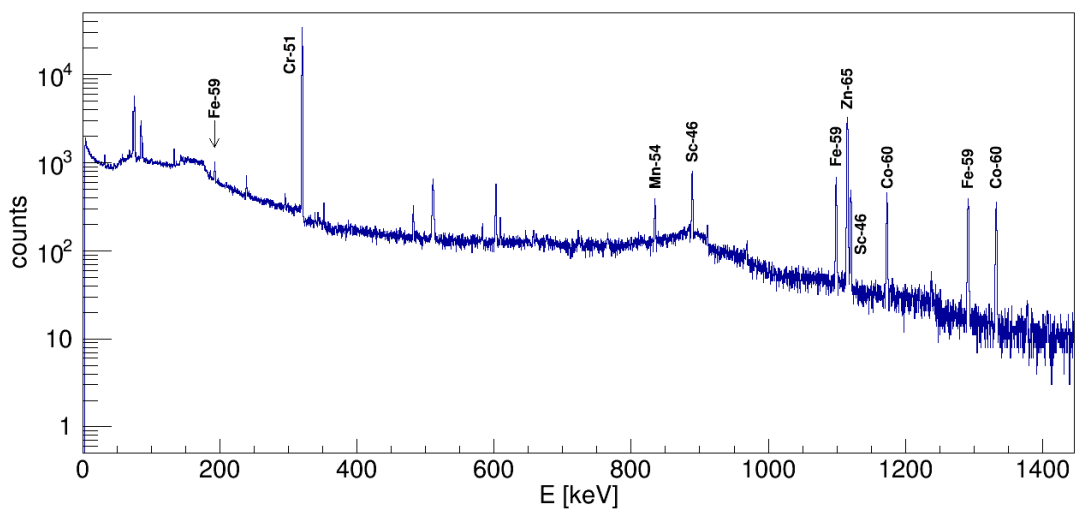


Figure 5.3 The  $\gamma$ -ray spectrum for aluminium.

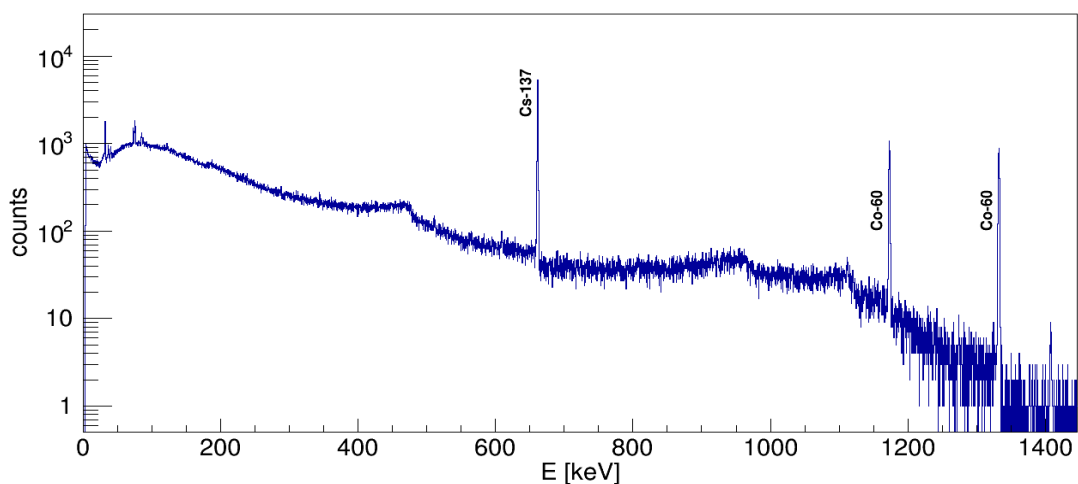
Figure 5.4 The  $\gamma$ -ray spectrum for ion-exchange resin barrel 1091.

Table 5.1 Measured and calculated activities of nuclides found in the concrete sample.

Nuclide	Half-life	Peak Confidence	Activity Bq/unit	Relative Uncertainty	Activity Bq/g	Inventory Calculated Bq/g
$^{22}\text{Na}$	2.603 y	1	1.8E+02	11%	1.2E-02	6.3E-08
$^{60}\text{Co}$	<b>5.274 y</b>	<b>0.998</b>	<b>3.7E+02</b>	<b>11%</b>	<b>2.5E-02</b>	<b>2.6E-02</b>
$^{65}\text{Zn}$	243.9 d	0.999	3.5E+02	12%	2.4E-02	1.9E-33
$^{152}\text{Eu}$	<b>13.52 y</b>	<b>0.996</b>	<b>1.4E+04</b>	<b>2.3%</b>	<b>9.6E-01</b>	<b>8.1E-01</b>

Table 5.2 Measured and calculated activities of nuclides found in the Flualtal sample.

Nuclide	Half-life	Peak Confidence	Activity Bq/unit	Activity Uncertainty	Relative Uncertainty	Activity Bq/g	Inventory Calculated Bq/g
$^{51}\text{Cr}$	27.70 d	1.000	4.4E+00	3.7E-01	8%	1.3E+00	4.8E+01
$^{54}\text{Mn}$	312.2 d	0.999	4.6E-01	7.0E-02	15%	1.3E-01	1.6E+00
$^{58}\text{Co}$	70.86 d	0.999	6.7E-01	6.9E-02	10%	1.9E-01	2.1E+00
$^{59}\text{Fe}$	44.50 d	0.998	2.3E+00	1.4E-01	6%	6.6E-01	5.2E+00
$^{60}\text{Co}$	1925 d	0.999	8.8E+00	2.2E-01	2.5%	2.6E+00	2.4E+01

Table 5.3 Measured and calculated activities of nuclides found in the aluminium sample.

Nuclide	Half-life	Peak Confidence	Activity Bq/unit	Activity Uncertainty	Relative Error	Activity Bq/g	Inventory Calculated Bq/g
<sup>46</sup> Sc	83.79 d	1	3.9E+00	1.1E-01	3%	5.4E+00	1.9E+01
<sup>51</sup> Cr	27.7 d	0.998	5.1E+02	2.4E+01	5%	7.0E+02	2.9E+03
<sup>54</sup> Mn	312.2 d	1	1.3E+00	1.0E-01	8%	1.8E+00	1.0E+01
<sup>59</sup> Fe	44.5 d	0.995	9.8E+00	2.8E-01	3%	1.4E+01	5.3E+01
<sup>60</sup> Co	1925 d	0.996	3.8E+00	1.1E-01	3%	5.2E+00	2.2E+01
<sup>65</sup> Zn	243.9 d	0.999	5.9E+01	1.8E+00	3%	8.1E+01	3.9E+02

Table 5.4 Measured activities of nuclides found in the ion-exchange resin.

Barrel Number	Mass g	Calibration	Activity (Bq/g)		
			<sup>60</sup> Co	<sup>125</sup> Sb	<sup>137</sup> Cs
1091	45400	Full	4.6E+00		1.4E+01
1092	47600	Full	1.7E-01		1.7E+00
1093	43600	Full	4.3E-01		3.7E+00
1094	52400	Full	1.2E+00		2.6E+01
1095	40000	Full	6.3E+00		6.5E+01
1096	35000	Full	1.8E-01		1.6E+00
1097	39200	Full	1.7E-01		4.9E+00
1098	40800	Full	9.4E+00		1.5E+01
1099	44200	Full	3.8E-02	1.3E-01	4.2E-01
1100	40200	Full	2.5E+00		4.1E+01
1101	22200	Half	8.3E+00		1.6E+01
1102	43000	Full	1.3E-01	3.8E-01	6.7E+00
1103	23400	Half	2.4E+01		1.8E+01
		Average (Bq/g)	4.4E+00	4.0E-02	1.7E+01
		Half-life	5.271 y	2.759 y	30.08 y
		Release Level (Bq/g)	0.1	0.1	0.1
		Time Until Safe Release	~ 29 years	-	~ 222 years

## 5.5 Understanding the peak analysis performed by Genie 2000

To demonstrate and understand the peak fitting method, the peak analysis is performed manually using the efficiency curves for the different geometries shown in figure 4.3a-c. In the detector, the exact photopeak has Gaussian energy broadening. The Genie 2000 software performs a peak analysis by fitting a Gaussian function onto the peak area. Thus, a manual Gaussian fit is performed by first converting the original spectra to a non-binary format so that the counts per channel can be read out, and then fitting a Gaussian function to these values. A region of channels is identified as the channels corresponding to a photopeak when there is a sharp increase and subsequent decrease in the number of counts in that region. This is done for one peak of a selected representative nuclide in each of the samples.

Using the background measurements performed, a background subtraction is performed by simply subtracting the number of counts in the background spectrum from the original spectrum, channel by channel. The background measurements were performed for approximately the same amount of time as the original spectrum.

Each of the chosen peaks is fitted, and the result is a Gaussian function which is integrated to find the total number of counts. The activity is determined in the following equation:

$$\text{Activity} = \frac{\text{Total counts}}{\text{Live time} \times \text{Peak intensity} \times \text{Efficiency}}$$

where the efficiency is found from studying the efficiency curve in figure 4.3a-c. The results are summarised and compared to values reported by Genie 2000 in table 5.5. Comparing the last two columns show relatively good agreement, given the rough estimate of the efficiency used in the hand calculation. Of course, this is not a verification of the Genie 2000 result because these calculations are not completely independent of the Genie 2000 software - the efficiency curve used to calculate these values was generated by Genie 2000.

Table 5.5 Comparison of manually calculated activities to values reported by Genie 2000, for selected representative nuclides and  $\gamma$  peaks.

Sample	Peak energy (keV)	Total counts	Live time (s)	Peak intensity	Efficiency	Activity (Bq)	Reported activity (Bq)
Concrete	152Eu: 344	55045	343489.1	26.5%	$4.5 \times 10^{-5}$	$1.34 \times 10^4$	$1.46 \times 10^4$
Fluental	60Co: 1332	6258.6	58579.3	100%	0.02	5.34	8.85
Aluminium	51Cr: 320	65811	60868.6	9.8%	0.05	221	506
Ion-exchange resin barrel 1091	137Cs: 662	31233	3600	85.1%	$1.5 \times 10^{-5}$	$6.80 \times 10^5$	$6.57 \times 10^5$



## Chapter 6: Conclusions

### 6.1 VTT's decommissioning procedure

The decommissioning of Finland's first nuclear reactor is a significant opportunity to learn as much as possible about the process of decommissioning, specifically regarding rules, limitations and legislation in Finland. Lessons learned and knowledge gained (in terms of environmental impact or transport safety analysis, for example) can be applied once Finland's two NPPs require decommissioning.

An important part of the decommissioning procedure is site characterisation. This involves creating a radioactive inventory for the facility, which is necessary for the planning of the required waste packaging, interim storage and final disposal of decommissioning waste. It is also necessary for the radiation safety of the workers performing the dismantling. Although not required by Finnish law, but according to common practice, VTT has produced an activity inventory by modelling and calculations.

The FiR 1 reactor has been modelled with its three dimensional geometry using MCNP to determine the neutron flux at different points in the geometry. This neutron flux is given as input information to the ORIGEN-S code, along with the irradiation history of the reactor. This includes accurate knowledge of the total irradiation hours, detailed knowledge of the reactor operating and cooling times for the years 1976-2015, and the addition of the BNCT unit in the years 1993-1996. Some assumptions have been made for the years 1962-1976 from which time less information is available. The final input parameter for the ORIGEN-S code is the material composition of the region being studied. The result is a nuclide-wise list of activities that is compared to measured data for verification.

ISOCS equipment was used for  $\gamma$ -ray measurements of four different types of samples: concrete, Fluenta, aluminium, and the AMBERLITE IRN150 ion-exchange resin. Data analysis was performed using Genie 2000 software to obtain the nuclide-wise list of activities for comparison.

After ICP-MS to determine accurate sample composition, large differences are still found to exist between calculated and measured results, although these differences are more systematic than initial results. This is possibly due to uncertainty in the placement of the samples within the small plastic canisters.

Although in concrete the calculated and measured activities for  $^{60}\text{Co}$  and  $^{152}\text{Eu}$  agree at least to the same order of magnitude, the activities for the remainder of the nuclides do not agree. It is possible  $^{154}\text{Eu}$  has been misidentified as  $^{22}\text{Na}$  since both nuclides have the 1274.5 keV line. When considering the formation mechanism of  $^{65}\text{Zn}$ , it is found that the required activating element is not present in the material composition in the ORIGEN-S calculation, and so the calculation is unable to accurately predict the  $^{65}\text{Zn}$  activity.

No calculated data are available for the ion-exchange resin, but  $\gamma$ -ray spectra for 13 barrels were measured for the purposes of comparison with regulatory release levels for safe disposal. The highest activity is found to come from  $^{137}\text{Cs}$ , indicating the possibility of a leaking fuel rod. The results indicate that the barrel contents will meet release criteria in approximately 222 years.

In the context of the decommissioning procedure at VTT, these measurements form part of the site characterisation as shown outlined in red in figure 1.10. However, analysis of these samples requires much time and effort. Once dismantling begins in 2018, the large volume of materials and structures to be characterised means it will not be possible to spend as much time on each sample. One of the key issues is that, especially with structures built several decades ago, small impurities are not included in given material compositions because they are not important when it comes to mechanical properties. They are, however, crucial in neutron activation and activity calculation. Having a detailed sample composition, including impurities, will definitely save time when it comes to predicting activities.

## 6.2 ISOCS equipment

The ISOCS equipment has adequately performed its designated tasks, especially in the pre-dismantling phase where in situ measurements are practically the only measurements possible. Its mounting station is mobile and allows measurements in every direction, which can be combined with collimators to adjust the field of view. In addition to this, one of the main advantages of this system is the ease of efficiency calibrations that can be performed. No calibration sources are required for the efficiency calibration, and although ISOCS is based on a set of MCNP calculations, no MCNP modelling is required from the user.

## 6.3 Recommendations for future work

Future work should include optimising the characterisation procedure so that the least amount of time can be spent per sample in both its measurement and its analysis while still producing enough statistics. A more complete characterisation should also be performed by including  $\alpha$  and  $\beta$  measurements of samples. A very important source of activity for the FiR 1 reactor is  $^3\text{H}$  which should be studied in detail.

**Addendum A: Relevant STUK regulations regarding decommissioning.**

- 302** “Pursuant to Section 8 of Government Decree 717/2013 and the optimisation principle of Section 2 of the Radiation Act, the processing and storage of operational waste shall be so designed that the average annual dose to the most exposed individuals of the population, arising from the processing and storage of operational waste as designed, does not exceed the 0.01 mSv constraint.”
- 303** “The annual dose to the most exposed individuals of the population arising as a result of an operational occurrence or accident shall remain below the values indicated below (Government Decree 717/2013, Sections 9 and 10):
- a. 0.1 mSv as a result of an anticipated operational occurrence;
  - b. 1 mSv in the event of a Class 1 postulated accident; and
  - c. 5 mSv in the event of a Class 2 postulated accident”
- 304** “The decommissioning of a nuclear power plant shall be designed based on the objective referred to in para. 302 concerning planned activities, according to which the annual dose constraint of 0.01 mSv shall not be exceeded, and on the dose constraints for operational occurrences and accidents specified in para. 303.”
- 308** “The basic radiation protection requirement for the clearance of nuclear waste is that the annual dose to any member of the public or worker handling the waste does not exceed the constraint of 0.01 mSv, and that the radiation exposure arising from the cleared waste is otherwise kept as low as reasonably achievable. This dose constraint applies to the clearance of materials arising from the operation or dismantling of a single nuclear power plant or other nuclear facility.”
- 309** “The basic radiation protection requirement for the clearance of the buildings and the site of a nuclear facility is that the typical annual dose to the most exposed individual arising from the use of the cleared site and buildings is not more than 0.01 mSv. In a case-specific clearance procedure where the future use of the site and the buildings is restricted, an annual dose of an individual up to 0.1 mSv may be permitted based on radiation protection optimisation. Furthermore, it must be demonstrated by means of analyses that even if the restrictions imposed on the use of the site were to fail, the annual dose arising from use of the buildings and occupancy at the site would remain below 1 mSv with high certainty.”

- 403** “According to Section 7g(1) of the Nuclear Energy Act, the design of a nuclear facility shall provide for the facility’s decommissioning. According to subsection 2, when the operation of a nuclear facility has been terminated, the facility shall be decommissioned in accordance with a plan approved by the Radiation and Nuclear Safety Authority (STUK). Dismantling the facility and other measures taken for the decommissioning of the facility may not be postponed without due cause.”
- 404** “In the design stage of a nuclear facility, a decommissioning strategy shall be established that at least defines the implementation stages with timetables, an outline of the dismantling and waste management solutions adopted, and the end state of the facility site. If the strategy involves a prolonged period of monitored storage prior to the dismantling of the facility, this shall be justified by considerations such as radiation protection optimisation, co-implementation of the decommissioning with other nuclear facilities, or the availability of disposal facilities.”
- 405** “Since its commissioning, a nuclear facility shall have a sufficiently detailed decommissioning plan commensurate with the type and state of the facility in place that is based on the adopted decommissioning strategy. During the operation of the facility, the strategy and plan shall be regularly reviewed and updated where necessary to ensure that they can be used as the basis for the final decommissioning plan drafted after the permanent shutdown of the facility.”
- 406** “According to Section 20 of Government Decree (717/2013), the design of a nuclear power plant shall take account of the decommissioning of plant units so as to limit the volume of waste destined for final disposal, accumulating during their dismantling, and the radiation exposure of workers due to the dismantling of the plant, and to prevent radioactive materials from spreading into the environment during decommissioning and when the waste is processed. These principles shall also apply to the design of other nuclear facilities.”
- 408** “During the design, construction, operation and particularly in connection with final shutdown of a nuclear facility, information concerning the facility that is of use when the decommissioning plan of the facility is kept up to date and when the facility is decommissioned shall be sought out, collected and recorded.”
- 424** “At an operating nuclear facility, activity and surface contamination measurements shall be carried out and the results recorded on a regular basis to provide baseline data for planning and designing the decommissioning of the facility.”

- 425** “At a permanently closed nuclear facility, a comprehensive activity and contamination level survey and recording programme shall be implemented to update the activity data used as the baseline in the final decommissioning plan. The activity and contamination level data shall be updated as the decommissioning proceeds whenever significant changes to them can be assumed to have occurred.”
- 427** “When the decommissioning of a nuclear facility has been completed, a survey of activity and contamination levels shall be carried out to demonstrate that the quantities of radioactive materials remaining in the buildings and soil at the facility site comply with the clearance requirements (paras. 309 and 415).”
- 415** “Buildings left undismantled may be cleared following the general procedure and without restrictions if the average surface activity contamination on the walls, floors and ceilings inside the buildings is less than  $0.4 \text{ Bq/cm}^2$  ( $4,000 \text{ Bq/m}^2$ ). Furthermore, surface activity contamination on any area of one square metre shall be less than  $10,000 \text{ Bq}$ . These surface contamination levels may be applied to nuclide compositions typically occurring at nuclear power plants.”
- 436** “One of the design objectives of a nuclear facility shall be the facilitation of its eventual decommissioning. In the design of the facility, due account shall be taken of the following considerations in particular:
- a. Materials shall be so selected as to minimise the generation and spreading of radioactive materials and to facilitate the cleaning of surfaces.
  - b. The removal of large components, the handling of activated components and the decontamination of systems shall be possible.
  - c. Use can be made of the structures and systems of the facility when the facility is being decommissioned.”
- 437** “When the decontamination, dismantling, transfer, cutting and packing techniques used in the decommissioning of a nuclear facility are selected, an important selection criterion shall be that the radiation exposure of workers, the releases of radioactive materials and the waste volumes generated are kept as low as reasonably achievable. The risk for potential accidents shall be assessed, and to accommodate them, priority shall be given to methods that are proven or otherwise deemed appropriate.”

**Addendum B: All spectra not shown in Chapter 5.**

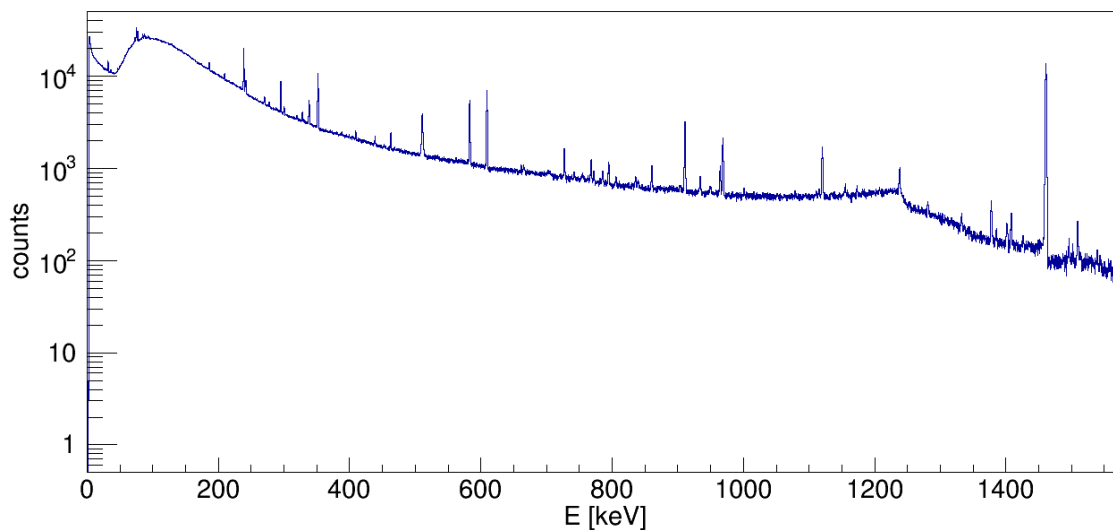


Figure B.1 The  $\gamma$ -ray spectrum for the concrete background measurement.

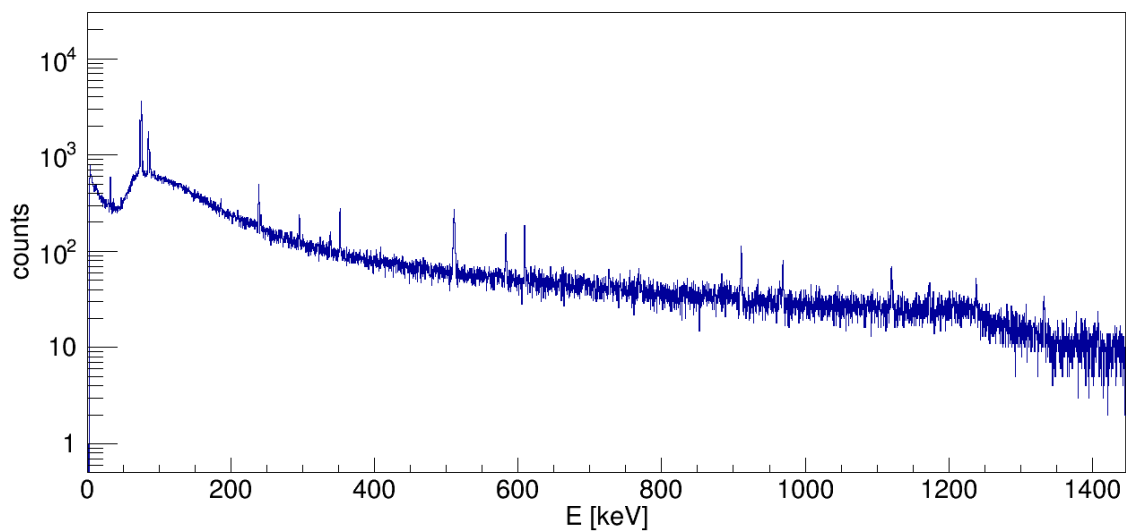


Figure B.2 The  $\gamma$ -ray spectrum for the Fluental and Aluminium background measurement.

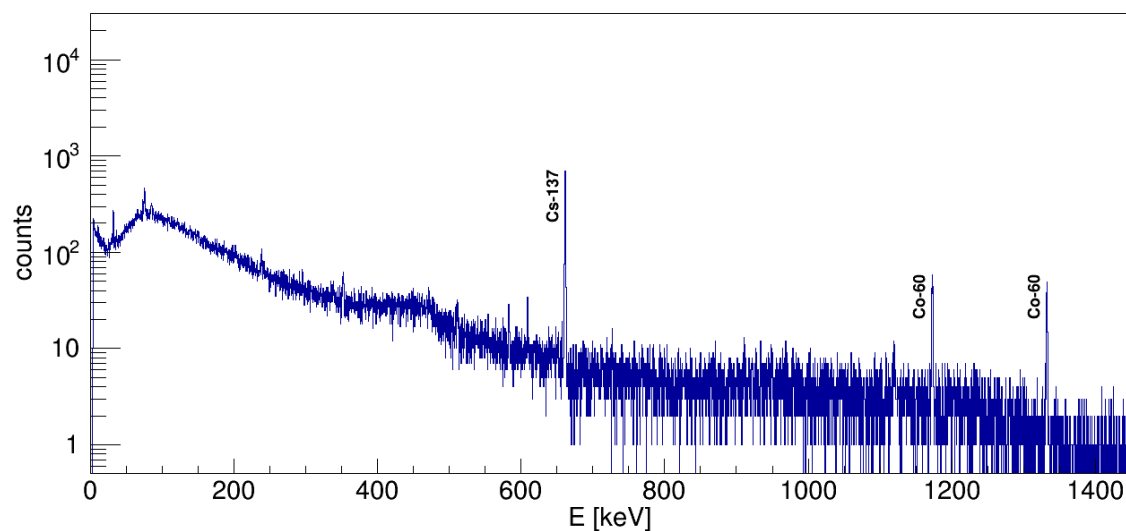


Figure B.3 The  $\gamma$ -ray spectrum for ion-exchange resin barrel 1092.

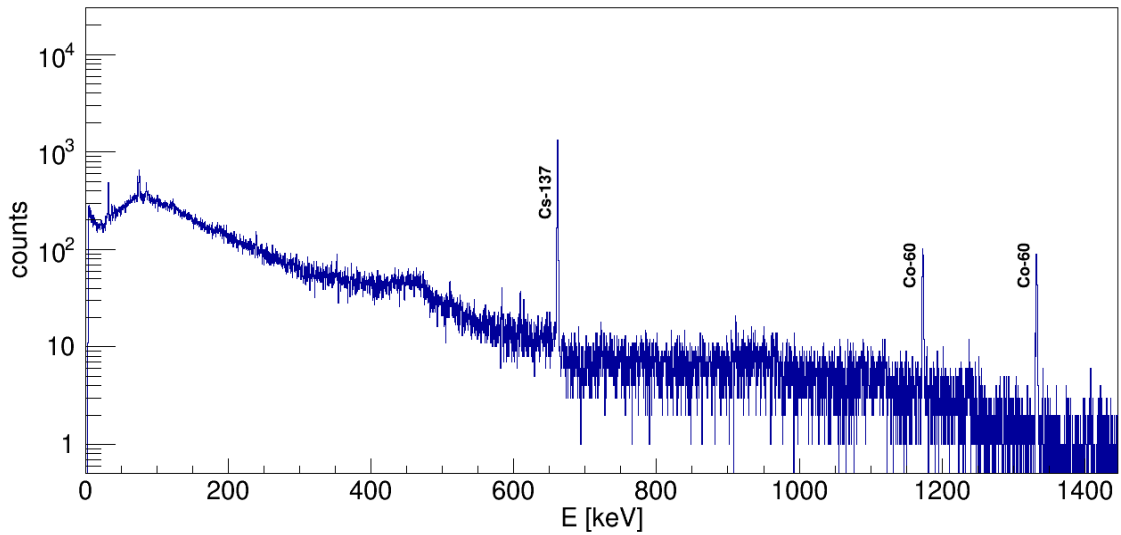


Figure B.4 The  $\gamma$ -ray spectrum for ion-exchange resin barrel 1093.

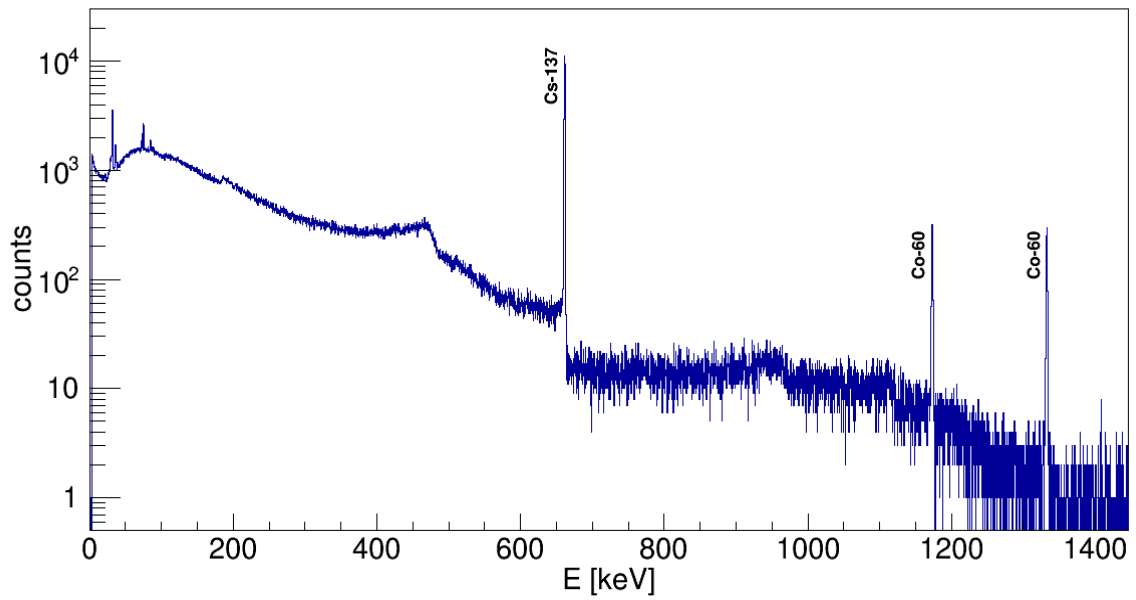


Figure B.5 The  $\gamma$ -ray spectrum for ion-exchange resin barrel 1094.

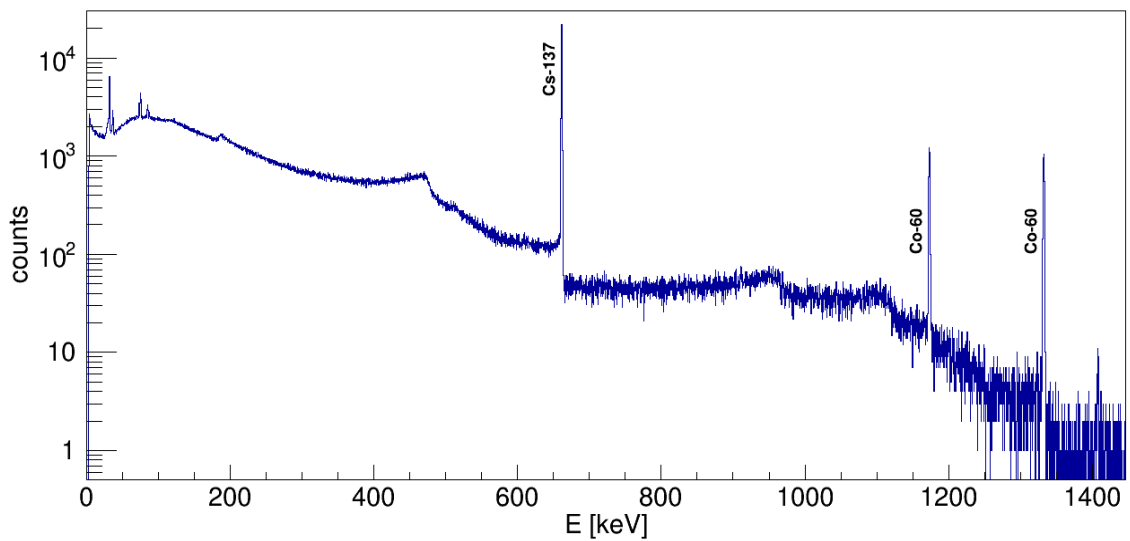


Figure B.6 The  $\gamma$ -ray spectrum for ion-exchange resin barrel 1095.

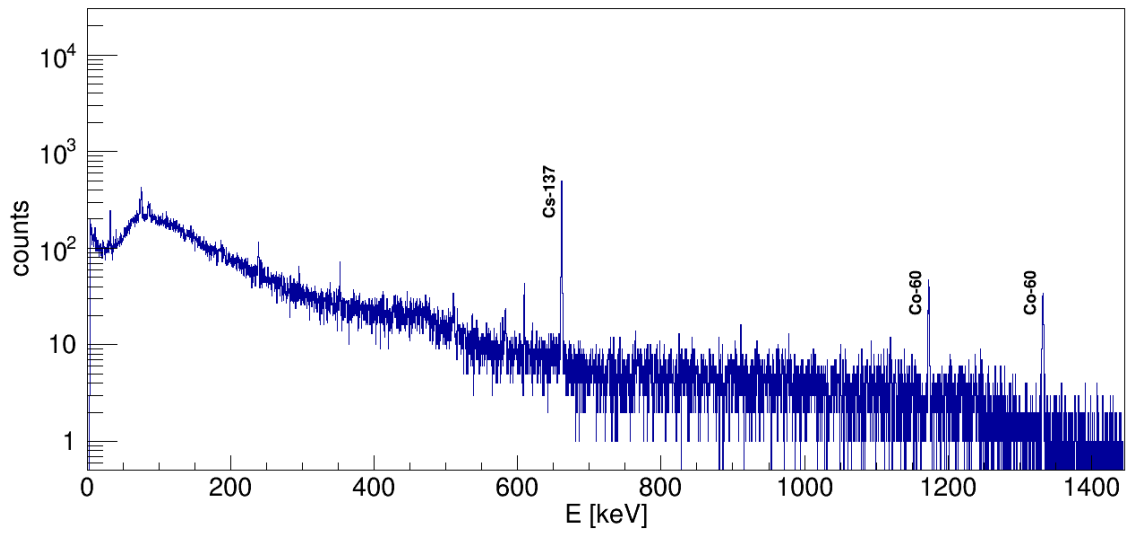


Figure B.7 The  $\gamma$ -ray spectrum for ion-exchange resin barrel 1096.

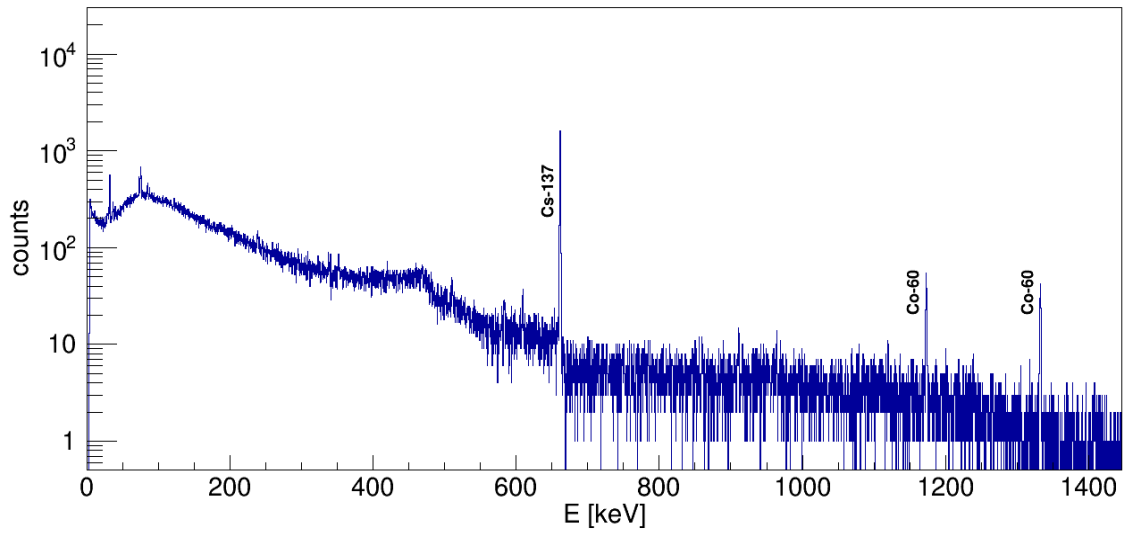


Figure B.8 The  $\gamma$ -ray spectrum for ion-exchange resin barrel 1097.

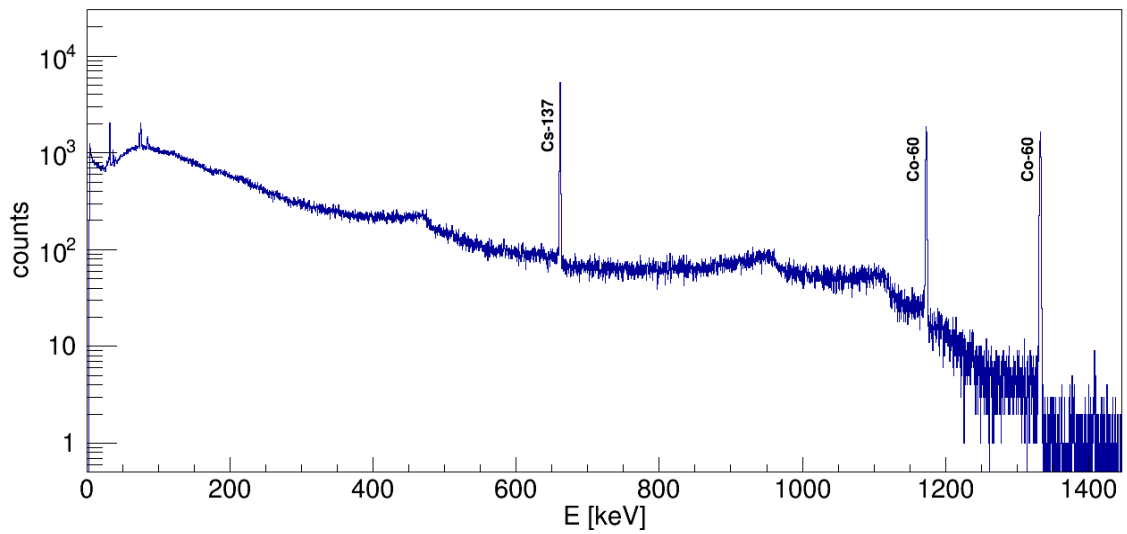


Figure B.9 The  $\gamma$ -ray spectrum for ion-exchange resin barrel 1098.



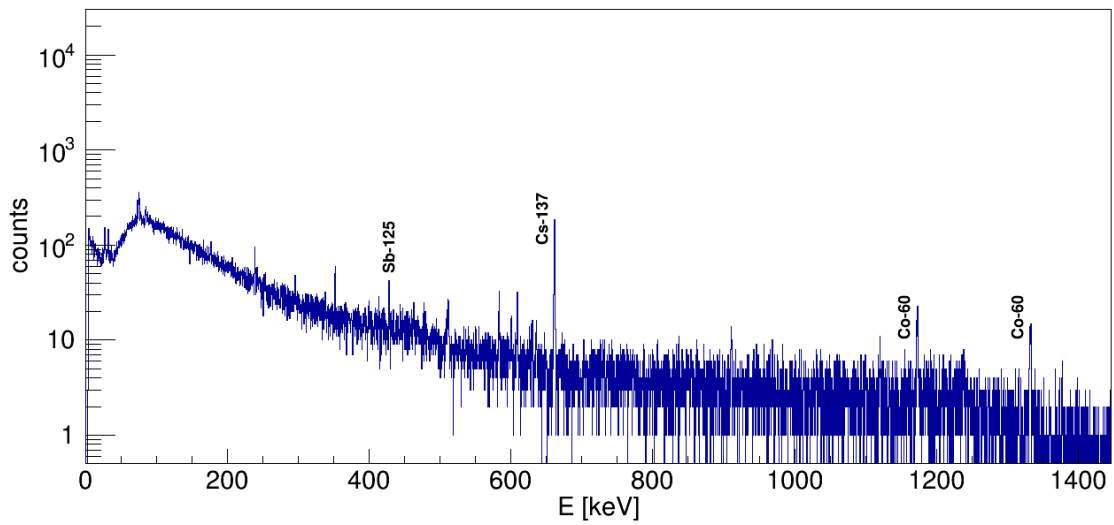


Figure B.10 The  $\gamma$ -ray spectrum for ion-exchange resin barrel 1099.

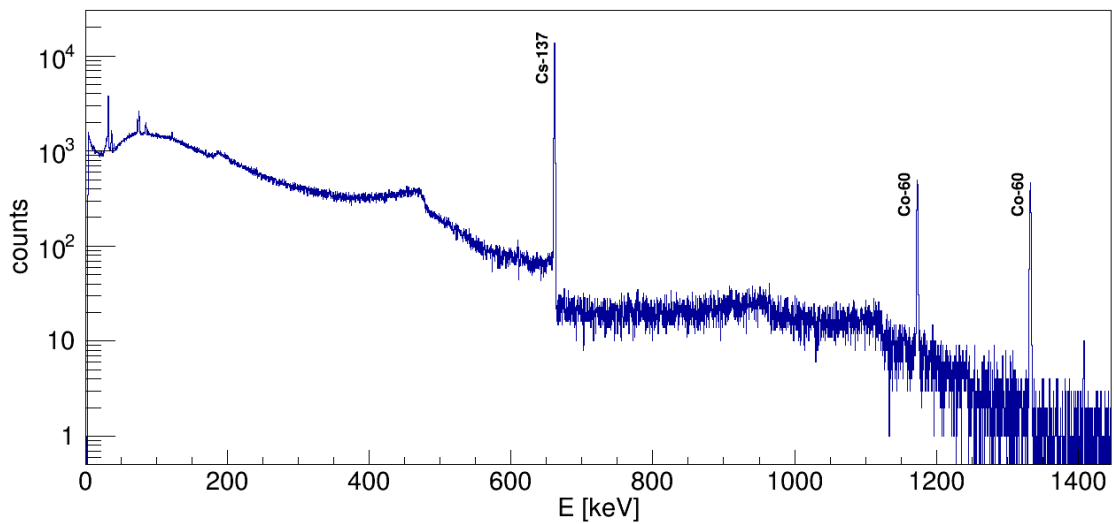


Figure B.11 The  $\gamma$ -ray spectrum for ion-exchange resin barrel 1100.

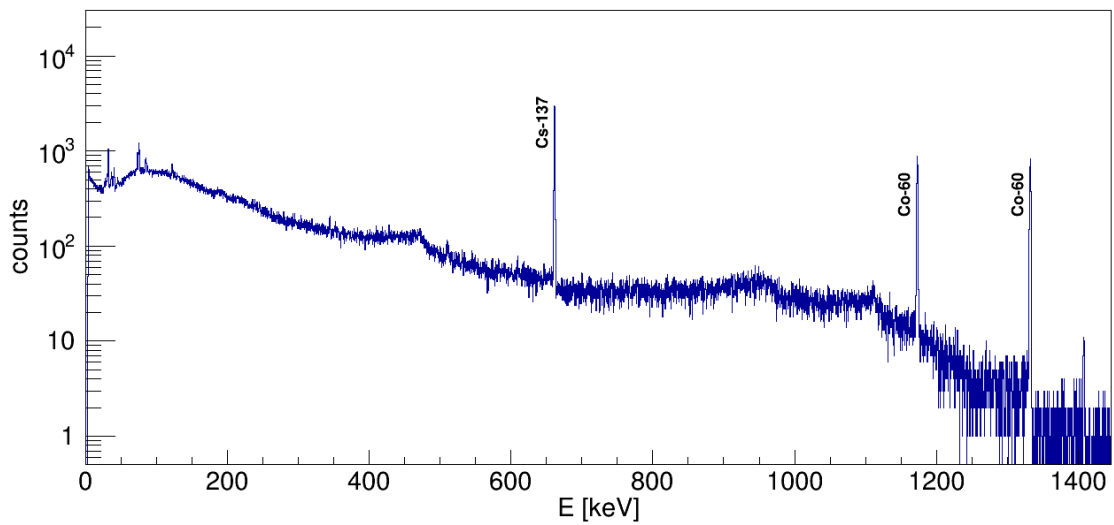


Figure B.12 The  $\gamma$ -ray spectrum for ion-exchange resin barrel 1101.

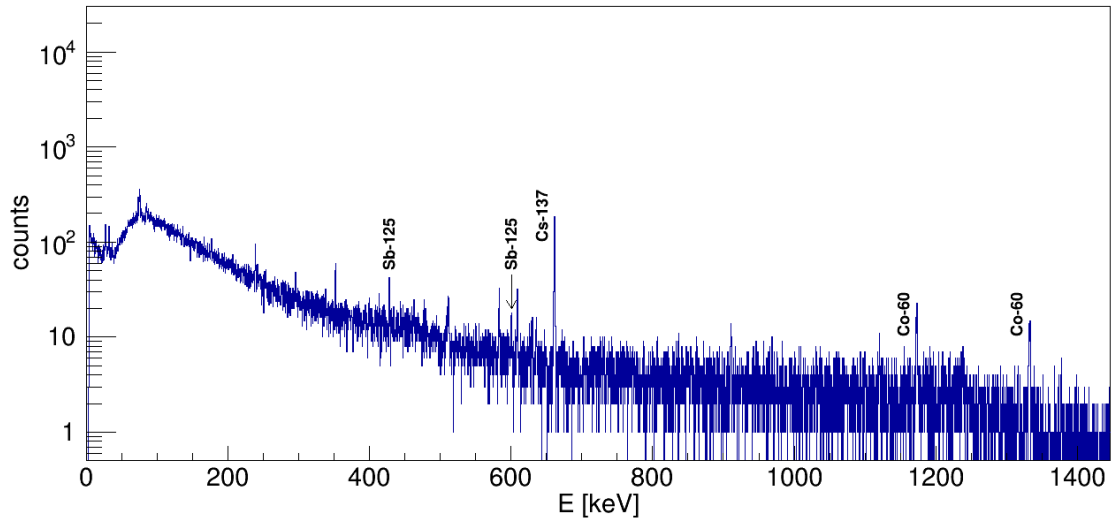


Figure B.13 The  $\gamma$ -ray spectrum for ion-exchange resin barrel 1102.

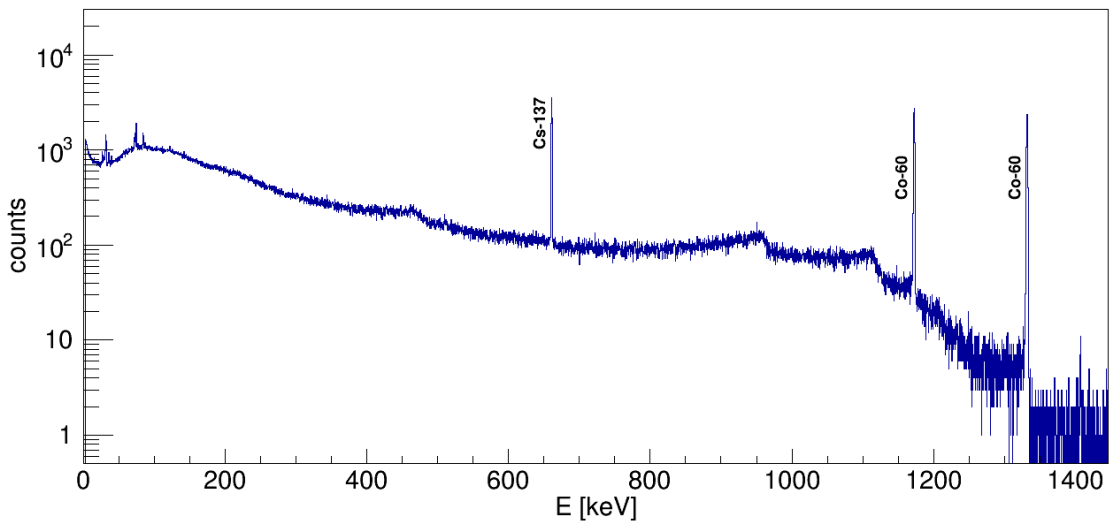


Figure B.14 The  $\gamma$ -ray spectrum for ion-exchange resin barrel 1103.

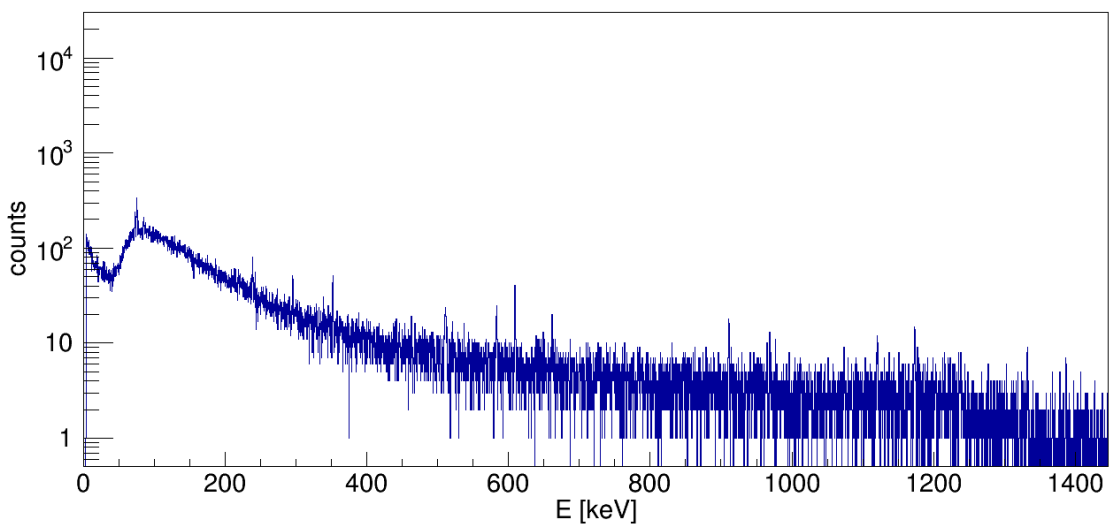


Figure B.15 The  $\gamma$ -ray spectrum for the ion-exchange resin background measurement.

**Addendum C: Gamma-ray energies used in activity calculations.**Table C.1 Concrete:  $\gamma$ -ray energies used in activity calculation.

Radionuclide	$\gamma$ -ray energy (keV)	Peak intensity (%)	Activity Bq/g
$^{22}\text{Na}$	1274.54	99.94	1.2E-02
$^{60}\text{Co}$	1173.22	100.00	2.6E-02
	1332.49	100.00	2.4E-02
$^{65}\text{Zn}$	1115.52	50.75	2.4E-02
$^{152}\text{Eu}$	121.78	28.40	1.2E+00
	244.69	7.49	1.0E+00
	344.27	26.50	9.8E-01
	411.11	2.21	9.8E-01
	443.98	3.11	1.1E+00
	778.89	12.74	9.6E-01
	867.32	4.16	1.0E-01
	964.01	14.40	9.2E-01
	1085.78	10.00	9.9 E-01
	1112.02	13.30	9.5 E-01
	1407.95	20.70	8.8 E-01

Table C.2 Flualtal 1:  $\gamma$ -ray energies used in activity calculation.

Radionuclide	$\gamma$ -ray energy (keV)	Peak intensity (%)	Activity Bq/g
$^{51}\text{Cr}$	320.08	9.83	1.3E+00
$^{54}\text{Mn}$	834.83	99.97	1.3E-01
$^{58}\text{Co}$	810.76	99.40	1.9E-01
$^{59}\text{Fe}$	192.34	3.11	4.4E-01
	1099.22	56.50	8.1E-01
	1291.56	43.20	5.8E-01
$^{60}\text{Co}$	1173.22	100.00	2.5E+00
	1332.49	100.00	2.6E+00

Table C.3 Aluminium 1:  $\gamma$ -ray energies used in activity calculation.

Radionuclide	$\gamma$ -ray energy (keV)	Peak intensity (%)	Activity Bq/g
<sup>46</sup> Sc	889.25	99.98	5.5E+00
	1120.51	99.99	5.4E+00
<sup>51</sup> Cr	320.08	9.83	7.0E+02
<sup>54</sup> Mn	834.83	99.97	1.8E+00
<sup>59</sup> Fe	142.65	1.03	1.2E+01
	192.34	3.11	1.4E+01
	1099.22	56.50	1.4E+01
	1291.56	43.20	1.3E+01
<sup>60</sup> Co	1173.22	100.00	5.3E+00
	1332.49	100.00	5.1E+00
<sup>65</sup> Zn	1115.52	50.75	8.1E+01

Table C.4.1 Ion-exchange resin barrel 1091:  $\gamma$ -ray energies used in activity calculation.

Radionuclide	$\gamma$ -ray energy (keV)	Peak intensity (%)	Activity Bq/g
<sup>60</sup> Co	1173.22	100.00	4.6E+00
	1332.49	100.00	4.7E+00
<sup>137</sup> Cs	661.65	85.12	1.4E+01

Table C.4.2 Ion-exchange resin barrel 1092:  $\gamma$ -ray energies used in activity calculation.

Radionuclide	$\gamma$ -ray energy (keV)	Peak intensity (%)	Activity Bq/g
<sup>60</sup> Co	1173.22	100.00	4.7E-06
	1332.49	100.00	4.8E-06
<sup>137</sup> Cs	661.65	85.12	4.6E-05

Table C.4.3 Ion-exchange resin barrel 1093:  $\gamma$ -ray energies used in activity calculation.

Radionuclide	$\gamma$ -ray energy (keV)	Peak intensity (%)	Activity Bq/g
<sup>60</sup> Co	1173.22	100.00	4.2E-01
	1332.49	100.00	4.5E-01
<sup>137</sup> Cs	661.65	85.12	3.7E+00

Table C.4.4 Ion-exchange resin barrel 1094:  $\gamma$ -ray energies used in activity calculation.

Radionuclide	$\gamma$ -ray energy (keV)	Peak intensity (%)	Activity Bq/g
$^{60}\text{Co}$	1173.22	100.00	1.2E+00
	1332.49	100.00	1.2E+00
$^{137}\text{Cs}$	661.65	85.12	2.6E+01

Table C.4.5 Ion-exchange resin barrel 1095:  $\gamma$ -ray energies used in activity calculation.

Radionuclide	$\gamma$ -ray energy (keV)	Peak intensity (%)	Activity Bq/g
$^{60}\text{Co}$	1173.22	100.00	6.3E+00
	1332.49	100.00	6.3E+00
$^{137}\text{Cs}$	661.65	85.12	6.5E+01

Table C.4.6 Ion-exchange resin barrel 1096:  $\gamma$ -ray energies used in activity calculation.

Radionuclide	$\gamma$ -ray energy (keV)	Peak intensity (%)	Activity Bq/g
$^{60}\text{Co}$	1173.22	100.00	1.8E-01
	1332.49	100.00	1.7E-01
$^{137}\text{Cs}$	661.65	85.12	1.6E+00

Table C.4.7 Ion-exchange resin barrel 1097:  $\gamma$ -ray energies used in activity calculation.

Radionuclide	$\gamma$ -ray energy (keV)	Peak intensity (%)	Activity Bq/g
$^{60}\text{Co}$	1173.22	100.00	1.7E-01
	1332.49	100.00	1.8E-01
$^{137}\text{Cs}$	661.65	85.12	4.9E+00

Table C.4.8 Ion-exchange resin barrel 1098:  $\gamma$ -ray energies used in activity calculation.

Radionuclide	$\gamma$ -ray energy (keV)	Peak intensity (%)	Activity Bq/g
$^{60}\text{Co}$	1173.22	100.00	9.3E+00
	1332.49	100.00	9.5E+00
$^{137}\text{Cs}$	661.65	85.12	1.5E+01

Table C.4.9 Ion-exchange resin barrel 1099:  $\gamma$ -ray energies used in activity calculation.

Radionuclide	$\gamma$ -ray energy (keV)	Peak intensity (%)	Activity Bq/g
$^{60}\text{Co}$	1173.22	100.00	-
	1332.49	100.00	3.8E-02
$^{125}\text{Sb}$	427.89	29.33	1.2E-01
	463.38	10.35	2.1E-01
$^{137}\text{Cs}$	661.65	85.12	4.2E-01

Table C.4.10 Ion-exchange resin barrel 1100:  $\gamma$ -ray energies used in activity calculation.

Radionuclide	$\gamma$ -ray energy (keV)	Peak intensity (%)	Activity Bq/g
$^{60}\text{Co}$	1173.22	100.00	2.5E+00
	1332.49	100.00	2.6E+00
$^{137}\text{Cs}$	661.65	85.12	4.1E+01

Table C.4.11 Ion-exchange resin barrel 1101:  $\gamma$ -ray energies used in activity calculation.

Radionuclide	$\gamma$ -ray energy (keV)	Peak intensity (%)	Activity Bq/g
$^{60}\text{Co}$	1173.22	100.00	8.2E+00
	1332.49	100.00	8.3E+00
$^{137}\text{Cs}$	661.65	85.12	1.6E+01

Table C.4.12 Ion-exchange resin barrel 1102:  $\gamma$ -ray energies used in activity calculation.

Radionuclide	$\gamma$ -ray energy (keV)	Peak intensity (%)	Activity Bq/g
$^{60}\text{Co}$	1173.22	100.00	1.3E-01
	1332.49	100.00	1.3E-01
$^{125}\text{Sb}$	176.33	6.89	3.7 E-01
	427.89	29.33	3.6 E-01
	600.56	17.80	4.3 E-01
	635.90	11.32	3.1 E-01
	671.41	1.81	8.0 E-01
$^{137}\text{Cs}$	661.65	85.12	6.7E+00

Table C.4.13 Ion-exchange resin barrel 1103:  $\gamma$ -ray energies used in activity calculation.

Radionuclide	$\gamma$ -ray energy (keV)	Peak intensity (%)	Activity Bq/g
$^{60}\text{Co}$	1173.22	100.00	2.4E+01
	1332.49	100.00	2.4E+01
$^{137}\text{Cs}$	661.65	85.12	1.8E+01

## Addendum D: Results of the ICP-MS analysis.

Table D.1 Results of the ICP-MS analysis.

Sample	unit	Li7(LR)	B11(LR)	Sr88(LR)	Zr90(LR)	Mo95(LR)	Ag107(LR)	Cd111(LR)	Sn118(LR)	Cs133(LR)	Ba137(LR)
Fluential 1	[ppb]	4.8E+05	<1632	4.7E+02	3.7E+03	3.7E+02	1.5E+01	2.8E+01	3.5E+02	<37,9	<2067
	RSD [%]	7.5E-01	2.2E+00	6.4E-01	3.3E+00	2.6E+00	7.7E+00	1.5E+01	1.4E+00	9.3E+01	8.5E+00
Fluential 2	[ppb]	5.5E+05	<2626	<354	4.1E+03	4.9E+02	1.8E+01	3.9E+01	3.3E+02	6.2E+01	<3326
	RSD [%]	2.9E+00	3.2E+00	3.7E+00	1.4E+00	7.5E+00	5.9E+00	3.3E+01	7.0E+00	2.7E+00	8.8E+00
Aluminium 1	[ppb]	< 73,1	1.9E+03	<37,9	6.1E+03	3.0E+03	1.7E+02	5.1E+02	8.3E+03	<6,54	<356
	RSD [%]	2.0E+01	1.1E+01	1.1E+01	1.3E+00	1.1E+00	3.1E-01	1.2E+00	9.5E-01	1.6E+01	9.5E+00
Aluminium 2	[ppb]	< 46,8	1.9E+03	<24,3	4.4E+03	2.9E+03	1.6E+02	4.8E+02	7.8E+03	<4,19	<228
	RSD [%]	1.1E+01	5.2E+00	9.6E+00	2.6E-01	1.2E+00	6.3E-01	1.3E+00	1.5E+00	1.2E+01	1.9E+00

Sample	unit	Ta181(LR)	W182(LR)	Re185(LR)	Ti205(LR)	Pb208(LR)	Bi209(LR)	Th232(LR)	U238(LR)	Na23(MR)	Mg24(MR)
Fluential 1	[ppb]	1.9E+01	8.0E+03	<1,28	<19,4	1.6E+03	1.0E+01	2.3E+01	1.0E+02	4.1E+05	3.9E+03
	RSD [%]	1.1E+01	2.5E+00	3.0E+01	1.2E+01	2.2E+00	1.5E+01	1.3E+01	2.2E+00	2.2E+00	2.5E+00
Fluential 2	[ppb]	1.5E+01	<163	<2,06	<31,3	3.5E+03	3.6E+01	1.2E+01	1.1E+02	4.2E+05	2.2E+03
	RSD [%]	7.2E+00	4.6E+00	2.6E+02	4.4E+00	7.2E-01	5.1E+00	3.1E+00	6.3E-01	2.2E+00	6.6E+00
Aluminium 1	[ppb]	<0,515	1.2E+03	7.0E-01	2.6E+02	2.2E+04	5.3E+01	1.1E+02	1.1E+03	<1161	1.1E+07
	RSD [%]	4.9E+00	8.0E-01	1.9E+01	1.9E+00	4.3E-01	1.4E+00	7.4E-01	1.3E+00	4.9E+00	1.3E+00
Aluminium 2	[ppb]	<0,330	1.1E+03	<0,141	2.6E+02	2.2E+04	5.3E+01	1.0E+02	1.1E+03	<744	1.0E+07
	RSD [%]	7.6E+00	7.2E-01	7.0E+01	6.8E-01	1.1E+00	3.1E+00	1.4E+00	2.3E+00	1.9E+01	1.5E+00

Sample	unit	Al27(MR)	Si28(MR)	P31(MR)	S32(MR)	Ca44(MR)	Sc45(MR)	Ti47(MR)	V51(MR)	Cr52(MR)	Mn55(MR)
Fluential 1	[ppb]	2.4E+08	5.4E+05	7.8E+03	8.6E+04	4.0E+04	1.2E+01	1.5E+04	1.5E+04	<9878	<6062
	RSD [%]	5.4E-01	1.8E+00	1.8E+00	1.9E+00	2.6E+00	1.3E+01	2.9E+00	1.2E+00	1.2E+00	4.5E+00
Fluential 2	[ppb]	2.6E+08	5.4E+05	7.8E+03	8.0E+04	<5023	1.4E+01	1.6E+04	1.6E+04	<14448	<9756
	RSD [%]	7.3E-01	2.6E+00	8.1E-01	3.2E+00	3.1E+01	1.8E+01	4.2E+00	3.0E+00	2.5E+00	8.6E+00
Aluminium 1	[ppb]	8.9E+08	3.7E+06	1.2E+03	<1602	1.2E+03	9.5E+01	1.3E+05	3.1E+04	1.9E+06	7.3E+05
	RSD [%]	1.5E+00	1.2E+01	9.2E+00	9.7E+00	8.7E+00	1.8E+00	4.0E+00	2.2E+00	9.7E-01	6.6E-01
Aluminium 2	[ppb]	9.2E+08	3.8E+06	8.9E+02	<1026	1.5E+03	8.9E+01	1.3E+05	2.9E+04	1.8E+06	7.1E+05
	RSD [%]	6.5E-01	8.4E+00	2.6E+00	7.2E+00	2.9E+00	8.1E-01	5.5E-01	3.2E-01	2.9E-01	1.4E+00

Sample	unit	Fe56(MR)	Co59(MR)	Ni60(MR)	Cu63(MR)	Zn66(MR)	Ga69(MR)	K39(HR)	Ge72(HR)	As75(HR)	Se77(HR)	Se78(HR)
Fluential 1	[ppb]	1.1E+05	2.6E+02	6.0E+03	4.3E+03	3.8E+03	5.0E+04	4.1E+04	1.1E+03	<12,4	<88,8	4.3E+06
	RSD [%]	3.1E-01	8.4E-01	1.4E+00	1.4E+00	1.5E+00	5.4E-01	5.0E+00	3.9E-01	3.0E-01	1.1E+00	1.2E+00
Fluential 2	[ppb]	1.0E+05	2.6E+02	6.3E+03	1.9E+03	3.9E+03	5.3E+04	1.6E+04	1.8E+03	<20,0	<143	4.8E+06
	RSD [%]	2.2E+00	3.6E+00	3.2E+00	5.9E+00	5.7E+00	2.2E+00	9.4E+00	3.4E-01	3.3E+00	4.3E-01	3.2E+00
Aluminium 1	[ppb]	3.5E+06	8.3E+02	1.6E+04	1.7E+06	2.9E+05	7.7E+04	<239	3.2E+02	1.1E+02	3.8E+02	1.3E+06
	RSD [%]	3.7E-01	3.7E+00	2.5E+00	5.9E-01	9.6E-01	2.5E+00	1.5E+00	1.5E+00	1.7E+01	6.8E+02	3.2E-01
Aluminium 2	[ppb]	3.4E+06	8.0E+02	1.5E+04	1.6E+06	2.7E+05	7.7E+04	<153	2.4E+02	1.5E+02	1.1E+03	1.2E+06
	RSD [%]	1.7E+00	2.4E+00	1.0E+00	1.1E+00	7.8E-01	1.6E+00	1.9E+00	1.4E+00	1.5E+01	1.9E+01	1.2E+00

ppb = parts per billion; RSD = relative standard deviation; LR = low range; MR = medium range; HR = high range.

## References

- [1] Maffei, B. The Physics of Energy Sources - Nuclear Fission. The University of Manchester [Online] [access 2016, 14 June]; Available: [http://www.jb.man.ac.uk/~bm/Teaching/en\\_sources/Lecture\\_notes/Lecture6\\_fission\\_notes.pdf](http://www.jb.man.ac.uk/~bm/Teaching/en_sources/Lecture_notes/Lecture6_fission_notes.pdf)
- [2] How Nuclear Reactors Work [Online] [access 2016, 14 June]; Available: <http://www.nei.org/Knowledge-Center/How-Nuclear-Reactors-Work>
- [3] Neutron Activation Analysis [Online] [access 2016, August 27]; Available: <http://www.naa-online.net/theory/equations/>
- [4] Nuclear Cross Sections and Neutron Flux [Online] [access 2016, 14 June]; Available: <http://www.free-ed.net/sweethaven/misctech/nuclear/Lesson0202.pdf>
- [5] Neutron Moderators in Nuclear Reactors [Online] [access 2016, 30 July]; Available: <http://www.nuclear-power.net/neutron-moderator/>
- [6] Omar S. Nuclear Reactor Coolants [Online] 2011 [access 2016, 30 July]; Available: <http://large.stanford.edu/courses/2011/ph241/omar1/>
- [7] Background on Reactor Pressure Vessel Issues [Online] [access 2016, 30 July]; Available: <http://www.nrc.gov/reading-rm/doc-collections/fact-sheets/prv.html>
- [8] Nuclear Power Plant Parts: A Look at the Parts of a Nuclear Power Plant [Online] [access 2016, 30 July]; Available: <http://www.argoturbo.com/blog/nuclear-power-plant-parts>
- [9] Research Reactors. World Nuclear Association [Online] 2016 [access 2016, August 20]; Available: <http://www.world-nuclear.org/information-library/non-power-nuclear-applications/radioisotopes-research/research-reactors.aspx>
- [10] Research Reactors. World Nuclear Association. [Online] [access 2016, 2 February]; Available: <http://www.world-nuclear.org/info/Non-Power-Nuclear-Applications/Radioisotopes/Research-Reactors/>
- [11] Bunn G, Braun C, Steinhausler F. Nuclear terrorism potential: Research reactors vs power reactors [Online] [access 2015, November 2]; Available: [https://cisac.fsi.stanford.edu/sites/default/files/Nuclear\\_Terrorism\\_Potential\\_Res\\_vs.\\_Power\\_Rctrs.pdf](https://cisac.fsi.stanford.edu/sites/default/files/Nuclear_Terrorism_Potential_Res_vs._Power_Rctrs.pdf)



[12] Nuclear Power Reactors. World Nuclear Association [Online] [access 2016, 30 July]; Available:

<http://www.world-nuclear.org/information-library/nuclear-fuel-cycle/nuclear-power-reactors/nuclear-power-reactors.aspx>

[13] Nuclear Power Reactors. World Nuclear Association [Online] 2016 [access 2016, August 20]; Available: <http://www.world-nuclear.org/information-library/nuclear-fuel-cycle/nuclear-power-reactors/nuclear-power-reactors.aspx>

[14] Decommissioning Nuclear Facilities. World Nuclear Association. [Online] [access 2015, March 20] ; Available: <http://www.world-nuclear.org/info/Nuclear-Fuel-Cycle/Nuclear-Wastes/Decommissioning-Nuclear-Facilities/>

[15] Samseth J. Closing and Decommissioning Nuclear Power Reactors. United Nations Environment Programme. [Online] [access 2015, March 20]; Available: [http://www.unep.org/yearbook/2012/pdfs/UYB\\_2012\\_CH\\_3.pdf](http://www.unep.org/yearbook/2012/pdfs/UYB_2012_CH_3.pdf)

[16] Regulations [Online] [access 2015, March 20]; Available: [http://www.stuk.fi/julkaisut\\_maaraykset/viranomaisohjeet/en\\_GB/yvl/](http://www.stuk.fi/julkaisut_maaraykset/viranomaisohjeet/en_GB/yvl/)

[17] Radioactivity Measurements at Regulatory Release Levels. OECD NEA Publication No. 6186. 2006.

[18] Radiological Characterisation of Shut Down Nuclear Reactors for Decommissioning Purposes. Technical Reports Series No. 389. IAEA Publication [Online] 2009 [access 2015, November 12]; Available: [http://www-pub.iaea.org/MTCD/publications/PDF/TRS389\\_scr.pdf](http://www-pub.iaea.org/MTCD/publications/PDF/TRS389_scr.pdf)

[19] The Decommissioning of Nuclear Reactors and Related Environmental Consequences. United Nations Environment Programme [Online] 2011 [access 2015, March 20]; Available: [http://na.unep.net/geas/getUNEPPageWithArticleIDScript.php?article\\_id=70](http://na.unep.net/geas/getUNEPPageWithArticleIDScript.php?article_id=70)

[20] Evans JC, Lepel EL, Sanders RW, Wilkerson CL, Silker W, Thomas CW, et al. Long-Lived Activation Products in Reactor Materials. Pacific Northwest Laboratory. Washington; 1984.

[21] Number of nuclear reactors operable and under construction. World Nuclear Association. [Online] [access 2016, August 20]; Available: [www.world-nuclear.org/nuclear-basics/global-number-of-nuclear-reactors.aspx](http://www.world-nuclear.org/nuclear-basics/global-number-of-nuclear-reactors.aspx)

- [22] Nuclear power plants, world-wide. European Nuclear Society [Online] 2016 [access 2016, August 20]; Available: <https://www.euronuclear.org/info/encyclopedia/n/nuclear-power-plant-world-wide.htm>
- [23] Decommissioning Nuclear Facilities. World Nuclear Association [Online] 2016 [access 2016, August 20]; Available: <http://www.world-nuclear.org/information-library/nuclear-fuel-cycle/nuclear-wastes/decommissioning-nuclear-facilities.aspx>
- [24] Operational Status of Research Reactors. IAEA Research Reactor Database [Online] 2016 [access 2016, August 20]; Available: <https://nucleus.iaea.org/RRDB/Reports/Container.aspx?Id=A1>
- [25] Radioactive Waste Management in Finland - STUK [Online] [access 2015, April 8]; Available: [http://www.stuk.fi/ydinturvallisuus/ydinjatteet/ydinjate/en\\_GB/ydinjate/\\_files/12222632510021180/default/fin\\_country\\_profile.pdf](http://www.stuk.fi/ydinturvallisuus/ydinjatteet/ydinjate/en_GB/ydinjate/_files/12222632510021180/default/fin_country_profile.pdf)
- [26] Carlsson T, Kotiluoto P, Vilkkamo O, Kekki T, Auterinen I, Rasilainen K. Chemical aspects on the final disposal of irradiated graphite and aluminium: A literature survey. VTT Technical Research Centre of Finland; 2014.
- [27] Kotiluoto P, Rätty A. FiR 1 activity inventories for decommissioning planning. VTT Technical Research Centre of Finland; 2015. [Available upon request].
- [28] Savolainen S, Kortensniemi M, Timonen M, Reijonen V, Kuusela L, Uusi-Simola J, et al. Boron neutron capture therapy (BNCT) in Finland: Technological and physical prospects after 20 years of experiences. *Physica Medica* 2013;29:233-248.
- [29] Reilly D, Ensslin N, Smith Jr H, Krelner S. Passive Nondestructive Assay of Nuclear Materials (Rinard P. Chapter 12: Neutron Interactions with Matter). Virginia: National Technical Information Service; 1991.
- [30] Salehi D, Sardari D, Salehi M. Evaluation of Design Neutron Filters in BNCT. Open Access Scientific Reports [Online] 2012 [access 2015, November 2]; Available: [www.omicsonline.org/scientific-reports/2155-9619-SR-537.pdf](http://www.omicsonline.org/scientific-reports/2155-9619-SR-537.pdf)
- [31] Rätty A, Kotiluoto P. FiR1 TRIGA Activity Inventories for Decommissioning Planning. Delivered at International Symposium on Preparation for Decommissioning (PREDEC 2016). Lyon; 2016.

- [32] Kotiluoto P, Hiismäki P, Auterinen I, Seppälä T, Aschan C. *Frontiers in Neutron Capture Therapy (Chapter: Shielding Design and Calculations for the Finnish BNCT Facility)*. Springer US; 2001.
- [33] Seppälä T. *FiR1 Epithermal Neutron Beam Model and Dose Calculation for Treatment Planning in Neutron Capture Therapy*. [Doctoral Dissertation]. Helsinki: University of Helsinki; 2002.
- [34] Auterinen I, Salmenhaara SEJ. *The 250 kW FiR 1 TRIGA Research Reactor - International Role in Boron Neutron Capture Therapy (BNCT) and Regional Role in Isotope Production, Education and Training*. IAEA Publication [Online] 2007 [access 2015, November 12]; Available: [http://www-pub.iaea.org/MTCD/publications/PDF/P1360\\_ICRR\\_2007\\_CD/Papers/I.H.%20Auterinen.pdf](http://www-pub.iaea.org/MTCD/publications/PDF/P1360_ICRR_2007_CD/Papers/I.H.%20Auterinen.pdf)
- [35] *Predisposal Management of Low and Intermediate Level Nuclear Waste and Decommissioning of a Nuclear Facility*. STUK Guide YVL D.4; 2013.
- [36] *Disposal of low and intermediate-level waste in Finland*. STUK. [Online] [access 2016, 26 March]; Available: <http://www.stuk.fi/web/en/topics/nuclear-waste/disposal-of-low-and-intermediate-level-waste-in-finland>
- [37] Kekki T, Tiitta A. *Evaluation of the radioactive waste characterisation at the Olkiluoto nuclear power plant*. STUK; 2000.
- [38] *Disposal of spent fuel in Finland*. STUK. [Online] [access 2016, 26 March]; Available: <https://www.stuk.fi/web/en/topics/nuclear-waste/disposal-of-spent-fuel-in-finland>
- [39] *Properties of Radiation* [Online] [access 2015, November 18]; Available: <http://www.physics.isu.edu/radinf/properties.htm>
- [40] Ragheb M. *Gamma Rays Interaction with Matter* [Online] 2016 [access 2016, August 20]; Available: <http://mragheb.com/NPRE%20402%20ME%20405%20Nuclear%20Power%20Engineering/Gamma%20Rays%20Interactions%20with%20Matter.pdf>
- [41] Knoll GF. *Radiation Detection and Measurement, Fourth Edition*. John Wiley & Sons, Inc; 2010.
- [42] Msezane BM. *The Study of High Spin States in <sup>196</sup>Hg*. [Master's Thesis]. MangaZe: University of Zululand; 2006.

- [43] Gamma Attenuation [Online] [access 2016, August 29]; Available: [http://www.radioactivity.eu.com/site/pages/Gamma\\_Attenuation.htm](http://www.radioactivity.eu.com/site/pages/Gamma_Attenuation.htm)
- [44] Hubbell JH, Seltzer SM. Tables of X-Ray Mass Attenuation Coefficients and Mass Energy-Absorption Coefficients (version 1.4). National Institute of Standards and Technology, Gaithersburg, MD. [Online] 2004 [access 2016, September 1]; Available: <http://physics.nist.gov/xaamdi>
- [45] The Neutrino. The NEMO experiment [Online] [access 2016, August 29]; Available: <http://nemo.in2p3.fr/physics/neutrinos.php>
- [46] Electron Capture [Online] [access 2016, August 29]; Available: [http://www.radioactivity.eu.com/site/pages/Electron\\_Capture.htm](http://www.radioactivity.eu.com/site/pages/Electron_Capture.htm)
- [47] Fission. Oregon State University [Online] [access 2016, August 29]; Available: <http://oregonstate.edu/instruct/ch374/ch418518/Chapter%2011%20Fission.pdf>
- [48] Reilly D, Ensslin N, Smith Jr H, Krelner S. Passive Nondestructive Assay of Nuclear Materials (Smith Jr H, Lucas M. Chapter 3: Gamma Ray Detectors). Virginia: National Technical Information Service; 1991.
- [49] Neutron Activation Analysis Scanning Fabry-Perot Interferometers [Online] [access 2016, August 29]; Available: <https://www.thorlabs.com/tutorials.cfm?tabID=e9d2d96f-1efd-4ef0-bb17-fa2ca60f8a8d>
- [50] Kotiluoto P. Adaptive Tree Multigrids and Simplified Spherical Harmonics Approximation in Deterministic Neutral and Charged Particle Transport. [Doctoral Dissertation]. Helsinki: University of Helsinki; 2007.
- [51] Liquid Scintillation Counting [Online] [access 2015, June 25]; Available: [http://www.bio.huji.ac.il/upload/beta\\_counter\\_protocol.pdf](http://www.bio.huji.ac.il/upload/beta_counter_protocol.pdf)
- [52] Hoeppener-Kramar U, Pimpl M, Wilmann F. Application of procedures for low level radionuclide analysis in environmental monitoring for the purpose of clearance measurements of materials from decommissioning of nuclear facilities. *Journal of Radioanalytical and Nuclear Chemistry* 1997;226(1-2):99-103.
- [53] Remeikis V, Plukis A, Juodis L, Gudelis A, Lukauskas D, Druteikiene R, et al. Study of the nuclide inventory of operational waste for the RBMK-1500 reactor. *Nuclear Engineering and Design* 2009;239:813-818.

- [54] Søgaard-Hansen J. NKS-R Decommissioning Seminar: Scaling Factors in Clearance Measurements on Decommissioning Waste at Danish Decommissioning [Online] 2013 [access 2015, November 12]; Available: [http://projects.hrp.no/nks-decom-2013/files/2016/07/Scaling\\_factors\\_in\\_clearance\\_measurements\\_on\\_decommissioning\\_waste\\_dd\\_soegaard\\_paper\\_nks2013.pdf](http://projects.hrp.no/nks-decom-2013/files/2016/07/Scaling_factors_in_clearance_measurements_on_decommissioning_waste_dd_soegaard_paper_nks2013.pdf)
- [55] Determining and Use of Scaling Factors for Waste Characterisation in Nuclear Power Plants. IAEA Publication [Online] 2009 [access 2015, November 12]; Available: [http://www-pub.iaea.org/MTCD/publications/PDF/Pub1363\\_web.pdf](http://www-pub.iaea.org/MTCD/publications/PDF/Pub1363_web.pdf)
- [56] Radiological Characterisation of Shut Down Nuclear Reactors for Decommissioning Purposes. Technical Reports Series No. 389. IAEA Publication [Online] 2009 [access 2015, November 12]; Available: [http://www-pub.iaea.org/MTCD/publications/PDF/TRS389\\_scr.pdf](http://www-pub.iaea.org/MTCD/publications/PDF/TRS389_scr.pdf)
- [57] Perevezentsev AN, Bell AC, Rivkis LA, Filin VM, Gushin VV, Belyakov MI, et al. Comparative study of the tritium distribution in metals. *Journal of Nuclear Materials* 2008;372:263-276.
- [58] Matsuyama M, Watanabe K, Hasegawa K. Tritium assay in materials by the bremsstrahlung counting method. *Fusion Engineering and Design* 1998;39-40:929-936.
- [59] Hou X. Radiochemical analysis of radionuclides difficult to measure for waste characterisation in decommissioning of nuclear facilities. *Journal of Radioanalytical and Nuclear Chemistry* 2007;273(1):43-48.
- [60] Hou X. Rapid analysis of  $^{14}\text{C}$  and  $^3\text{H}$  in graphite and concrete for decommissioning of a nuclear reactor. *Applied Radiation and Isotopes* 2005;62:871-882.
- [61] Warwick PE, Kim D, Croudace IW, Oh J. Effective desorption of tritium from diverse solid matrices and its application to routine analysis of decommissioning materials. *Analytica Chimica Acta* 2010;676:93-102.
- [62] Zweben SJ, Johnson DW, Hill KW, Ku LP, LeMunyan G, Loesser D, et al. Methods for the measuring surface tritium inside TFTR using beta decay. *Review of Scientific Instruments* 1995;66:357-359.
- [63] Pomme S, Hardeman F, Robouch P, Etxebarria N, Arana G. Neutron Activation Analysis with  $K_0$ -standardisation: General Formalism and Procedure. Nuclear Spectrometry, Radiation Protection Department: SCK.CEN [Online] 1997 [access 2016, August 23]; Available: [http://www.iaea.org/inis/collection/NCLCollectionStore/\\_Public/29/032/29032874.pdf](http://www.iaea.org/inis/collection/NCLCollectionStore/_Public/29/032/29032874.pdf)

- [64] Lamarsh JR. Nuclear Reactor Theory. Ontario: Addison-Wesley Publishing Company, Inc.; 1996.
- [65] Background on Tritium, Radiation Protection Limits, and Drinking Water Standards. United States Nuclear Regulatory Commission [Online] 2016 [access 2016, May 15]; Available: <http://www.nrc.gov/reading-rm/doc-collections/fact-sheets/tritium-radiation-fs.html>
- [66] Decommissioning of Medical, Industrial and Research Facilities. IAEA Safety Standards Series. IAEA Publication [Online] 1999 [access 2015, November 12]; Available: [http://www-pub.iaea.org/MTCD/publications/PDF/P078\\_scr.pdf](http://www-pub.iaea.org/MTCD/publications/PDF/P078_scr.pdf)
- [67] Live Chart of Nuclides [Online] [access 2015, October 15]; Available: <https://www-nds.iaea.org/relnsd/vcharthtml/VChartHTML.html>
- [68] X-5 Monte Carlo Team. MCNP – A General Monte Carlo N-Particle Transport Code, Version 5, Volume 1: Overview and Theory. 2008.
- [69] Gauld IC, Hermann OW, Westfall RM. ORIGEN-S: A Scale System Module to Calculate Fuel Depletion, Actinide Transmutation, Fission Product Buildup and Decay, and Associated Radiation Source Terms (Version 6.1). 2011.
- [70] The Bateman Equations. Reactor Physics: K TH Royal Institute of Technology [Online] [access 2016, August 30]; Available: <http://neutron.kth.se/courses/transmutation/Bateman/Bateman.html>
- [71] Larsson A, Lundgren K. Assessment of Radioactivity Inventory in Swedish LWRs at Time of Decommissioning. WM2014 Conference [Online] 2014 [access 2016, January 28]; Available: <http://www.wmsym.org/archives/2014/papers/14279.pdf>
- [72] Pavelescu AO, Geprava DG. CANDU Radiotoxicity Inventories Estimation - A Calculated Experiment Cross-check for Data Verification and Validation [Online] 2006 [access 2016, June 29]; Available: [http://www.nipne.ro/rjp/2007\\_52\\_1-2/0137\\_0149.pdf](http://www.nipne.ro/rjp/2007_52_1-2/0137_0149.pdf)
- [73] Glozman EP, Akhmetova RS. Chemical composition of bitumen components, Chemistry and Technology of Fuels and Oils 6(5). 1970.
- [74] Lewan MD, Maynard JB. Factors controlling enrichment of vanadium and nickel in the bitumen of organic sedimentary rocks. Geochimica et Cosmochimica Acta 46(12). 1981.
- [75] Nuclear Energy Act 990/1987; amendments up to 342/2008 included. Ministry of Trade and Industry, Finland [Online] [access 2016, June 28]; Available: [www.finlex.fi/en/laki/kaannokset/1987/en19870990.pdf](http://www.finlex.fi/en/laki/kaannokset/1987/en19870990.pdf)

- [76] Return of Research Reactor Spent Fuel to the Country of Origin: Requirements for Technical and Administrative Preparations and National Experiences (Proceedings of a technical meeting held in Vienna, August 2006). IAEA Publication; 2008.
- [77] IAEA Safety Standards: Decommissioning of Facilities. General Safety Requirements Part 6. IAEA Publication [Online] 2014 [access 2015, October 15]; Available: <http://www-pub.iaea.org/MTCD/publications/PDF/Pub1652web-83896570.pdf>
- [78] Troiani F, Bienvenu P, Dale C, Delepine JJ, Fachinger J, Gallego C, et al. Destructive Analyses for the Quality Checking of Radioactive Waste Packages. European Commission; 2001.
- [79] Rätty A, Kotiluoto P. FiR1 Activity Inventories for Decommissioning Planning. VTT research report VTT-R-03599-16; 2016.
- [80] AMBERLITE™ IRN150 Resin Product Data Sheet [Online] [access 2015, 1 December]; Available:  
[http://msdssearch.dow.com/PublishedLiteratureDOWCOM/dh\\_06b2/0901b803806b2d43.pdf?filepath=liquidseps/pdfs/noreg/177-02225.pdf&fromPage=GetDoc](http://msdssearch.dow.com/PublishedLiteratureDOWCOM/dh_06b2/0901b803806b2d43.pdf?filepath=liquidseps/pdfs/noreg/177-02225.pdf&fromPage=GetDoc)
- [81] In Situ Gamma Spectroscopy with ISOCS, an In Situ Object Counting System. Canberra Application Note [Online] [access 2015, September 7]; Available:  
[http://www.canberra.com/literature/gamma\\_spectroscopy/application\\_notes/InSitu-ISOCS-M2352.pdf](http://www.canberra.com/literature/gamma_spectroscopy/application_notes/InSitu-ISOCS-M2352.pdf)
- [82] Akkurt I, Gunoglu K, Arda SS. Detection Efficiency of NaI(Tl) Detector in 511-1332 keV Energy Range. Science and Technology of Nuclear Installations 2014 [Online] 2013 [access 2016, September 16]; Available: <https://www.hindawi.com/journals/stni/2014/186798/>
- [83] McClelland P, Lewis V. Measurement Good Practice Guide No. 34: Radiometric Non-Destructive Assay. National Physical Laboratory. Middlesex; 2003.
- [84] Genie™ 2000 Spectroscopy Software: Customization Tools. Canberra Industries, Inc; 2013.
- [85] Genie™ 2000 Basic Spectroscopy Software. Canberra Industries [Online] [access 2015, September 7]; Available: [www.canberra.com/products/radiochemistry\\_lab/.../G2K-BasicSpect-SS-C40220.pdf](http://www.canberra.com/products/radiochemistry_lab/.../G2K-BasicSpect-SS-C40220.pdf)G2K-BasicSpect:
- [86] Genie™ 2000 Interactive Peak Fit. Canberra Industries [Online] [access 2015, September 7]; Available: [http://www.canberra.com/products/radiochemistry\\_lab/pdf/IPF-C37116.pdf](http://www.canberra.com/products/radiochemistry_lab/pdf/IPF-C37116.pdf)

[87] Genie™ 2000 Gamma Analysis Software. Canberra Industries [Online] [access 2015, September 7]; Available: [http://www.canberra.com/products/radiochemistry\\_lab/pdf/Gamma-Analysis-SS-C40221.pdf](http://www.canberra.com/products/radiochemistry_lab/pdf/Gamma-Analysis-SS-C40221.pdf)

[88] Laboratoire National Henri Becquerel. Tables of evaluated data [Online] [access 2016, October 15]; Available: [http://www.nucleide.org/DDEP\\_WG/DDEPdata\\_by\\_Z.htm](http://www.nucleide.org/DDEP_WG/DDEPdata_by_Z.htm)